The Silesian University of Technology
Faculty of Mechanical Engineering
Department of Fundamentals of Machinery Design

Doctoral dissertation

Comparative analysis of the drone configuration in terms of stability criteria

MSc, Eng. Paulina Zenowicz

Supervisor:
Prof. Wojciech Moczulski, PhD, DSc

Gliwice, 2024

Contents

1. Introduction

Unmanned Aerial Vehicles (UAVs) like aircraft are becoming increasingly popular across all sectors, including science and the private industry. Thanks to advancements in modern lightweight materials and electronic components, UAVs can be designed as small, agile drones or with a large wingspan capable of transporting heavy loads from one location to another (Ucgun, Yuzgec and Bayilmis 2021).

With their independence and flexibility, UAVs have a multitude of applications, such as military operations, surveillance, monitoring, telecommunications, medical supply delivery, and rescue missions. Despite the potential for drones, there are still design challenges that must be addressed to ensure that they are effective for specific applications (Heaphy, et al. 2017).

Unmanned Aerial Vehicles (UAVs) can be categorized into two groups based on their flight altitudes - High Altitude Platforms (HAPs) and Low Altitude Platforms (LAPs). HAPs typically reach altitudes of up to 17 km above sea level and flight are quasi-stationary. Alternatively, LAPs can fly at altitudes ranging from several dozen meters to several kilometers, are more flexible and can move quickly. UAVs can also be classified based on their type - fixed-wing and rotary-wing UAVs. Fixed-wing UAVs, like small planes, have more mass, speed and need to move forward to stay up, compared to rotary-wing UAVs (Mozaffari, et al. 2019).

1.1. UAV classification

Unmanned Aerial Vehicles, like other aircraft, can be classified based on various variables. The designed structures differ depending on the missions they are to perform, each structure has individual features that may prove crucial when planning a given drone mission, such as the ability to hover in the air or long flight duration. Based on the literature (Fotouhi, et al. 2019, Arjomandi 2007, Mozaffari, et al. 2019), UAVs were divided according to flight altitude, type of structure and mass [Fig. 1].

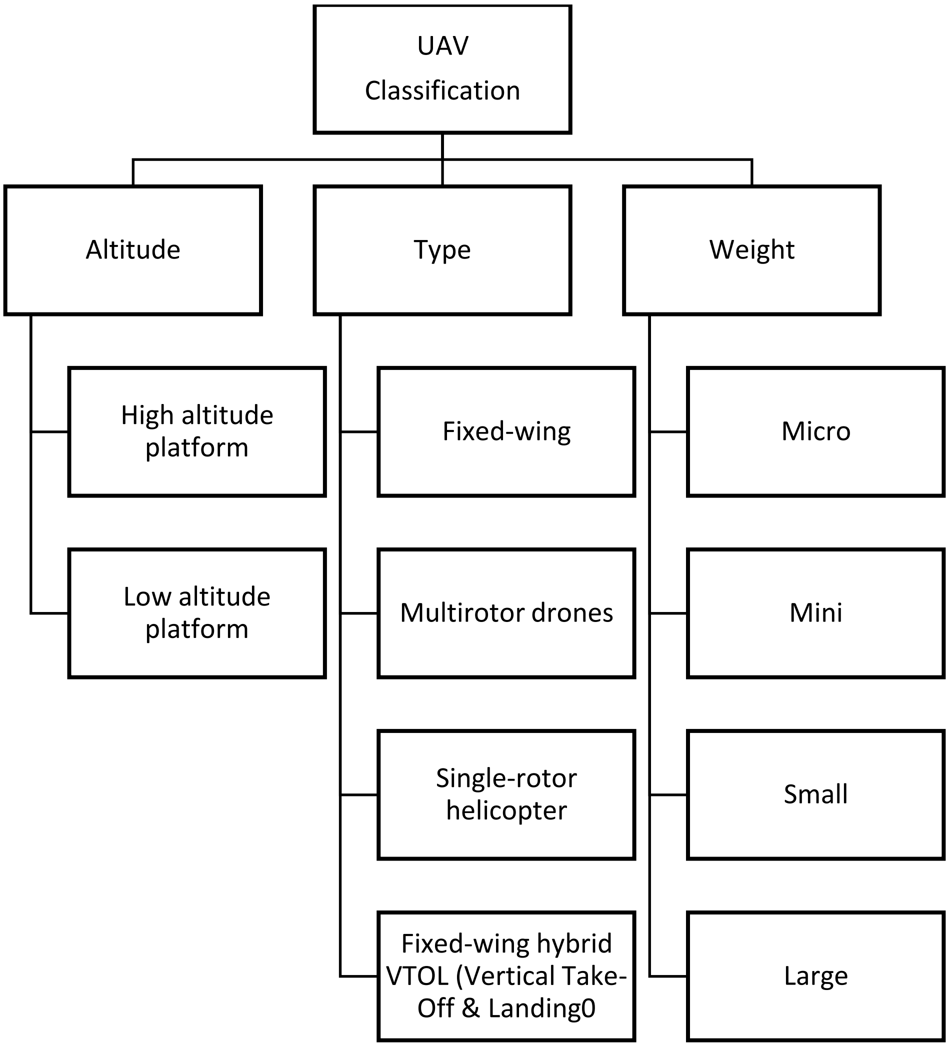

Fig. 1 UAV Classification (Mozaffari, et al. 2019, Fotouhi, et al. 2019)

UAV's classification according to flight altitude:

- High altitude platform (HAPs)
  - Long endurance (Days or months).
  - Wide coverage.
  - Quasi-stationary.
  - Altitude above 17 km.
- Low altitude platform (LAPs)
  - Fast and flexible deployment.
  - Quick mobility.
  - Cost-effective.
  - Typically flies up to several hours.

Division by body structure (Lee, Kim and Chu 2021):

- Fixed-wing – these drones resemble classic airplanes, they fly ability is caused by the airflow around the wing when the aircraft is in motion and Flight endurance of this type of UAV is usually higher than other constructions and they can fly over long distances. The cost of producing such a drone is usually higher compared to producing other types and requires greater flying skills of the pilot. For take-off, there is a need for a runway or a catapult, and for landing a runway or a parachute (Elmeseiry, Nancy and Ismail 2021).

- Multirotor drones – these are the most often used drones by professionals and hobbyists. They are classified according to the number of rotors. Ease of production, piloting and the possibility of vertical take-off make them the most popular unmanned structures. The disadvantages of such structures are related to the limited flight endurance and the amount of energy needed to stabilize the flight (Saeed, et al. 2015).
- Single-rotor helicopter – structurally it resembles a small helicopter, it has one large rotor and one smaller one on the tail, they have a longer flight time and are more stable than multi-rotors, they are more expensive to produce than multi-rotors due to the size of the main rotor. Single-rotor drones require more skill to fly them in the air properly (Carholt, et al. 2016).
- Fixed-wing hybrid VTOL (Vertical Take-Off & Landing) - has the best features of both the rotor and fixed wing, a fixed-wing hybrid will have multiple rotors that can be attached at the tip of the wings or in the middle of the wings, taking into account the wings must rotate appropriately to perform VTOL (Joshi, Tripathi and Ponnalgu 2019).

Division by weight (Coban and Oktay 2018):

- Micro: Less than two kilograms.
- Mini: Greater than 2 kg and less than 20 kg.
- Small: Greater than 20 kg and less than 150 kg.
- Large: Greater than 150 kg.

1.2. Overview of tail units used in the drones

A comparative analysis was conducted on various types of tail structures employed in aviation. The diverse configurations of airplane tail constructions encompass a range of key elements that significantly influence its performance, stability, and overall characteristics during flight (Kurnyta, et al. July 10-13, 2018). Greater surface area, sweep angle and location of the tail can increase or decrease the control of the aircraft during manoeuvring, and therefore its effect on the stability of the aircraft in flight (Abdulwahab, et al. 2013). For example, an inverted V-tail arrangement can improve lateral stability, especially at high angles of attack. When choosing a given configuration, it is worth relying on the assessment of experienced designers and pilots. Evaluating the performance of different tail variants in real conditions can provide valuable information regarding reliability, effectiveness and control difficulty.

It should be noted that the intricate nature of tail aerodynamics requires an interdisciplinary analysis, considering both engineering and piloting aspects. Only through a holistic approach to this issue is it possible to effectively understand the impact of the tail on the flight characteristics of aircraft and optimize their design with a focus on safety and operational efficiency.

The following configurations were proposed for further analysis, taking into account the use of the aircraft as well as its other structural elements, such as the structure of the fuselage, wings and the selection of the propulsion source:

- Conventional tail unit

The common tail structure represents the most common model. It consists of a single vertical stabiliser located in the tapered rear section of the fuselage and a single horizontal stabiliser divided into two parts, located on one side of each vertical stabiliser wing. For many aircraft, a conventional layout provides adequate stability and control with minimal structural weight (Whalen, et al. 2016).

- V-tail and inverted V design

The intended advantage of the V-tail design is the ability of two surfaces to perform the same function as the three required in the traditional tail and its modifications. A V-shaped tail, when properly proportioned, can achieve as high level of stability as a conventionally configured tail. A potential drawback of the V-tail arrangement is the generation of torque by deflecting the rudders; however, this effect can be minimized by transforming the tail into an A-shaped (inverted V) configuration (Gracia-Hernandez, Cuerno-Rejado and Perez-Cortes 2018).

- Boom-tail construction

The lack of a standard tail section allows for flexibility in cargo location. By placing equipment, fuel or other cargo between the booms, it is possible to adjust the position of the aircraft's centre of gravity, which translates into the optimization of flight parameters.

A boom-tail can generate more aerodynamic drag than a classic configuration, potentially affecting the aircraft's usability in certain applications (Weiss 2023).

All analysed tail configurations were presented in figure Fig. 2.

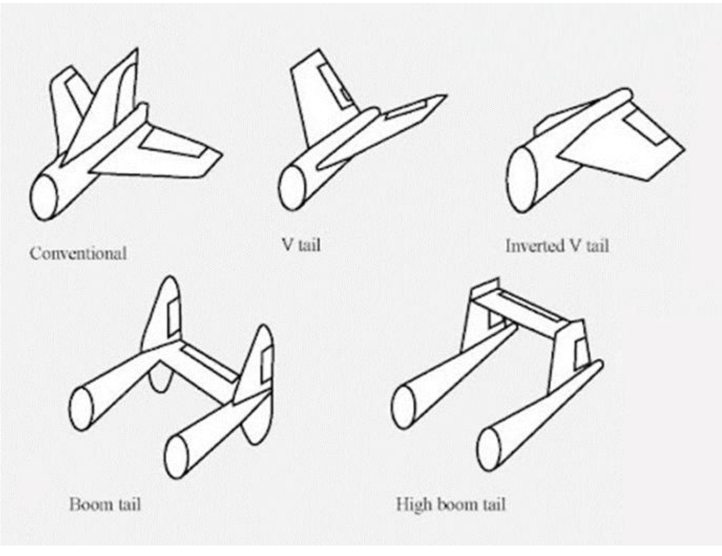

Fig. 2 Tail units (What, When, How - Tail designs 2023)

1.3. Overview of existing solutions

Unmanned aerial vehicle classification can be done due to many parameters. Agostino et al. in their work (Agostino, et al. 2006), presented the clasiffication according to the weight, range, and duration of the flight, cruising altitude, and loads acting on the wings. The parameters they adopted when determining the distribution are presented in Tables (Tab 1– Tab 4).

Tab 1 UAVs classification by weight (Agostino, et al. 2006)

Designation	Weight Range	Example
Super Heavy	>2000 kg	Global Hawk
Heavy	200 – 2000 kg	A-160
Medium	50 – 200 kg	Raven
Light	5 – 50 kg	RPO Midget
Micro	<5 [kg]	Dragon Eye

Tab 2 UAVs classification by Range and Endurance (Agostino, et al. 2006)

Category	Endurance	Range	Example
High	>24 hours	>1500 km	Predator B
Medium	5 – 24 hours	100 – 400 km	Silver Fox
Low	< 5 hours	< 100 km	Pointer

Tab 3 UAVs classification by maximum altitude (Agostino, et al. 2006)

Category	Max Altitude	Example
Low	< 1000 m	Pointer
Medium	1000 – 10000 m	Finder
High	> 10000 m	Darkstar

Tab 4 UAVs classification by wing loading (Agostino, et al. 2006)

Category	Wing loading kg/m2	Example
Low	<50	Seeker
Medium	50-100	X -45
High	>100	Global Hawk

As part of the work, a literature review on unmanned aerial platforms was performed. The analysis revealed the existence of many solar-powered or high-altitude platforms. Only a few platforms meet the conditions regarding electric power supply, high flight altitude, and the possibility of long-term flight exceeding 24 hours. The platforms that come closest to meeting the required assumptions are presented below:

1.3.1. Aurora Oddyseus:

Aurora's Odysseus (Fig. 3) (Sciences n.d.) aircraft is a high-altitude pseudo-satellite that can change how we use the sky. At a fraction of the cost of a satellite and powered by the sun, Odysseus offers vast new possibilities for those who need to stay connected and informed.

Carries a class-leading 63.5 kg of payload to above of 18288 m. Provides 900 watts maximum or continuous 250 watts of power. Operable year-round between medium latitudes and 6 months at sub-arctic latitudes. Autonomously maintains its position for months on end in any stratospheric condition. Generates zero emissions and operates far above other aircarfts and weather conditions. Odysseus brings endurance and autonomy to a wide variety of missions. Its global reach, flexible payload capacity and persistent, solar-powered flight enable longer missions and better data quality (Sciences n.d.).

Fig. 3 Aurora Oddyseus (Sciences n.d.)

1.3.2. X-HALE

The X-HALE (Cesnik, et al. December 2012) is a flexible, high-aspect-ratio, wing-boom-tail type aircraft. It has an 8-m span (constructed with eight identical 1-m sections) 0.2-m chord; four 0.83-m booms with horizontal tails attached and five motor pods with propellers, batteries, and processor boards (Fig. 4). X-HALE has a mass of 11 kg with an anticipated flight speed ranging from 10 to 19 m/s (Cesnik and Su 4 - 7 January 2011, Cesnik, et al. December 2012, Kamran and Hammad 2013).

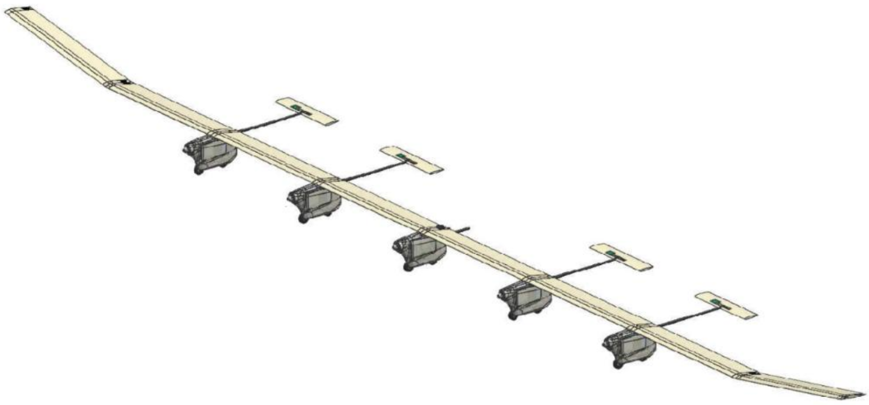

Fig. 4 X-HALE CAD (Cesnik, et al. December 2012)

1.3.3. HELIPLAT

HAVE/UAV (High Altitude Verylong Endurance / Unmanned Air Vehicle) HELIPLAT (Frulla 2002) (HELIos PLATform) (Fig. 5). The vehicle should climb to 17-20 km by mainly taking advantage of direct sun radiation and thereafter maintaining a level flight; during the night, a fuel cell energy storage system would be use. A first configuration was worked out, following a preliminary parametric study. The platform is a monoplane with 8 brushless motors, a twin-boom tail type with a long horizontal stabiliser and two rudders. A preliminary structural design of a scale-sized technological demonstrator was completed to manufacture a proof-of-concept structure of HELIPLAT and perform a static test on it. A computer program has been developed for designing the anisotropic wing box, lay-up and thicknesses, leading to a maximum tip deflection of about 1.5 m.

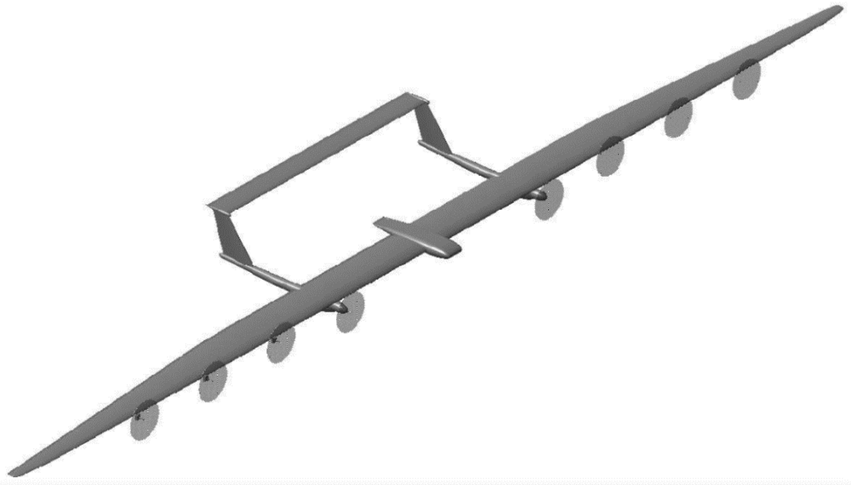

Fig. 5 HELIPLAT (HELIos PLATform) (Frulla 2002)

1.3.4. Sky-Sailor

Sky-Sailor (Fig. 6) (Noth, Engel and Siegwart 2006) version 1 is a motor glider with a structural weight of only 0.6 kg for a wingspan of 3.2 m and a wing surface of 0.776 m2. The resulting total weight including motors, propeller, solar cells, batteries and controller is around 2.5 kg (Noth, Engel and Siegwart 2006, Noth, Siegwart and Engel 2006).

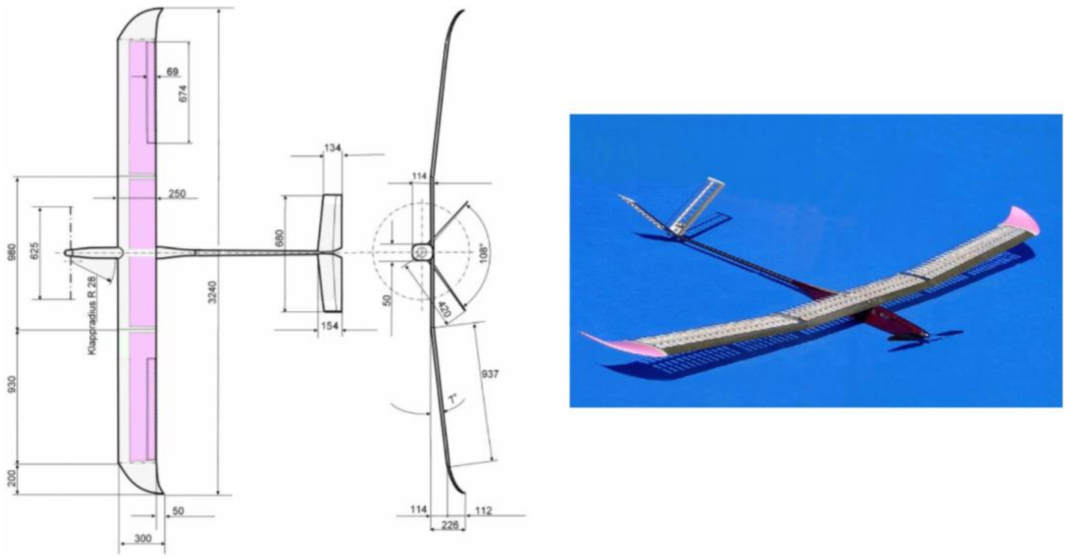

Fig. 6 Mechanical structure of Sky-Sailor (Noth, Engel and Siegwart 2006, Montgomery and Mourtos 2016)

1.3.5. SoLong UAV

The SoLong (Fig. 7) kg (Zhu, Guo and Hou 2014) was established by AC Propulsion Inc., a company that specializes in high-efficiency, electric propulsion. Alan Cocconi, the founder, chairman, and chief engineer of AC Propulsion, funded the project himself. The objective of the SoLong was to demonstrate a multi-day solar-powered flight. The SoLong was a solar-powered monoplane with a wingspan of 4.75 m, a wing area of 1.5 m2, a battery that weighs

5.6 kg (Sanyo 18650 lithium-ion (Li-ion) batteries with 220 Wh/kg), 76 SunPower A300 solar cells, and a total mass of 12.6 kg (Zhu, Guo and Hou 2014).

Fig. 7 SoLong UAV (Zhu, Guo and Hou 2014)

1.3.6. Airbus Zephyr 7

The Zephyr 7 (Fig. 8) with a 23 m wingspan, 55 kg weight, and 5 kg payload, has two propellers driven by electric motors and uses the energy from solar panels during the day and lithium-sulfur batteries at night (D'Oliveria, de Melo and Devezas 2016, Airbus 2018)

Fig. 8 Zephyr HALE UAV family (D'Oliveria, de Melo and Devezas 2016)

1.3.7. NASA Helios

The Helios Prototype (Fig. 9) was an enlarged version of the Centurion flying wing, which flew a series of test flights at NASA's Dryden Flight Research Center in late 1998. The aircraft has a wingspan of 75.3 m, 21.5 m greater than the Centurion 2, 1/2 times that of its solar-powered Pathfinder flying wing, and longer than the wingspans of either the Boeing 747 jetliner or Lockheed C-5 transport aircraft (Dunbar 2009, Pietreanu and Iordache 2018).

Fig. 9 NASA Helios (Dunbar 2009)

As a summary of the literature review for long endurance UAVs done above, a tabular summary (Tab 5) has been prepared, taking into account the individual parameters of the presented aircraft.

Tab 5 Presentation of the existing Long Endurance UAVs (K. Zenowicz 2023)

Name	X-HALE (Cesnik and Su 4 - 7 January 2011)	Helios Platform (HELIPLAT) (Romeo, Frulla and Cestino 2005)	Sky-sailor (Noth, Siegwart and Engel 2006)	SoLong (Zhu, Guo and Hou 2014)	Airbus Zephyr 7 (D'Oliveria, de Melo and Devezas 2016)	NASA Helios (Gibbs 2017)	Units
Wing span	8	73	3.2	4.75	22.5	75.3	[m]
Chord	0.2	2.41	0.25	3.16	1.9	2.4	[m]
Platform area	1.6	176	0.8	1.5	4.6	180.7	[m2]
Aspect Ratio	40	33	12.9	15	11.6	30.9	[-]
Max Gross Takeoff Weight	11.1	815	2.6	12.6	53	929	[kg]
Length of aircraft	1.01	7	1.8	2.2	No data	5	[m]
Number of motors	5	8	1	1	2	14	[-]
Speed range	10-19	14-38	7-11	12.2-22.5	No data	8.5-12.1	[m/s]
Endurance	45 minutes	26 days	27 hours	48 hours	14 days	14 hours	[-]
Power/Weight	25.5	10.2	~10	63.5	No data	22.6	[W/kg]
Altitude	No data	17 -20	5.5	8	21	29.5	[km]

The vast majority of the presented platforms use a multiple fuselage system. Each design uses a different tail unit. Based on the above, it can be assumed that there is a need to conduct research on the optimal arrangement of the tail unit due to the lack of one optimal solution for all platforms equipped with more than one fuselage.

1.4. UAV regulations

Poland is a member country of the European Union and therefore must comply with drone regulations introduced by the European Union Aviation Safety Agency (EASA) (European Union Aviation Safety Agency 2022). In addition to these regulations, Poland also has country-specific regulations. A drone may be operated in the "Open" category if:

- The drone has one of the Class 0, 1, 2, 3 or 4 identification tags.
- The drone was purchased before January 1, 2023, without a class designation as above.
- The aircraft has a maximum takeoff weight of less than 25 kg (55 lb).
- The remote control keeps the drone at a safe distance from people.
- A drone will not fly directly over people unless it has a class label or is lighter than 250 g (0.55 lb). (See the operation subcategories: A1, A2 and A3 to find out where is possible to fly a drone.)
- The remote pilot will maintain a visual line of sight (VLOS) or be assisted by an unmanned aircraft observer.
- The remote controller will not operate the drone above 120 m (400 ft).
- The drone will not carry any hazardous goods and will not drop any material

Open subcategories:

The open category is divided into three additional subcategories that introduce additional rules. Subcategory determination is based on the class identification label and the weight of the aircraft.

<u>A drone may be operated in the "Open" A1 category if:</u>

- The drone is marked with class identification label 0 or 1.
- If marked as C1, the drone operator must be registered with the EASA.
- A C0 labeled drones max takeoff weight does not exceed 250g (0.55 lbs).
- A C1 labeled drones max takeoff weight does not exceed 900g (1.98 lbs).
- Flight speed does not exceed 19 m/s (42 mph).
- The drone is not operated over crowds of people or in areas where drone operations are prohibited in a member state.

<u>A drone may be operated in the "Open" A2 category if:</u>

- The drone is marked with a Class 2 identification tag.
- The drone operator is registered with EASA and is at least 16 years old.
- The maximum take-off weight of C2-rated drones does not exceed 4 kg (8.81 lb).
- The drone is not used over crowds of people or in areas where drone operations are prohibited in a Member State.
- Flights are maintained at a horizontal distance of 30 m (98 ft) from uninvolved persons.

<u>A drone may be operated in the "Open" A3 category if:</u>

- The drone is marked with a Class 3 or 4 identification tag.
- The drone operator is registered with EASA and is at least 16 years old.
- The maximum takeoff weight of C3 or C4 drones does not exceed 4 kg (8.81 lb).
- Flights are conducted away from people and at a minimum distance of 150 m (492 ft) from urban areas.

Special category

The Special Category is reserved for drones that do not meet the requirements set out above under the Open Category due to an increased level of operational risk. A drone may be operated in a specific category if:

- The remote pilot operates according to a standard scenario issued by EASA or their National Aviation Authority (NAA).
- The operation is carried out under the Standard Scenario and a declaration must also be submitted to the NAA.
- The operation is not conducted under a standard scenario, the remote pilot must conduct a pre-defined risk assessment (PDRA) before the operation and obtain approval from the NAA.
- The operation is conducted by a remote pilot who holds a Light UAS Operator Certificate (LUC).

Certified category

The Certified category is used for drone operations that carry a high risk. This category covers large drones, which pose an inherent risk if something goes wrong. Drone operations should be classified in the certified category when the following conditions are met:

- The drone is certified by Art. 40 section 1 letter (a), (b) and (c) of Delegated Regulation (EU) 2019/945.

- The operation is performed under any of the conditions listed below:
  - Over large groups of people.
  - Includes the transportation of people.
  - Covers the transport of dangerous goods that may pose a high risk in the event of an accident.
- Operations should be classified as UAS operations in the certified category based on the risk assessment referred to in Article Remote Control Licensing.

1.5. Problems of aircraft design

The development of aircraft is a multifaceted task that requires expertise across various technologies. With ever-changing regulations, sophisticated software, and technological advancements, aircraft designers face numerous challenges (Mozaffari, et al. 2019). To achieve optimal aerodynamics, designers must consider the complexities of three-dimensional flight dynamics as aircraft navigate through airspace. The shape of wings, fuselage, and control surfaces are meticulously designed to minimize drag while maintaining key flight characteristics like stability and controllability. In the case of Unmanned Aerial Vehicles (UAVs), the weight of the aircraft is a critical factor that demands the use of modern composite materials with high strength, low weight, and resistance to atmospheric conditions. However, due to the anisotropic properties of these materials, numerical modeling becomes more intricate compared to lightweight metal alloys.

The development of engines with greater efficiency and lower emissions is essential in the context of environmentally friendly propulsion. This is particularly important for modern aircraft, including the subject of research in this doctoral thesis. These aircraft increasingly utilize electric motors and propulsion cells powered by energy from photovoltaic panels.

During the design process, it is crucial to consider power sources for critical avionics systems that impact the safety and reliability of aircraft. The constructions should meet rigorous safety standards, especially in emergencies. Additionally, the designed structures should consider various factors related to take-off, landing, and changing atmospheric conditions at different flight altitudes (Raymer 1992).

1.6. Purpose of the doctoral thesis

This doctoral dissertation aims to utilize advanced computational methods for conducting simulations of various tail configurations for a drone and understanding how they influence the stability of this aerial vehicle. The research focuses on advancing innovative approaches to designing drone configurations, taking into account both technological aspects and the impact of flight missions on the proposed structures. Within the scope of the work, key aerodynamic parameters have been identified for specific tail configurations, and their impact on the drone's stability has been analyzed.

The thesis encompasses a literature review on the design of aircraft, their configurations, and applications. Appropriate software and configuration were selected for further computations. Through conducting simulations, a comparison of results for different configurations in various flight phases was presented, and one configuration adapted to the conditions assumed for the application of the studied object and its flight mission was proposed.

It is anticipated that the doctoral thesis will contribute to the development of innovative solutions related to simulations for various drone configurations, enabling their better adaptation to diverse applications.

1.7. Thesis

The objective of this doctoral thesis is to develop innovative methods for the design and simulation of various drone configurations, aiming to enhance their universality and adaptability for diverse applications. The research will encompass comprehensive aspects of design, including aerodynamic parameters such as stability. The use of advanced computational tools is intended to facilitate the identification of different configuration solutions for specific mission scenarios, contributing to the improvement of operational efficiency in various fields, such as environmental monitoring. The anticipated results hold the potential for a significant contribution to the advancement of drone technology, supporting progress in the field of autonomous aircraft design.

THESIS: It is possible to select a configuration for the tail section of a given unmanned aerial vehicle (UAV) that is optimal in terms of meeting stability criteria. This selection considers typical flight profiles and the operational conditions determined by the intended application of the UAV. The optimization process may utilize results derived from both simulation-based and analytical approaches.

2. Subject of the research

The subject of the research of the above doctoral dissertation is an unmanned aircraft with extended flight endurance (HALE UAV). The structure was developed by SkyTech eLab and is one of the scaled models from the Twin Stratos UAV family (Polnor Leader 2019). The analyzed object is a conceptual aircraft. Twin Stratos was used in the project LEADER, partially supported by Norwegian Financing Mechanism, during which its durability and flight altitude parameters are to be used. In this work, a comparative analysis of various tail configurations for the Twin-Stratos drone was performed concerning its flight stability.

2.1. General Characteristics of the Twin Stratos UAV

UAV Twin Stratos is a project that includes various scales of the tested object. All of the objects have in common an unusual arrangement of hulls, type of power supply, selected type of drive and the arrangement of the tail part based on the "A" structure. As part of the development of the Twin Stratos concept, the following models of the tested object were developed.

- Twin Stratos 1:10 (TS110) – The aircraft is based on the general shape of the Twin Stratos design. Its task was to confirm the possibility of controlling the simplified control system used in the project.
- Twin Stratos 1:8 (TS18) – An aircraft simulating the propulsion system, and power supply and confirming the flight endurance parameters of the tested structure. Ultimately, the model on a given scale was replaced by a larger scale due to problems with using the number of photovoltaic panels to meet the flight parameters assumptions.
- Twin Stratos 1:7 (TS17) – A direct development of the TS18 design. The model uses a wing with changed geometry to increase the surface that can obtain electricity using photovoltaic panels.
- Twin Stratos 1:2 (TS12) – The Twin Stratos model is intended to confirm flight endurance parameters, and stratospheric flight altitudes and perform commercial missions. This is the first Twin Stratos platform to achieve HALE UAV (High Altitude Long Endurance - Unmanned Aerial Vehicle) parameters.
- Twin Stratos 1:1 (TS11) – Target Twin Stratos concept. The assumption is uninterrupted flight at stratospheric altitudes. A platform enabling research and commercial activities.

All presented Twin Stratos project aircraft are intended to confirm the ability to achieve key flight parameters for the Twin Stratos 1:1 platform. As part of the above doctoral dissertation, the TS17 aircraft will be analyzed (Fig. 10).

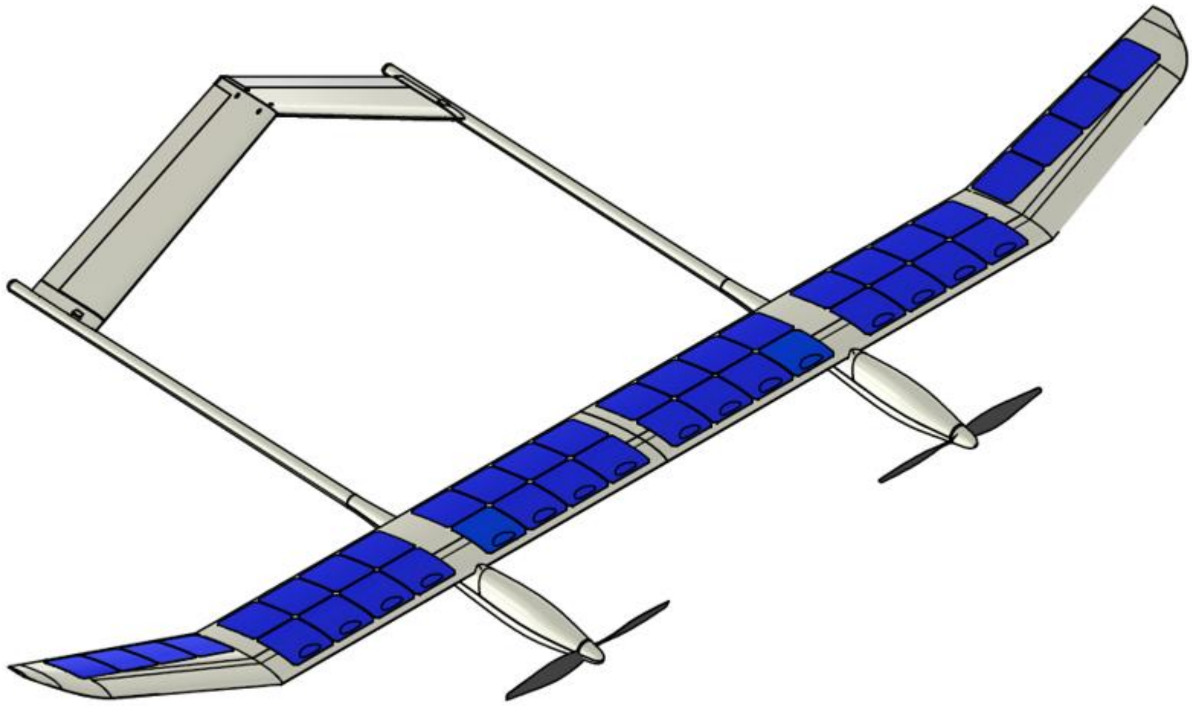

Fig. 10 Twin Stratos visualization 1:7

The aircraft was made by the initially adopted design (Fig. 11). The research aims to determine the possibility of using other solutions regarding the tail unit system.

Fig. 11 UAV TS17

The parameters of the analyzed object provided by SkyTech eLab are presented in the table (Tab 6). The parameters presented in the table were determined based on the calculation methodology developed by SkyTech eLab employees.

Tab 6 Parameters of TS17

Scale	1:7	Unit
Take off mass	9.8	[kg]
Aspect Ratio (AR)	14.46	[-]
Wing area	0.70	[m^2]
Maximum celling	5000	[m]
Assumed Maximum flight duration	24	[h]
Payload	2.5	[kg]
Middle chord	0.28	[m]
Wing Span [A]	3.6	[m]
Tail unit area	0.25	[m^2]
Length of aeroplane [C]	1.8	[m]
Height of tail unit [B]	0.29	[m]
Assumed motors power	300	[W]

The above parameters constitute the initial assumptions regarding the research carried out. All optimization changes presented in the subsequent chapters of the above work and the parameters obtained for the designed shapes were compared with the parameters presented in the table above. The graph presented in the graphic (Fig. 12) shows an example flight plan for the Twin Stratos 1:7 UAV. The assumed flight plan is associated with achieving a milestone in the form of a flight altitude of 5 km. This is a pre-defined flight plan.

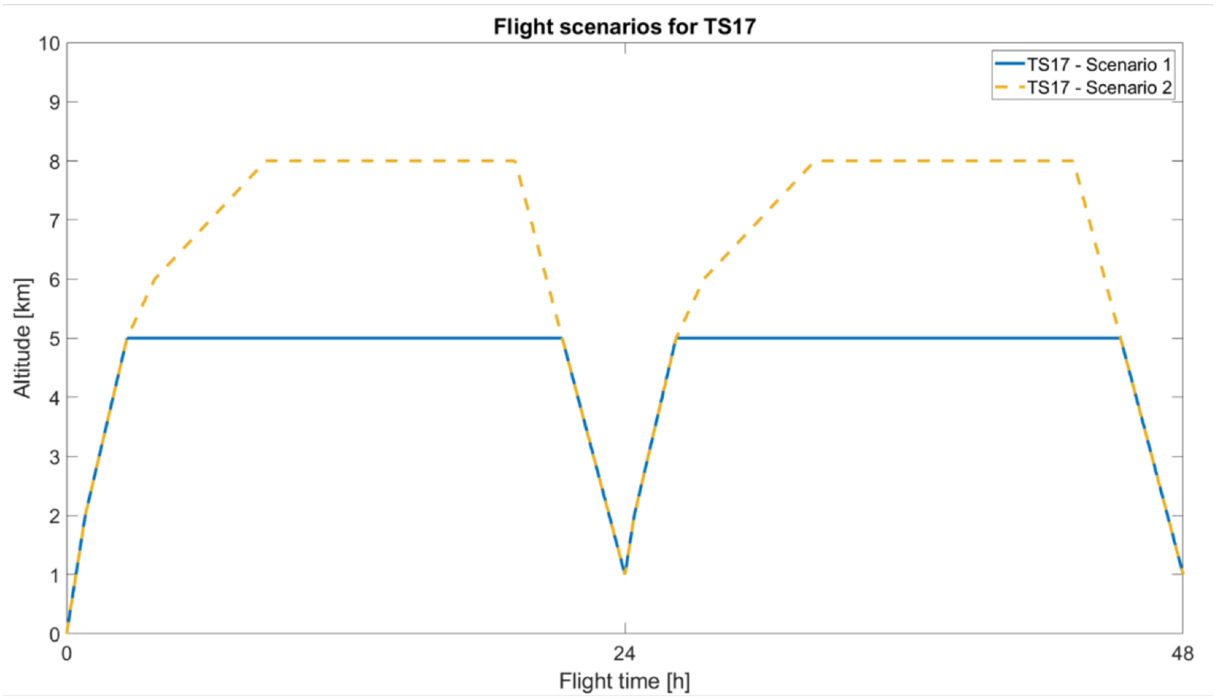

Fig. 12 Flight scenarios 1 for TS17 (Mateja, et al. 2023)

The presented scenario (Fig. 13) was developed to prove the possibility of long-lasting flight. Mathematical models based on it determine the correctness of the system used to obtain electricity using photovoltaic panels. The work presented by K. Mateja (Mateja, et al. 2023) confirms the possibility of achieving the assumed milestone related to flight endurance.

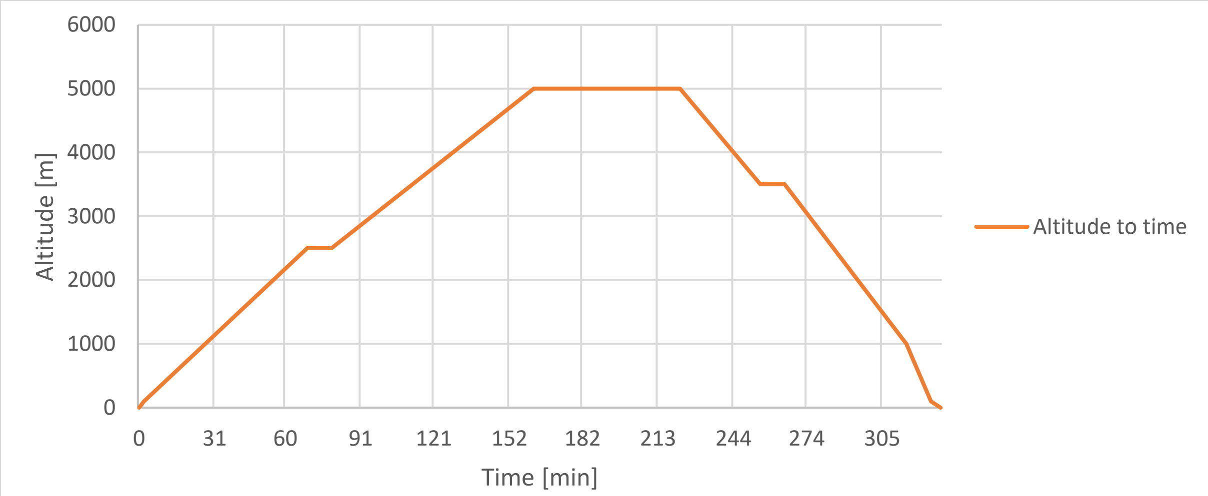

Fig. 13 Flight scenarios 2 for TS17

To meet the milestone related to achieving the planned flight altitude, a scenario presented in the visualization was developed (Fig. 14). The flight assumed during this scenario was aimed directly at achieving the milestone's planned flight altitude. For this purpose, the planned accuracy of the climb and flight stabilization stages during this manoeuvre was increased.

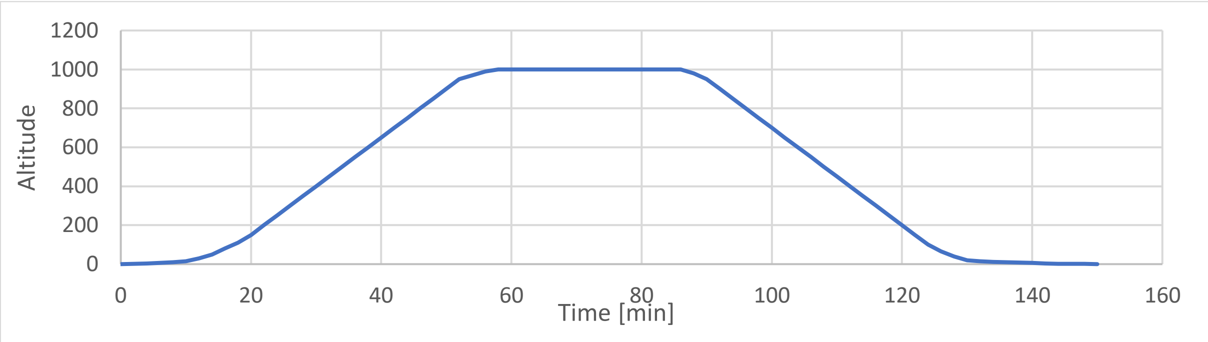

Fig. 14 Flight scenario assumed for analysis

To carry out the analyzes presented in the above doctoral thesis, a simplified flight plan was developed to determine uniform conditions for each of the tested configurations (Fig. 14). As part of the plan, the parameters of climb, descent and horizontal flight were adopted by those set for the research subject in the created version.

By safety guidelines, it is necessary to carry out analyzes for flight parameters determined based on the load envelope as flight critical points (Heintz, Rudol and Doherty 2007, Zheng, et al. 2021). Stability analysis aimed at determining the direct impact of the tail section on the flight stability of the tested object is based on parameters consistent with horizontal flight at the optimal speed and with the optimal angle of attack for each of the considered tail section concepts. When preparing the presented flight plan, no parameters related to the propulsion system of the tested object were taken into account, only the parameters declared by Sky Tech eLab.

2.2. Examples of applications of the considered UAV

High-altitude flight increases the efficiency of photovoltaic panels by minimizing the dispersion of solar radiation. Advanced mission planning algorithms and flight control systems enable the maximization of panel sunlight exposure while simultaneously reducing energy consumption through efficient utilization of air currents (Mateja, et al. 2023).

Aerodynamic optimization is essential, ensuring that the panels do not cause increased drag or interfere with the laminar flow around the main structural elements of the aircraft. Flight trajectory planning must also consider the Sun's changing position throughout the operational day.

Preliminary analyses of the planned Twin Stratos research platform allowed for the proposal of several applications in which it could be utilized. The capabilities pertaining to lifting capacity for additional equipment, a specific range of flight speed, the possibility of prolonged flight at a fixed altitude, and the ability to reach high ceilings suggest that this object could be used, among other things, in industries related to (F. Heintz 2007, Mozaffari, et al. 2019, Zheng, et al. 2021):

- Security and military,
- Telecommunications,
- Observation,
- Surveys of large areas,
- Cultivation supervision,
- Fire control,
- Meteorology,
- Air quality testing,
- Traffic intensity surveys.

The application concepts presented above may become the primary tasks of similar UAVs in the future. All of these activities can be classified into three fundamental aircraft capabilities: telecommunications, observation (Fig. 15), and measurement (K. Zenowicz 2023).

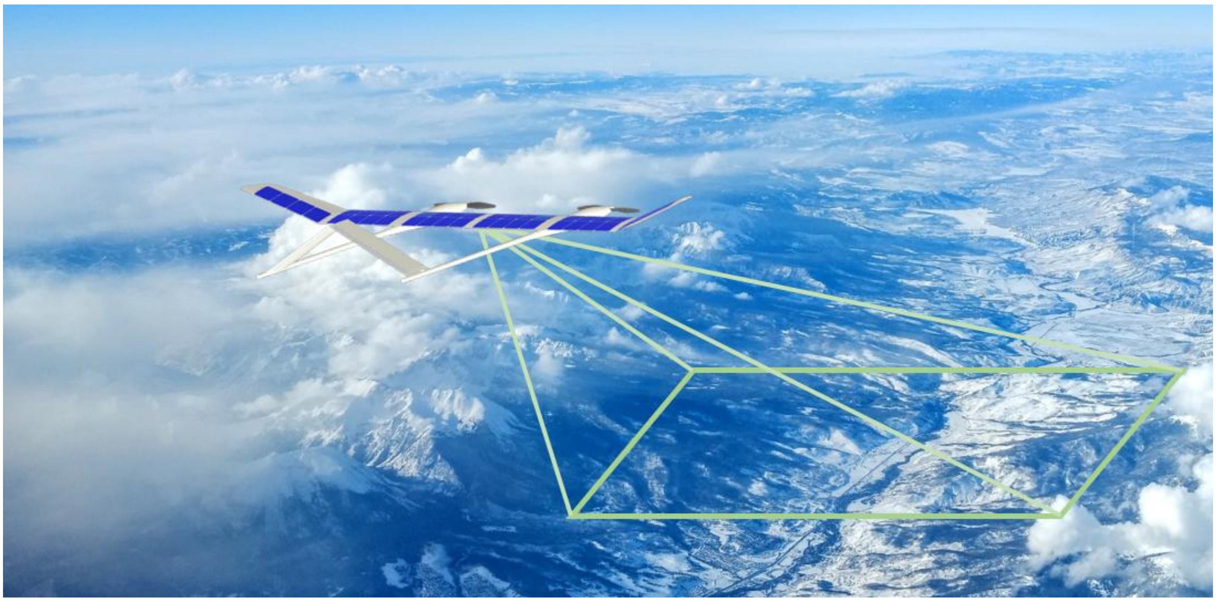

Fig. 15 Twin Stratos observation mode (K. Zenowicz 2023)

3. Review of the state of art

To maintain control and anticipate the performance and behavior of an aircraft during flight, it's crucial to evaluate its stability. This requires a detailed study of the forces and moments that affect the aircraft (Kemp. Jr. 2013). Within the framework of preparing a doctoral dissertation, it was necessary to conduct a literature review on the definition of aircraft stability, which was characterized as the ability to return to its initial state after a disturbance, such as a change in position in pitch, roll, or yaw (Fig. 16). Stability analyses and assessments are evaluated using advanced computational methods and flight testing.

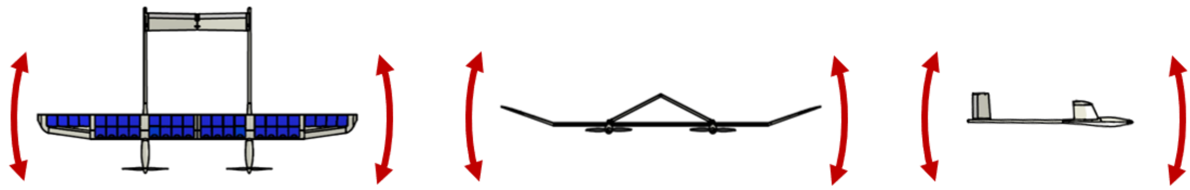

Fig. 16 Movement of the aircraft during the flight

Aircraft movements can be precisely described using a coordinate system assigned to the unmanned aerial vehicle (UAV). See figure (Fig. 17) and table (Tab 7) This system is composed of the following axes (Anderson, Introduction to Flight 2000, Lungu 2013, Tuzucu 2008):

- Long Axis (Y-axis): This represents the aircraft's longitudinal stability, related to pitching movements.

- Lateral Axis (X-axis): Corresponds to lateral stability, which involves rotation around the transverse axis, affecting rolling movements.

- Vertical Axis (Z-axis): Refers to directional stability, encompassing rotation around the vertical axis, which influences yawing movements.

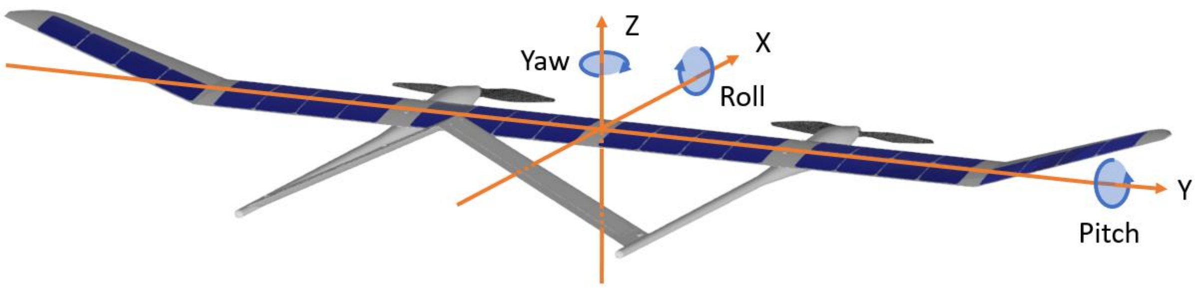

Fig. 17 Twin Stratos angular movements presentation

Tab 7 Summary of the conventions used for the moments and angular velocities (Embry-Riddle Aeronautical University 2024)

Axis	Moment	Moment Coefficient	Angular Displacement	Angular Velocity	Non-dimensional angular rate	Description
x	L	C_l	ϕ	p	$\bar{p}$	Roll
y	M	C_m	θ	q	$\bar{q}$	Pitch
z	N	C_n	β	r	$\bar{r}$	Yaw

During steady-state flight, aerodynamics principles highlight the correlation among the forces exerted on the aircraft. It is assumed that the sum of all vertical force components must be balanced and equal to zero (Z axis). This principle also applies to forces acting in both vertical directions considered (X, Y axis). This balance ensures flight stability, emphasizing the need for an equilibrium among lift, weight, thrust, and drag (Caughey 2011).

3.1. The influence of stability on UAV flight

To more accurately describe the behaviour of an aircraft in flight, stability can be divided into static and dynamic. Static stability concerns the tendency to return and maintain balance rather than motion, while dynamic stability mainly concerns the nature of an object's motion and its change over time. Visualization of static stability types are presented in Fig. 18 and Fig. 19.

Static stability types based on its return ability to steady state (Embry-Riddle Aeronautical University 2024, Struett 2012, Irving 2014, Boschetti, Cardenas and Amerio 2010):

- Positive static stability (statically stable):

An aircraft exhibits a tendency to revert to its initial orientation following disturbances. During a turn, when the control surfaces are set to their neutral position, there is no noticeable rolling motion or increase in the aircraft's roll angle.

- Neutral static stability (neutral stability):

It is the tendency of an aircraft to remain on a new flight path. If the UAV enters a turn and the controls are released, it will remain in the turn but will not roll or become steeper (Rodgers 1965).

- Negative static stability (statically unstable):

The behavior indicates a tendency to move away from the initial position. When an aircraft is pitched to a high angle, releasing the controls leads to further rolling, illustrating an increasing divergence from its original orientation.

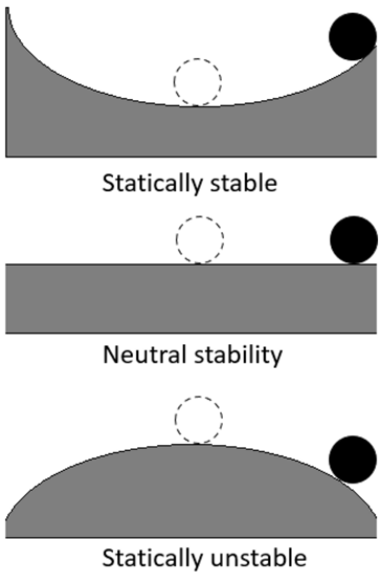

Fig. 18 various conditions of static stability (Nelson 1998)

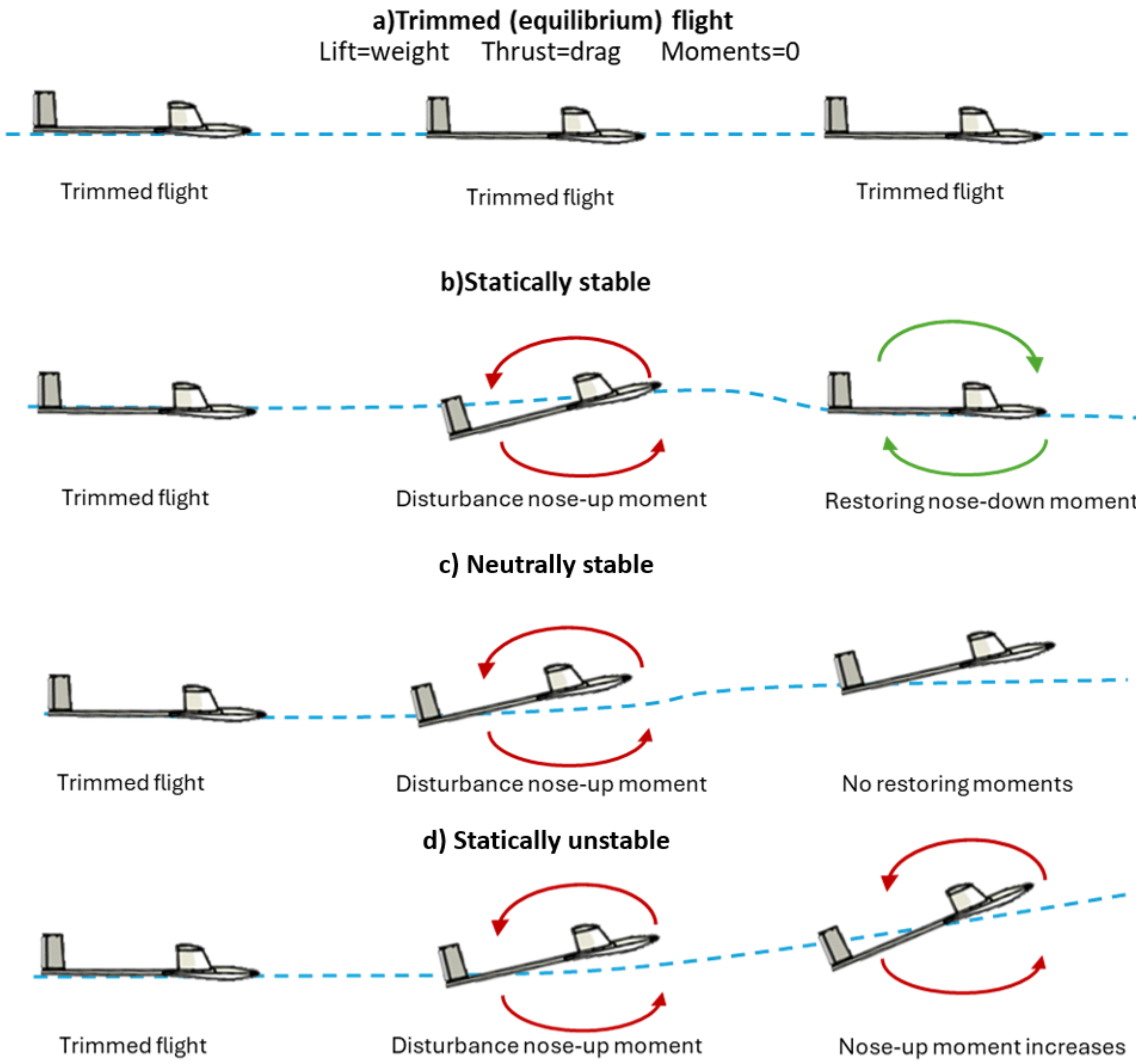

Fig. 19 Examples of static stability principles witch respect to pitch attitude (Embry-Riddle Aeronautical University 2024)

Types of dynamic stability due to its ability to return to a steady state (Embry-Riddle Aeronautical University 2024, Babister 2013). See Fig. 20:

- Positive dynamic stability(dynamically stable):

Following dynamic disturbances like turbulence or speed fluctuations, the aircraft demonstrates a tendency to revert to its original position or state of equilibrium. The UAV autonomously corrects deviations from its intended flight path, indicating a self-regulating tendency for maintaining stability.

- Neutral dynamic stability (neutral dynamically stable):

Following dynamic disturbances, the aircraft shows no inherent inclination to either return to or deviate from its equilibrium state.

- Negative dynamic stability (dynamically unstable):

When dynamic disturbances occur, the aircraft presents a tendency to deviate from its original position and equilibrium.

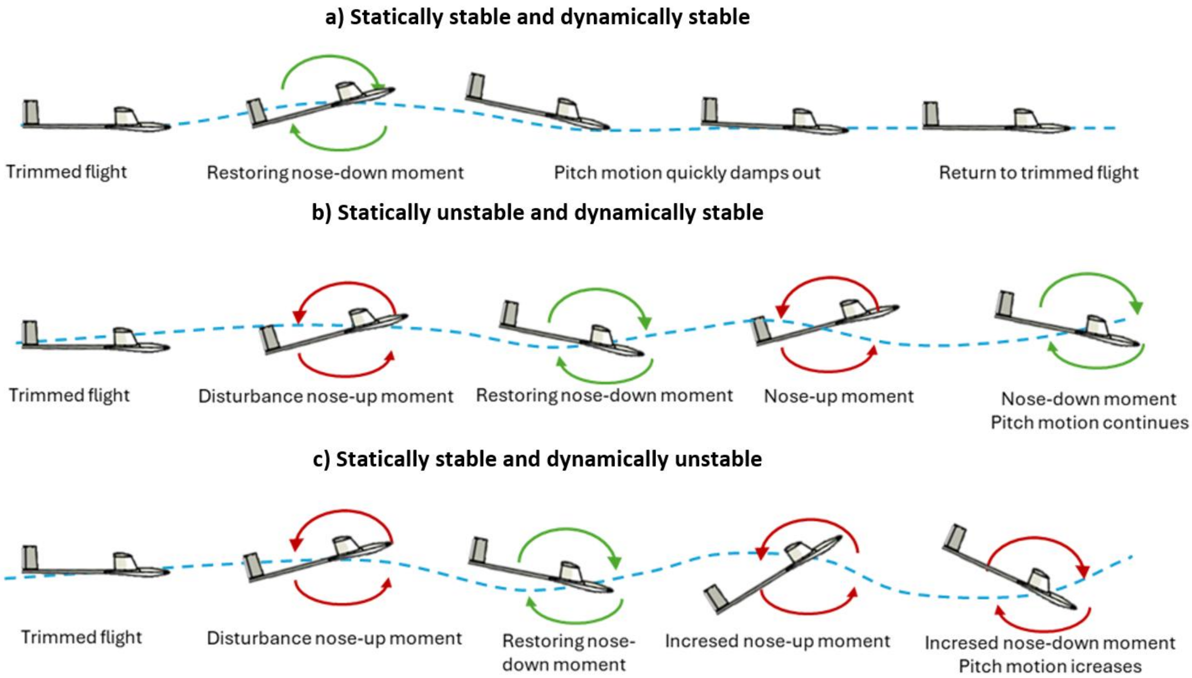

Fig. 20 Examples of differences in static and dynamic stability (Embry-Riddle Aeronautical University 2024)

3.2. Types of stability

Considering the designated axes and the coordinate system utilized by a specific Unmanned Aerial Vehicle (UAV), the following stability types can be defined:

- <u>Longitudinal Stability (Rotation around the Longitudinal Axis):</u>

Longitudinal stability in aviation pertains to an aircraft's sustainability for consistent pitch angle during flight. See Fig. 21. This stability is governed mainly by parameters as, aerodynamic derivatives, the aircraft's center-of-gravity position, flight altitude and speed (Ding 2023).

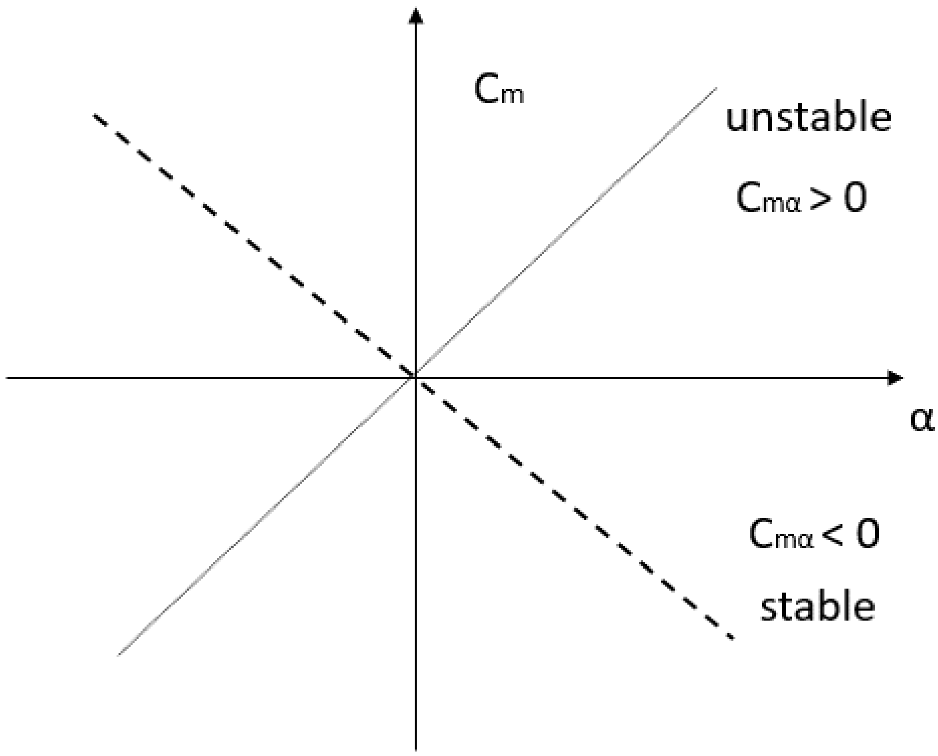

Fig. 21 Example of pitching moment coefficient vs angle of attack (Nelson 1998)

Assessment of this type of stability can be made using various methods, including:

- Estimating the Neutral Point (NP) and Stability Margin:

The Neutral Point indicates the location where the torque remains constant regardless of the angle of attack modification. The term "neutrally stable" in the context of the aircraft's longitudinal axis refers to the situation when its centre of gravity (CG) is located in front of the mentioned neutral point (Cusati, et al. 2022). The aerodynamic concept of this parameter in aircraft design is crucial for ensuring stability and control. The neutral point is defined as the location where the pitching moment remains constant regardless of changes in the angle of attack. Understanding and accurately determining the neutral point are fundamental aspects of designing aircraft with optimal stability characteristics (Wang, et al. 2021).

The stability margin in an aircraft is a metric associated with stability, defined as the spatial discrepancy between the center of gravity (CG) and the neutral point (NP), quantified in units of length (Fig. 22). This margin value facilitates the determination of the permissible forward shift of the CG relative to the NP while preserving stability (Embry-Riddle Aeronautical University 2024, Caughey 2011, Anderson, Aircraft Performance & Design 2012).

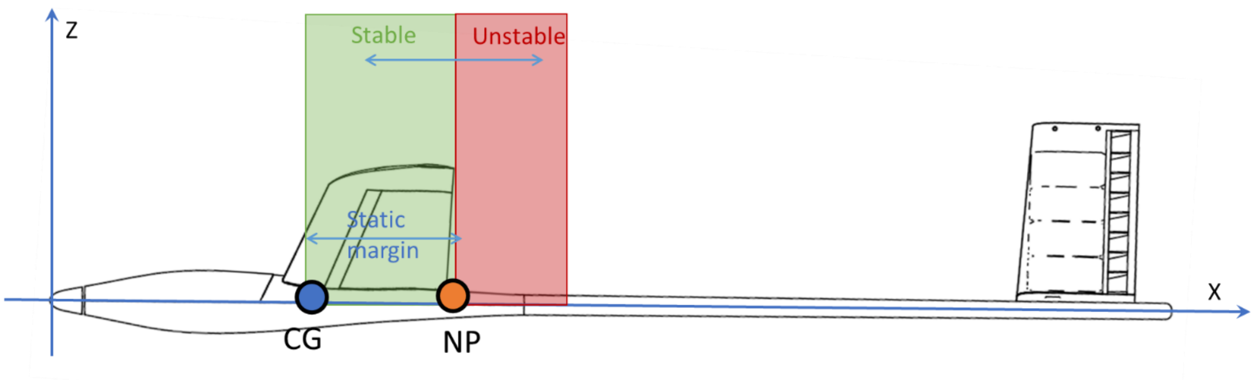

Fig. 22 Visualisation of static margin

$$SM = \big((NP - CG)/MAC\big)x100\% \quad (1)$$

Where

SM – Stability margin [%]

NP – neutral point [m]

CG – center of gravity [m]

MAC – mean aerodynamic chord of wing [m]

The stability margin is positive when the center of gravity is positioned ahead of the neutral point, thereby promoting stability. In turn, a negative stability margin indicates that the centre of gravity is behind the neutral point, which may lead to a loss of stability, especially during maneuvers as changes in the angle of attack.

- Determining Pitching Moment:

The longitudinal Pitching Moment (*Cm*) versus the angle of attack (α) can be graphed to visualize the stability characteristics. Negative slope of the *Cm* curve vs. α indicates stability (Anderson, Aircraft Performance & Design 2012, Slingerland 2003).

Pitching moment formula (Nelson 1998):

$$M = I_y\dot{q} + rp(I_x - I_z) + I_{xz}(p^2 - r^2) \quad (2)$$

- *M* - moment of force around the Y-axis (Pitch),
- I_x, I_y, I_z - moments of inertia around the X, Y, Z axes,
- I_{xy}, I_{xz}, I_{yz} - products of inertia,
- $\dot{p}, \dot{q}, \dot{r}$- derivatives of angular velocities,
- *p, q, r* - angular velocities around the X, Y, Z axes.

Flight tests to determine longitudinal static stability may involve checking several aspects (Adamczuk and Burek 2019, Edwards Air Force Base 1974, Nowakowski 2019, Nicolosi, Ciliberti, et al. 2020), like:

- Speed Stability,
- Flight Path Stability,
- Determining the location of neutral points (centers of neutral balance), the neutral point is defined as the location of the center of gravity at which the aircraft exhibits neutral static stability. Its location is constant for a given aerodynamic configuration of the aircraft,
- FRSR – Free Return Speed Range.

The position of the aerodynamic neutral point and the centre of gravity, and therefore the margin of longitudinal stability, can be determined in the CFD environment or by analytical methods.

- Lateral Stability (Rotation around the Transverse Axis)

Lateral stability pertains to the aircraft's capacity to revert to its initial alignment following a lateral roll. The evaluation of lateral stability can be conducted through the following equation (Nelson 1998):

  - Rolling Moment:

Rolling moment formula (Nelson 1998):

$$L = I_x\dot{p} - I_{xz}\dot{r} + qr(I_z - I_y) - I_{xz}pq \tag{3}$$

- *L* - moment of force around the X-axis (Roll),
- I_x, I_y, I_z - moments of inertia around the X, Y, Z axes,
- I_{xz}, - products of inertia measure of the uniformity of the distribution of mass about the x axis,
- $\dot{p}, \dot{q}, \dot{r}$- derivatives of angular velocities,
- p, q, r- angular velocities around the X, Y, Z axes.

To evaluate lateral stability, it may be essential to determine the rolling coefficient (*Cl*) as a function of the sideslip angle (β) to comprehend the aircraft's response to rotational dynamics. A positive value of *Cl* signifies stability (Nelson 1998). See Fig. 23.

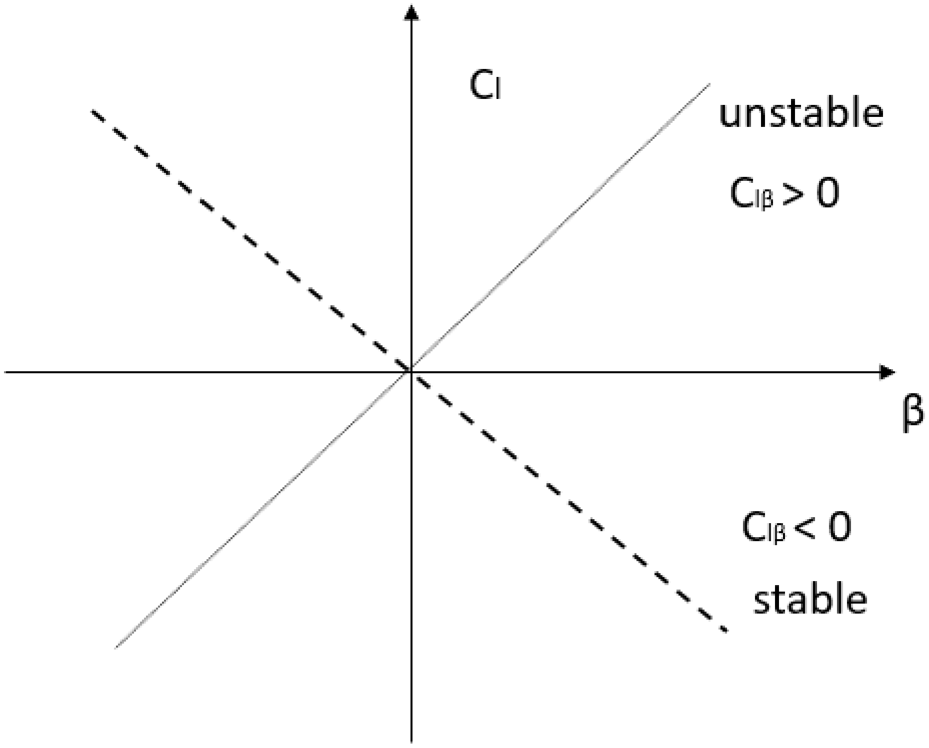

Fig. 23 Example of static roll stability (Nelson 1998)

- Dihedral Angle:

The dihedral angle is the angle between the wing and fuselage. A positive dihedral angle contributes to lateral stability by generating a restoring force when the aircraft tilts (Nelson 1998).

- <u>Directional Stability (Rotation around the Vertical Axis):</u>

Directional stability refers to the ability of an aircraft to maintain its course after a disturbance in the horizontal axis. See Fig. 24. To assess directional stability, the following methods can be used (Nelson 1998, Vecchia, Nicolosi and Ciliberti 2015):

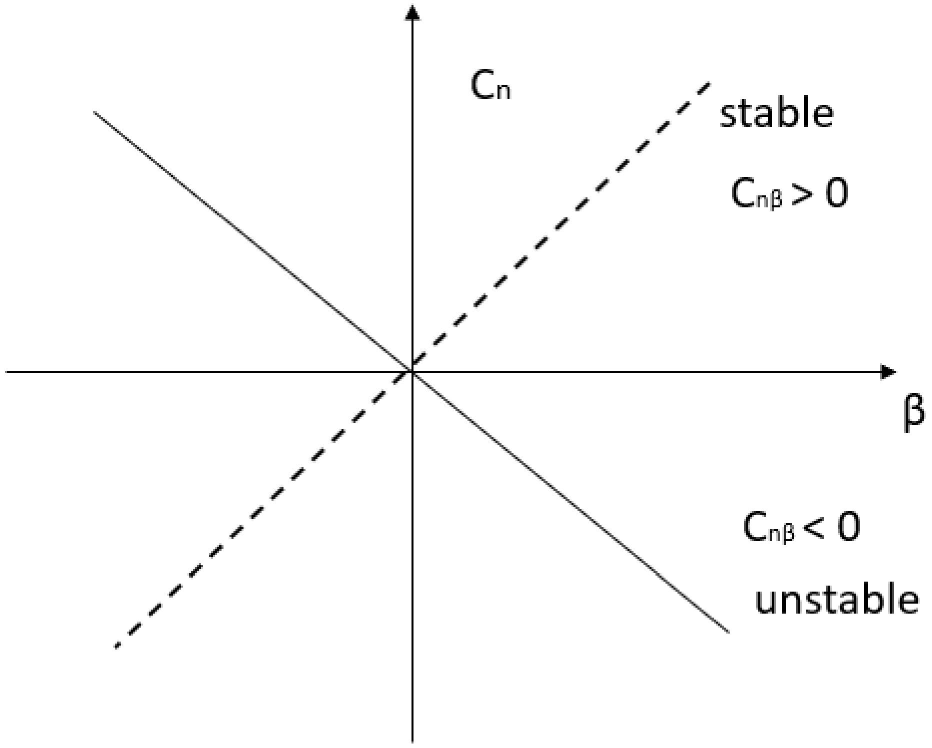

Fig. 24 Static directional stability (Nelson 1998)

- Yaw moment Calculation:

Yawing moment formula (Nelson 1998):

$$N = -I_{xz}\dot{p} + I_z\dot{r} + pq(I_y - I_x) + I_{xz}qr \tag{4}$$

- N - moment of force around the Z-axis (Yaw),
- I_x, I_y, I_z - moments of inertia around the X, Y, Z axes,
- I_{xy}, I_{xz}, I_{yz} - products of inertia,
- $\dot{p}, \dot{q}, \dot{r}$ - derivatives of angular velocities,
- p, q, r - angular velocities around the X, Y, Z axes.

To investigate the aircraft's reaction to directional motion, it is advisable to compute the yaw moment coefficient (*Cn*) relative to the slip angle (β). Stability is indicated by a positive Cn coefficient (Ciliberti, Nicolosi and Della Vecchia 2013).

- Area and Height of Vertical Tail Unit:

Appropriate dimensions of the vertical stabilizer are crucial for directional stability. Increasing the surface and height of the vertical stabilizer increases stability.

3.3.Classes of Tail Configurations for the Application

For the dual-tail aircraft as the research object, there are limitations regarding the possibilities for the use of the tail units. The doctoral thesis examined the most commonly used configurations, including the V and iverted V (A) shapes, conventional, boom-tail and high boom-taile. The thesis explores the influence of these configurations on the stability of the aircraft across different flight stages and includes parametric analyses of various tail configurations (Raymer 1992).

V shape and inverted V shape (A shape) tail configurations

The V-type and A-type tails positively affects the maneuverability and stability of the aircraft, especially at high angles of attack, which is beneficial in situations such as takeoff, landing or maneuvering in difficult conditions. An example of such configurations is shown in the Fig. 25. Whereas, this configurations may introduce some difficulties in maintaining stability in the turning (yaw) phase during flight, especially in aerodynamically complex conditions (Raymer 1992).

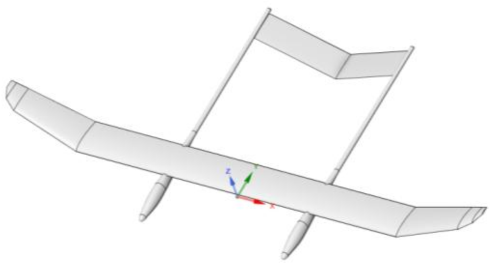

V shape configuration

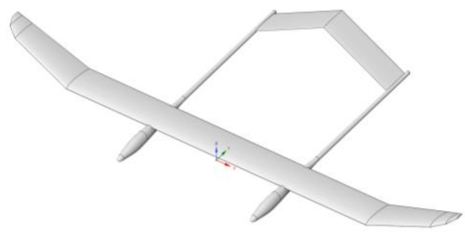

A shape configuration

Fig. 25 Example of V and A tail unit configuration

The design of V-tail or A-tail aircraft itself is more complex than the classic tail designs and generates more aerodynamic drag in the usual phases of flight, while aerodynamic drag decreases at high angles of attack (Raymer 1992).

Conventional tail

The conventional type tail is the most common tail configuration used in aviation, and is suitable for both small drones and large jets. An example of such a configuration is shown in the Fig. 26. This configuration is characterized by a simple design, generates low aerodynamic drag and provides good stability in the yaw phase. Compared to more advanced configurations, such as the V-tail, the conventional tail can be less maneuverable at high angles of attack and then generate more aerodynamic drag. This tail also has more weight compared to more modern configurations. It has good overall stability at medium airspeeds, which is advantageous for many aviation applications (Raymer 1992).

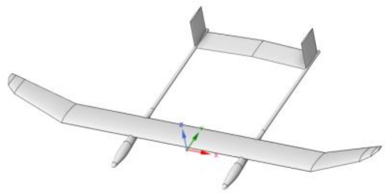

Fig. 26 Conventional tail unit

Boom Tail and High Boom Tail

A boom tail, also called a "T-tail" or "H-tail," is a design in which the horizontal stabilizers are placed on top of the vertical stabilizer. The examples considered are shown in the Fig. 27. Horizontal stabilizers on top of the vertical stabilizer allows to reduce the interaction of the control surfaces, which makes the UAV more contol, avoids air curl generated by the aircraft's engine, and minimizes the effect of the wings on the horizontal stabilizers, which has a costly effect on the stability of the aircraft. The design is heavier than that of a conventional tail system, and the tail is less maneuverable, but shows better maneuverability especially in the yaw phase (Raymer 1992).

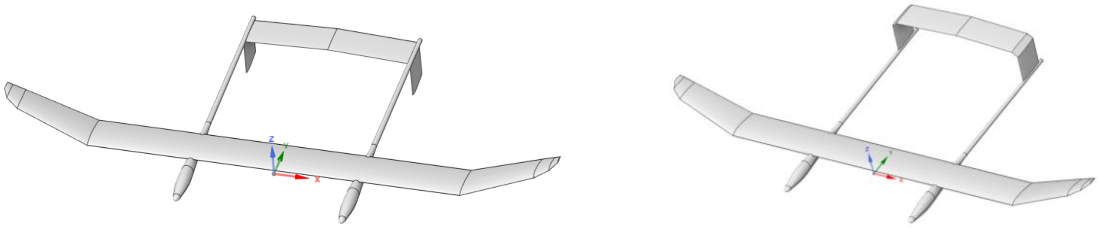

Boom tail unit High boom tail unit

Fig. 27 Boom tail & High boom tail

3.4.Stability testing methods and theorems

In an era of technological advances, aerospace engineers have access to tools that enable them to solve optimization problems in aircraft (UAVs) designs more quickly. These developments are facilitating experiments with a variety of configurations and design solutions, resulting in increased efficiency and speed in the design process, as well as the ability to create more complex and advanced designs. Numerical simulations are main tool, enabling modeling of aircraft behavior considering various operational conditions. As a result, it is possible to predict the response of structures to changing factors, which allows better adaptation of designs to specific requirements and flight conditions.

There are many methods that allow designers to resolve flying vehicles for special requrement. The primary method has been to create a physical, scaled model and use it for wind tunnel testing. This method was an important tool in the early stages of design (Raymer 1992, Anderson, Introduction to Flight 2000).

In addition, computational methods were used, such as Aeroprediction 2009 (AP09), which, using an accumulated database of tunnel test results, is used to predict the aerodynamic characteristics of tested objects (Moore and Moore 2008). A currently used advanced technique is the use of computer programs based on the Navier-Stokes equations, within the framework of computational fluid dynamics (CFD) methods. An example of software using this methodology is ANSYS-CFX, which allows detailed analysis of fluid flows and their interaction with objects (Muhammad Ahmad, et al. 2021). The Navier-Stokes equations are shown below (Glenn Reseaech Center 2021):

Where:

Coordinates - (*x,y,z*)
Time - *t*
Pressure - *p*
Density - ρ
Stress: τ
Velocity Components - (*u,v,w*)
Total Energy - *Et*
Heat Flux - *q*
Reynolds Number - *Re*
Prandtl Number - *Pr*

Continuity (Glenn Reseaech Center 2021):

$$\frac{\partial \rho}{\partial t}+\frac{\partial(\rho_u)}{\partial x}+\frac{\partial(\rho_v)}{\partial y}+\frac{\partial(\rho_w)}{\partial z}=0 \tag{5}$$

X-Momentum (Glenn Reseaech Center 2021):

$$\frac{\partial(\rho_u)}{\partial t}+\frac{\partial(\rho_u{}^2)}{\partial x}+\frac{\partial(\rho_{uv})}{\partial y}+\frac{\partial(\rho_{uw})}{\partial z}=-\frac{\partial p}{\partial x}+\frac{1}{Re_r}\left[\frac{\partial \tau_{xx}}{\partial x}+\frac{\partial \tau_{xy}}{\partial y}+\frac{\partial \tau_{xz}}{\partial z}\right] \tag{6}$$

Y-Momentum (Glenn Reseaech Center 2021):

$$\frac{\partial(\rho_v)}{\partial t}+\frac{\partial(\rho_{uv})}{\partial x}+\frac{\partial(\rho_v{}^2)}{\partial y}+\frac{\partial(\rho_{vw})}{\partial z}=-\frac{\partial p}{\partial y}+\frac{1}{Re_r}\left[\frac{\partial \tau_{xy}}{\partial x}+\frac{\partial \tau_{yy}}{\partial y}+\frac{\partial \tau_{yz}}{\partial z}\right] \tag{7}$$

Z-Momentum (Glenn Reseaech Center 2021):

$$\frac{\partial(\rho_w)}{\partial t}+\frac{\partial(\rho_{uw})}{\partial x}+\frac{\partial(\rho_{vw})}{\partial y}+\frac{\partial(\rho_w{}^2)}{\partial z}=-\frac{\partial p}{\partial z}+\frac{1}{Re_r}\left[\frac{\partial \tau_{xz}}{\partial x}+\frac{\partial \tau_{yz}}{\partial y}+\frac{\partial \tau_{zz}}{\partial z}\right] \tag{8}$$

Energy (Glenn Reseaech Center 2021):

$$\frac{\partial(E_r)}{\partial t}+\frac{\partial(uE_r)}{\partial x}+\frac{\partial(vE_r)}{\partial y}+\frac{\partial(wE_r)}{\partial z}=-\frac{\partial(up)}{\partial x}-\frac{\partial(vp)}{\partial y}-\frac{\partial(wp)}{\partial z}-\frac{1}{Re_r Pr_r}\left(\frac{\partial q_x}{\partial x}+\frac{\partial q_y}{\partial y}+\frac{\partial q_z}{\partial z}\right)+ \\ \frac{1}{Re_r}\left[\frac{\partial}{\partial x}\left(u\tau_{xx}+v\tau_{xy}+w\tau_{xz}\right)+\frac{\partial}{\partial y}\left(u\tau_{yx}+v\tau_{yy}+w\tau_{yz}\right)+\frac{\partial}{\partial z}\left(u\tau_{zx}+v\tau_{zy}+w\tau_{zz}\right)\right] \tag{9}$$

R_{er} is the Reynolds number reduced to some reference or characteristic scale that determines the relative importance of inertial forces versus viscous forces in fluid flow. It is used in equations to emphasize the effect of viscosity on the distribution of velocities and stresses within the fluid. Navier-Stokes equations allow aerospace engineers to model airflows around aircraft more effectively (Paskonov 2020). The use of these equations significantly affects aerodynamic analysis, allowing a detailed study of air-vehicle interaction, which translates into the optimization of aircraft design in the direction of increasing lift and reducing aerodynamic drag (ANSYS, Inc. 2013). Based on advanced analysis, it is possible to design aircraft with precisely defined objectives and achieve optimal flight parameters adequate to the intended missions (Sieradzki, Dziubiński and Galiński 2016). A very important aspect is also to design an aircraft that will be stable, and controllable during flight.

3.4.1. Analytical methods

A variety of analytical methods are used in aircraft stability studies:

- Linear stability analysis: This method focuses on linear modeling of the equations of motion around a fixed equilibrium configuration of an aircraft. It makes it possible to determine whether this configuration is stable or unstable, which is fundamental in the initial stages of design (Anderson, Introduction to Flight 2000).
- Stability derivative method - This analyzes the effect of aerodynamic changes, such as angular velocities or displacements, on the behavior of the aircraft (Donegan 1954). These derivatives are necessary to understand how the aircraft will respond to dynamic changes during flight (Nelson 1998).
- Modal analysis - This technique enable the identification of natural vibration frequencies and the corresponding vibration forms (mods) of an aircrafts structure. Controlling and understanding these mods is critical to ensuring both aerodynamic and structural stability (Kerschen, Peeters and Golinval 2013).
- Perturbation theory - Used to study the response of a system to small perturbations from its equilibrium position. With this method, it is possible to predict how small changes in external conditions or control parameters will affect the aircraft behavior (Ananthkrishnan 2004).

The analysis of the described object was carried out using the analytical method of linear stability analysis. These studies are divided into two types of analysis, static and dynamic (Stafiej 2000). Both types concidere the geometric relationships of the research object.

Longitudinal static stability

The state of longitudinal equilibrium is defined by the sum of moments with respect to the transverse axis of the analyzed object equal to zero (Stafiej 2000), i.e.:

$$M = M_{bu} + P_H \cdot L_H = 0 \tag{10}$$

Where:

M-pitching moment,
M_{bu}-pitching moment without control surfaces,
P_H-Lift force generated by control surfaces,
L_H-Control surface arm length

By dividing by $S \cdot q \cdot l$ the coefficient form of the equilibrium equation is obtained (Stafiej 2000):

$$C_m = Cm_{bu} + \frac{C_{Z_H} \cdot S_H \cdot q_H \cdot L_H}{q \cdot S \cdot l_0} \tag{11}$$

Where:

C_m – Pitching moment coefficient,
Cm_{bu} – Pitching moment coefficient without control surfaces,
C_{Z_H} – Lift force coefficient of control surfaces change,
S_H – Control surfaces area,
q_H – Dynamic pressure generated by flight speed acting on control surfaces,
q – Dynamic pressure generated by flight speed acting on analysed aircraft,
S – Main wing area,
L_0 – Mean aerodynamic chord.

Considering the designation $\chi_H = \frac{S_H \cdot L_H}{S \cdot L}$ and keeping in mind that for the analyzed object qH=q, relationship takes the form (Stafiej 2000):

$$C_m = Cm_{bu} + C_{Z_H} \cdot \chi_H = Cm_{bu} + \frac{dC_{Z_H}}{d\alpha_H} \cdot \chi_H \tag{12}$$

Where:

$\frac{dC_{Z_H}}{d\alpha_H}$ – slope of the lifting characteristic for infinite extension.
χ_H – Horizontal tail volume coefficient

The wing of the analyzed object undergoes a torsional deformation "ϕ" during flight, which, displacing the angular chords of the wing, affects the change in the angle of attack on the wing:

$\alpha_W = \alpha + \varphi$

Since torsional deformation cannot be ignored in flight, especially at high speed, it was included in the stability analysis.

The angle of attack at the height lip concideres the susceptibility of the wing is (Stafiej 2000):

$$\alpha_H = \alpha + \varphi - \varepsilon + \delta_H + \Delta\alpha_H \tag{13}$$

Where:

α_H – Control surfaces angle of attack,
δ_H – tail incidence angle,
$\Delta\alpha_H$ – Control surfaces angle of attack change,
δ – tilt angle,
ε – jet deflection angle
φ – Torsional deformation of the airfoil,

After taking this relationship into account, the equation takes the following form (Stafiej 2000):

$$Cm = Cm_{bu} + \frac{dC_z}{d\alpha_H} \cdot \chi_H (\alpha + \varphi - \epsilon + \delta_H + \Delta\alpha_H) \tag{14}$$

Given the equation of rudder deflection by a certain angle ($\Delta\alpha_H = \frac{d\alpha_H}{d\beta_H} \cdot k_\beta \cdot \beta_H$), the equation is as follows (Stafiej 2000):

$$Cm = Cm_{bu} + \frac{dC_{z_H}}{d\alpha_H} \cdot \chi_H \left(\alpha + \varphi - \epsilon + \frac{d\alpha_H}{d\beta_H} \cdot k_\beta \cdot \beta_H \right) \tag{15}$$

Where:

β_H – Control surfaces elevation angle,
k_β – Elevation correction factor (usually determined from the graph),
$d\beta_H$ – Control surfaces elevation angle change,

The reserve of longitudinal static stability was called (Stafiej 2000):

$$ZS = \frac{dCm}{dCz} = \frac{dCm_{bu}}{dCz} + \frac{dCz_H}{d\alpha_H} \cdot \chi_H \cdot \frac{d}{dCz} \cdot \left(\alpha + \varphi - \epsilon + \delta_H + \frac{d\alpha_H}{d\beta_H} \cdot k_\beta \cdot \beta_H \right) \tag{16}$$

Since the wedging angle of the height lip is constant (δ_H=const), so its derivative: $\frac{d\delta_H}{dCz} = 0$, so (Stafiej 2000):

$$ZS = \frac{dCm_{bu}}{dCz} + \frac{dCz_H}{d\alpha_H} \cdot \chi_H \cdot \left(\frac{d\alpha}{dCz} + \frac{d\varphi}{dCz} - \frac{d\epsilon}{dCz} + \frac{d\alpha_H}{d\beta_H} \cdot k_\beta \cdot \beta_H \right) \tag{17}$$

Assuming that the stub moment is treated as positive, the system is statically stable when ZS<0.

Longitudinal dynamic stability

An object is dynamically stable when it is capable of damping out over time the oscillations caused by taking it out of equilibrium. The issue reduces forces to solving the "characteristic equation" of a system of equations of motion (Stafiej 2000):

$$A \cdot r^4 + B \cdot r^3 + C \cdot r^2 + D \cdot r + E = 0 \tag{18}$$

Where: "r" is the root of the characteristic equation, and the quantities: *A, B, C, D* and *E* are functions of aerodynamic and structural parameters of the analyzed object or constants and so (Stafiej 2000):

$$A = 1 \tag{19}$$

$$B = Cx + \frac{dCz}{d\alpha} \cdot \overline{m_q} \tag{20}$$

$$C = \frac{dCz}{d\alpha} \cdot \overline{m_q} + \mu \cdot \overline{m_w} \tag{21}$$

$$D = \left(\overline{m_q} \cdot \frac{dCz}{d\alpha} + 1{,}5 \cdot \mu \cdot \overline{m_w}\right) \cdot Cx + \overline{m_q} \cdot \left(0{,}5 - K \cdot \frac{dCz}{d\alpha}\right) \cdot Cz^2 \tag{22}$$

$$E = \mu \cdot \overline{m_w} \cdot \frac{Cz^2}{2} \tag{23}$$

The quantities appearing in the above equations are determined by the relationship (Stafiej 2000):

$$\overline{m_q} = \frac{l_0}{i_y \cdot L_H} \cdot \chi_H \cdot \frac{dCz_H}{d\alpha_H} \tag{24}$$

$$i_y = \frac{l_y \cdot g}{Q \cdot L_H} \tag{25}$$

$$Q = m \cdot g \tag{26}$$

$$\mu = \frac{m \cdot g}{g \cdot \rho \cdot S \cdot l_0} = \frac{m}{\rho \cdot S \cdot l_0} \tag{27}$$

$$\overline{m}_w = \frac{l_0}{i_y \cdot L_H} \cdot \left[\chi_H \cdot \frac{dCz_H}{d\alpha_H} \cdot \left(1 - \frac{d\varepsilon}{d\alpha}\right) - t\frac{dCz}{d\alpha}\right] \tag{28}$$

$$t = \frac{t_{SC}}{l_0} \tag{29}$$

$$K = \frac{1 + \delta_C}{\Pi \cdot \lambda} \tag{30}$$

Where:
C_x – Drag coefficient,
Q – Analysed aircraft weight,
ρ – Air density,
g – Gravity acceleration,
λ – Aspect ratio,
δ_C – correction factor that include the wing outline and is dependent on the shape of the main lifting flap,
t_{SC} is determined as shown in the graphic of Fig. 28.

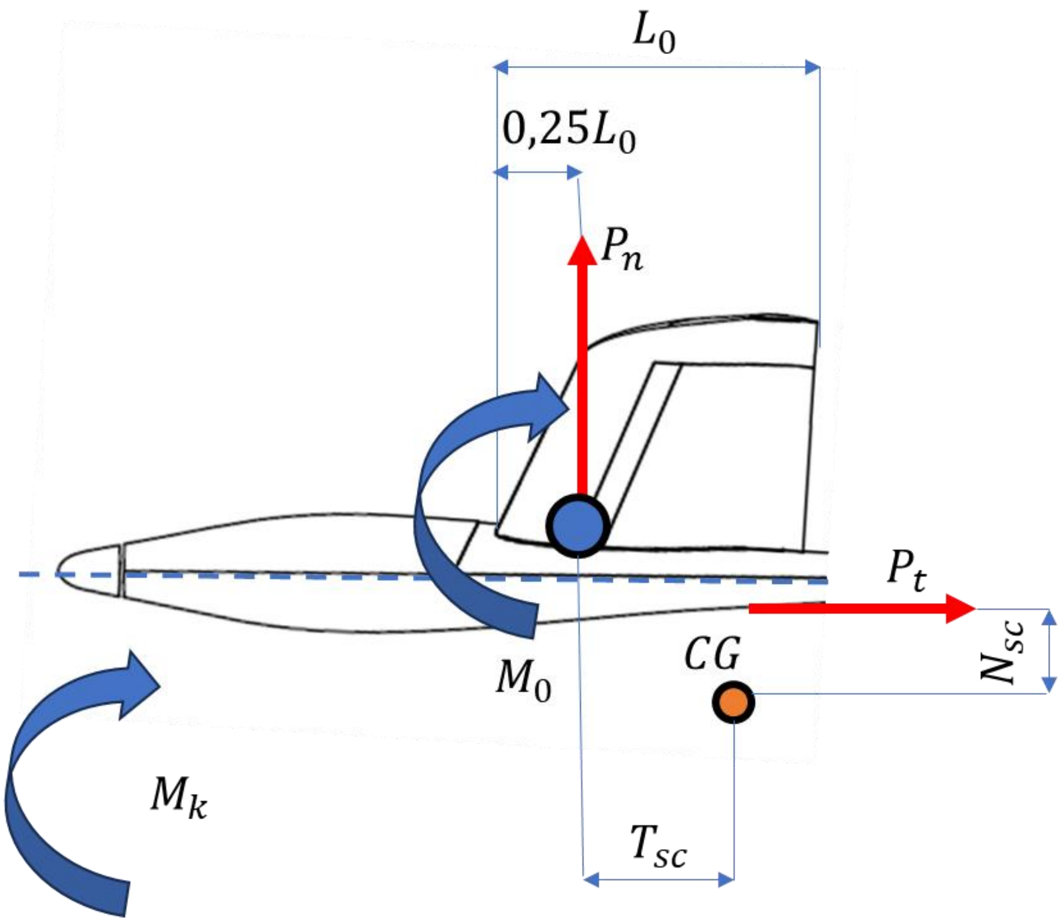

Fig. 28 The system of forces and moments with respect to the center of gravity of the test object.

A research object is dynamically stable, that is, it tends to extinguish oscillations over time, then when the elements of the characteristic equation have a negative sign as long as they are real, or as long as they are complex their real parts are negative. Such a state occurs when the expressions *A, B, C, D* and *E* are greater than zero, and the Routh Hurwitz discriminant (Stafiej 2000):

$$R = BCD - AD^2 - B^2E > 0 \quad (31)$$

Typically, the characteristic equation has two pairs of complex elements. Then the equation of the fourth degree, after introducing simplifying assumptions, can be replaced by the product of two equations of the second degree (Stafiej 2000):

$$(r^2 + B \cdot r + C) \cdot \left[r^2 + \left(\frac{D}{C} - \frac{BE}{C^2}\right) r + \frac{E}{C}\right] = 0 \quad (32)$$

The first result of equation gives a pair of complex elements r_1 i r_2 Which define the airplane fast, highly damped oscillations. The second result of equation yields a pair of composite elements that define slow less damped oscillations. During analysis, the most important thing is time $t_{1/2}$, in which the amplitude and period of *T* fluctuations are halved. Determining the elements of the equations in complex form (Stafiej 2000):

$$r = \xi + \eta_i \quad (33)$$

The time of decrease of the amplitude to half is determined by the relation (Stafiej 2000):

$$t_{\frac{1}{2}} = \frac{ln2}{(-\xi)}\tau_T \tag{34}$$

Where (Stafiej 2000):

$$\tau_T = \frac{\mu \cdot l_0}{V} \tag{35}$$

The period of fluctuation is determined by the formula (Stafiej 2000):

$$T = \frac{2 \cdot \pi}{\eta} \cdot \tau_T \tag{36}$$

Calculate the above relationships for fast and slow oscillations. As in the case of static stability, dynamic stability requires consideration of all calculated positions of the centers of gravity of the analyzed object in flight, since the expressions forming the coefficients of the characteristic equation depend on gravity center position.

3.4.2. Numerical Methods

The ANSYS CFX program uses a number of advanced numerical methods to analyze the dynamic stability of aircraft, including methods based on Reynolds-Averaged Navier-Stokes (RANS) equations and dynamic meshing techniques (Witanowski, Klonowicz and Lampart 2018, Muhammad Ahmad, et al. 2021). The RANS method makes enable to calculate the time of aerodynamic moments for a model oscillating around the center of gravity (Rizzi 2011). The use of a dynamic computational grid allows efficient modeling of harmonic motions, such as dipping and waving motions, which is crucial for separating the complex dynamic derivatives obtained in the forced oscillation process. ANSYS CFX also uses stationary and non-stationary simulations, which allows detailed aerodynamic analysis and investigation of aircraft dynamic stability (Goetzendorf-Grabowski and Antoniewski 2016). With these advanced numerical methods, more accurate modelling and analysis is possible, which contributes to ensuring the proper flight characteristics and safety of aircraft (Juliawan, et al. 2021, ANSYS, Inc. 2013, Lu, et al. 2019, Park, et al. 2017).

The XFLR5 program applies a range of numerical methods to the analysis of the aircraft aerodynamic stability, adapted to work at low Reynolds numbers.

The techniques used are (XFLR5 2023, Damiani, et al. 2019, Deperrois 2019, Mahdi and Elhassan 2012):

- Lifting Line Theory (LLT) – is based on a simplified wing model, where the airflow distribution is described as a continuous function along the wingspan. It is mainly used to calculate lift for wings, this method is not recommended for calculations for large angles of attack and does not take into account the three-dimensional effects of airflow around the wings.
- Vortex Lattice Method (VLM) - This method uses vortices acting on the surface of the aircraft's wings and tail system to calculate air circulation. The method takes into account the three-dimensional air flow.
- 3D Panel Method - The method uses a discretization of the body surface by means of panels (lobes) on which sources and double vortices are placed. The solution for the

potential flow is obtained by satisfying the Dirichlet or Neumann boundary conditions on each panel. This method requires more accurate geometry modeling, but is capable of modeling flows with high accuracy (Kubryński 1996).

3.4.3. Experimental Methods

In the process of determining the stability of aircraft, a variety of test methods are used to analyze their aerodynamic properties. Experimental methods include:

- Wind tunnel testing: allows accurate measurement of forces and moments acting on aircraft models under controlled airflow conditions to simulate various aviation situations (Nelson 1998, Rohlf, Schmidt and Irving 2012, Nicolosi, Corcione and Vecchia, Commuter Aircraft Aerodynamic Characteristics Through Wind Tunnel Tests 2016).
- Flight tests: these are used to collect operational data directly from aboard actual aircraft, allowing data obtained from other methods to be verified and the behavior of the aircraft to be evaluated in real-world conditionsch (Raymer 1992).
- Testing with moving mock-ups: This involves using scaled models capable of autonomous flight, allowing observation of their dynamics and stability under natural flight conditions (Nelson 1998).
- Computer simulations: although not an experimental method in the strict sense of the word, advanced simulation programs are a valuable tool to complement real tests, allowing analysis under virtual conditions (Juliawan, et al. 2021, ANSYS, Inc. 2013, Kubryński 1996).
- Cooper-Harper Test
  The Cooper-Harper Handling Qualities Rating Scale (HQR) is a subjective method of assessing the control of aircraft under various operational conditions. See figure Fig. 29. The Cooper-Harper scale includes ratings from 1 (excellent handling qualities) to 10 (unsatisfactory handling qualities, requiring immediate improvement) (Nelson 1998, Harper and Cooper 1966).

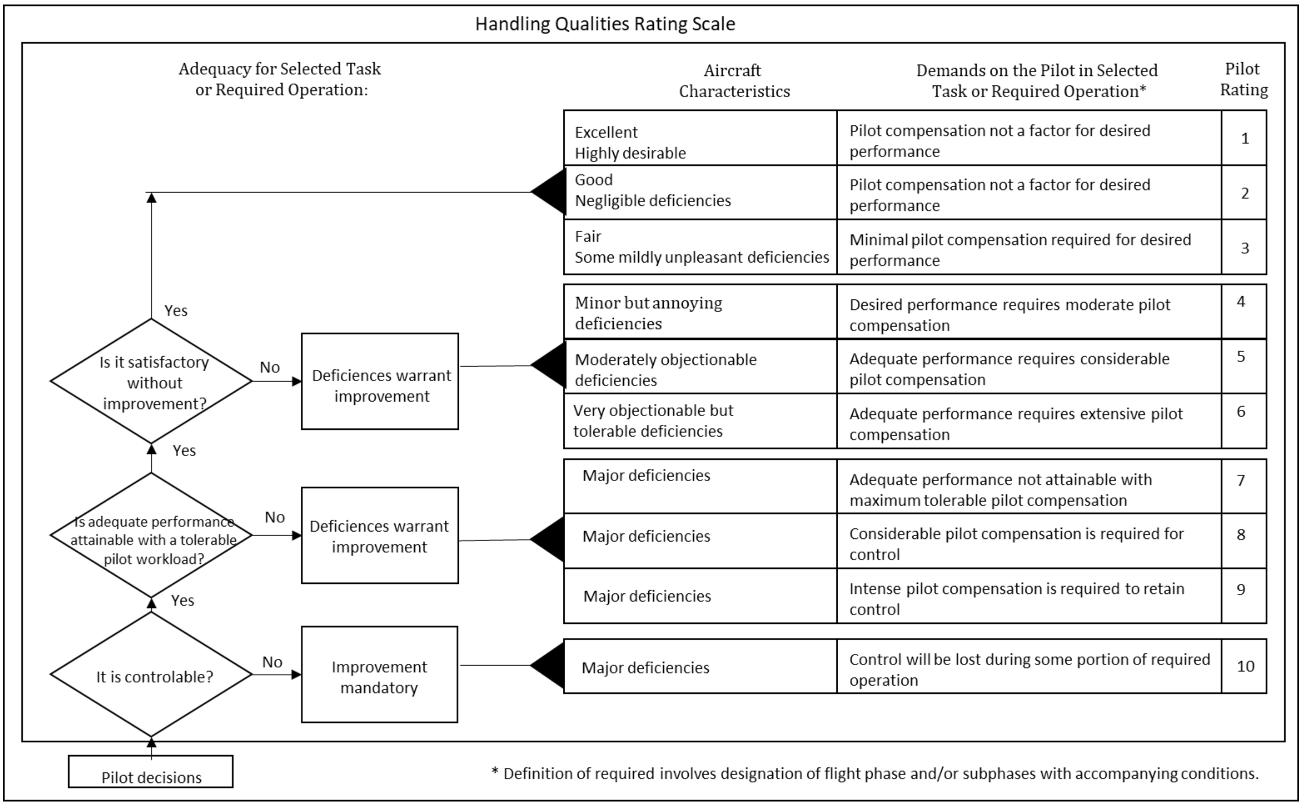

Fig. 29 Cooper-Harper Handling Qualities Rating Scale (HQR) [82]

4. Analysis methodology

The analysis methodology for the unmanned aerial vehicle presented in the dissertation considers many aspects of the design assumptions. The presented methodology was developed to conduct stability analyses of the Twin Stratos UAV and determine the optimal tail configuration for the test object in terms of stability. Fig. 30 shows a schematic diagram of the procedure for conducting the analyses presented in the following section.

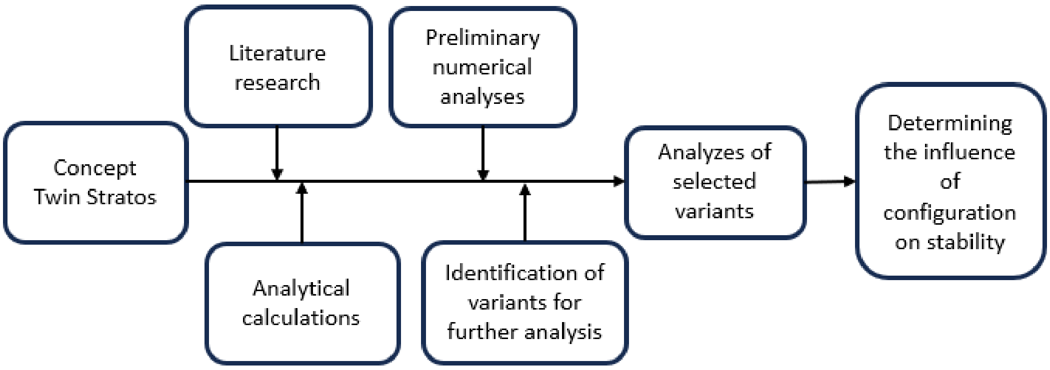

Fig. 30 Scheme of conducted analyses

Due to the analysis to be carried out, it is necessary to determine the variable and constant parameters for the optimized object. The assumptions for the variable and constant elements are presented in the chapter 4.2. Due to the complexity of the issue, it is necessary to define parameters related to the basic mission. The scheme for determining the requirements for the development concepts is presented in section 4.1.

4.1. Procedure diagram

The work identified a significant number of critical requirements and initial assumptions. Because of this, a diagram was developed to show the path for determining the requirements, initial assumptions, and interrelationships between successive stages of the work. See Fig. 31.

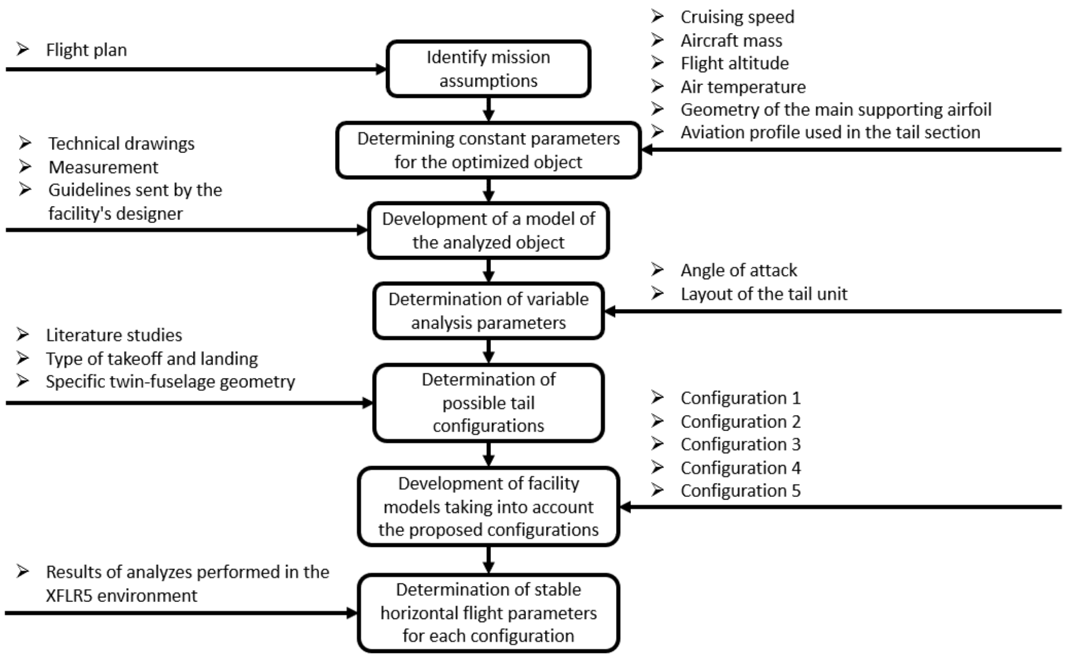

Fig. 31 Key parameters based on the stages of the conducted analyses

Based on the presented scheme, it is possible to identify the stages of research on the tail configurations under consideration. In the first stage, it was determined:

- What controllability parameters must the proposed configuration provide,
- what are the possible geometric and structural changes,
- what are the takeoff and landing restrictions caused by the takeoff system and landing gear configuration,
- whether configuration can be changed by adding control surfaces on the wings to improve flight stability.

By determining the above parameters, it was possible to develop further assumptions. Based on the preliminary analysis, it was possible to determine the assumptions for further stages of the work.

4.2. Development of the concepts shapes and geometric assumptions

Based on the data obtained from the team from Skytech Elab company, involved in the design of the subject of the research, fixed parameters and variable parameters were determined for each considered tail configurations. The assumptions for the Twin Stratos configuration in the form of the fuselage arrangement, the main lifting airfoil, and the location of the tail section and, more specifically, its distance from the trailing edge were determined to be invariant. The tail section in the form of the arrangement between the tail beams was specified as fixed. Tab 8 shows the exact list of fixed parameters.

Tab 8 Fixed parameters of analyzed tail configurations

Constant parameters		
Parameter	Symbol	Unit
Distance between hulls	L1	m
Height of the tail section	L2	m
Distance of the leading edge of the tail section to the trailing edge of the main lifting flap	L3	m
Angle of the leading edge of the tail section with respect to the fuselage axis	α1	°
Angle of the trailing edge of the tail section with respect to the axis of the fuselages	α2	°
Airfoil used in the tail section	-	-
The length of the chord of connection to the hulls	C1	m
Length of the chord in the axis of the aircraft	C2	m

In order to accurately determine the constant parameters, they are shown in the visualizations of Fig. 32 and Fig. 33.

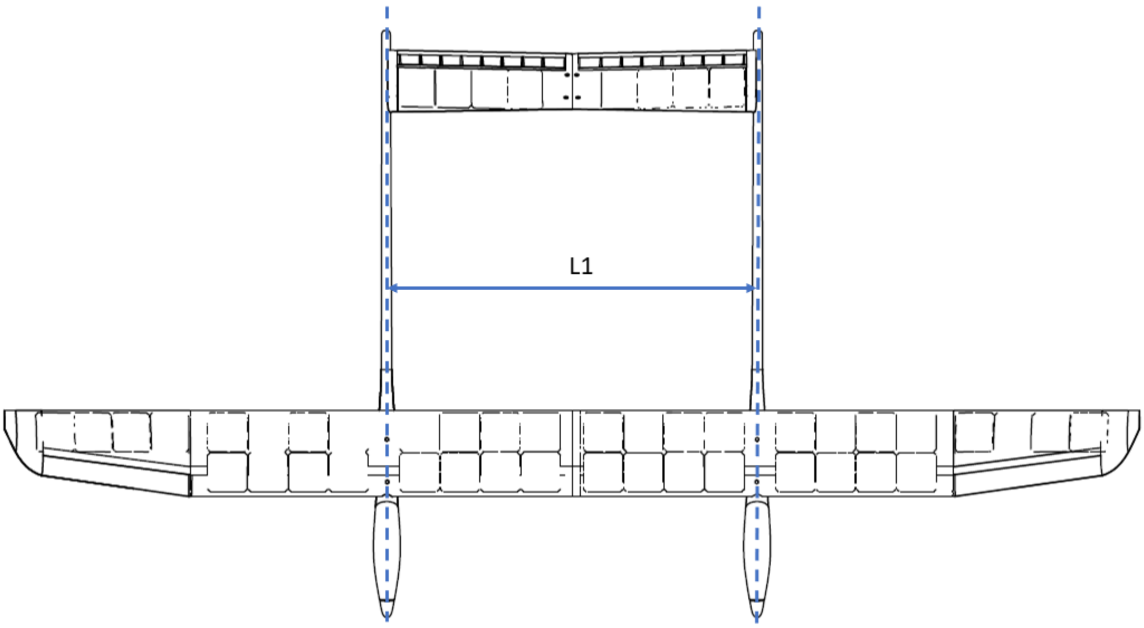

Fig. 32 Twin stratos top view with constant parameters

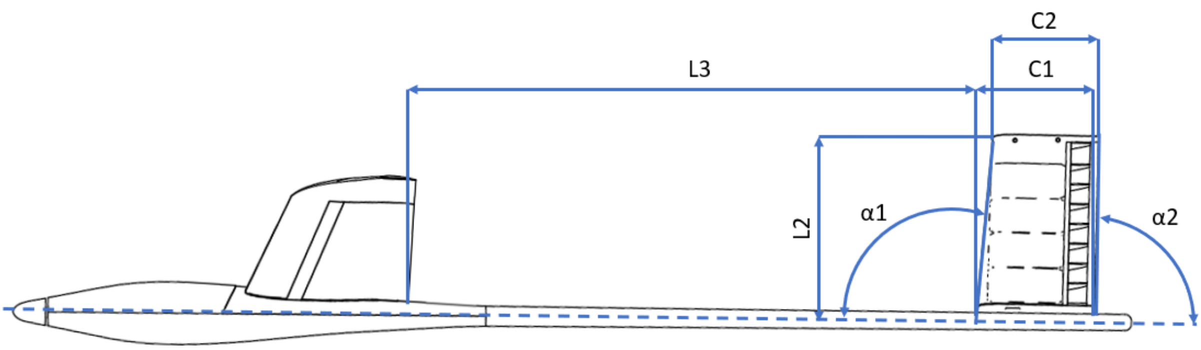

Fig. 33 Twin stratos side view with constant parameters

Considerations regarding potential modifications to the tail system were also needed to account for the positioning of the tail beam. This matter was addressed during the development of tail section requirements in collaboration with the design team responsible for the subject of the analysis. The placement of the tail beams is depicted in Fig. 34.

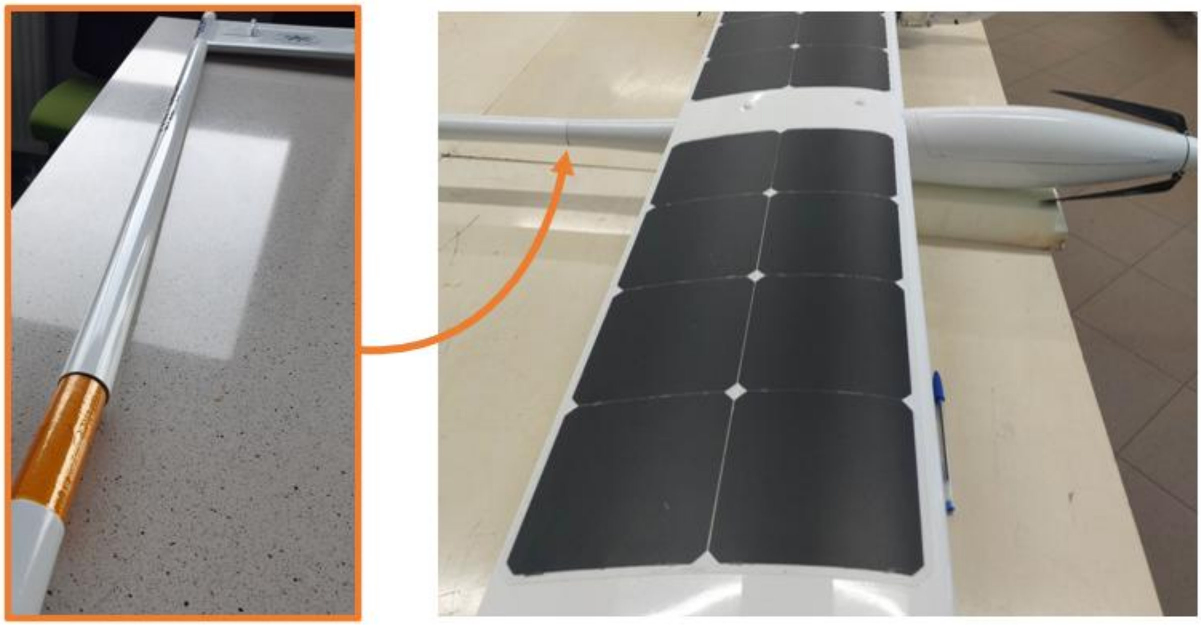

Fig. 34 Connection of the fuselage to the tail section

4.3. Determination of the masses, flight speed and CG location

The determination of flight parameters was prepared taking into account the representative mission (Zenowicz and Moczulski 2024). Due to the assumptions associated with horizontal flight and constant airspeed when conducting air analysis, level flight is the most relevant from the approach of the flight stability. Given the initial stage of the work, the focus was on aerodynamic optimization, without considering the internal structure of the aircraft (Mieloszyk and Goetzendorf-Grabowski 2017). See Fig. 35.

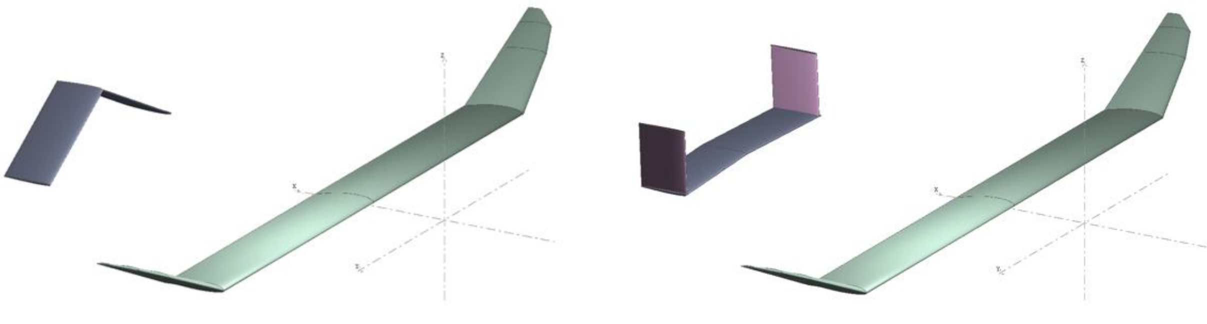

Fig. 35 Comparative view for different tail configurations

Determination of different tail configurations affects the position of the center of gravity of the subject of the research due to the different arrangement of structural, aircraft skin and electronic components and also by the different length of the airfoils themselves, so that the position of the center of gravity was approximated based on simple geometric relationships and scaling.

To establish the center of gravity for each configuration, a dynamic spreadsheet was created, enabling real-time recalculations based on the positioning of components within the geometrically modified sections of the test object. Utilizing this spreadsheet, the center of gravity is also visually represented in the graphic provided below in Fig. 36.

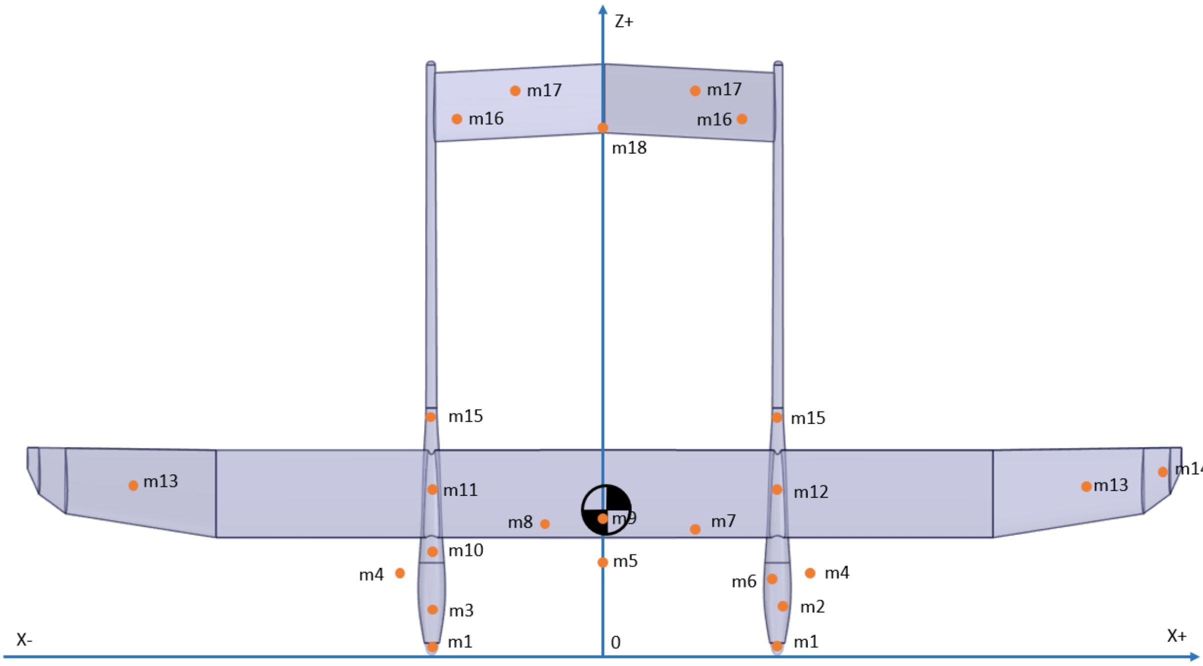

Fig. 36 Representation of component masses in the form of mass points defined on the TS17 coordinate system. m1 – m18 are the sum of the masses of the components in one location, taking into account their centers of gravity.

The remaining components for each configuration were identified as fixed, with their attachment points remaining constant. This approach allowed for the precise determination of the center of gravity for each configuration under consideration. The results of this analysis were referenced to the coordinate system illustrated in the visualization in Fig. 37.

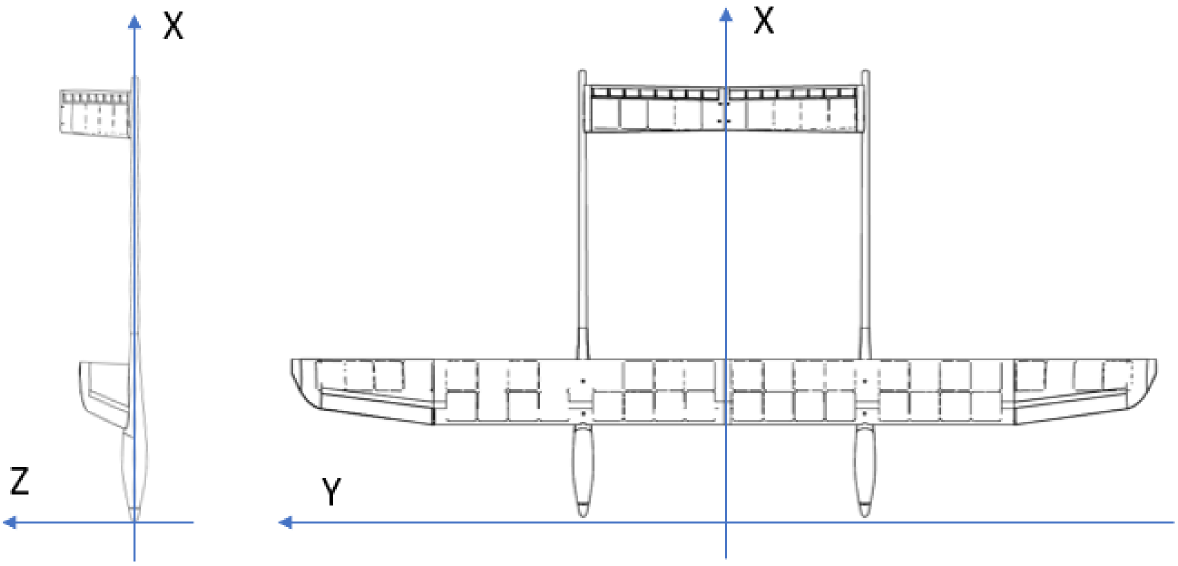

Fig. 37 The coordinate system adopted for the mass analyses

The locations of the centers of gravity for each of the considered configurations are shown in the table Tab 9.

Tab 9 CG location table for analysed tail configuration

Configuration	I	II	III	IV	V
CG position along the X axis [mm]	472	472	477	477	477
CG position along the Y axis [mm]	0	0	0	0	0
CG position along the Z axis [mm]	1	-22	-2	-5	13

Determining the centers of gravity for each of the proposed axis is an important part of the study due to the impact of the location of a given point on stability and the value of the stability margin. The location of the centers of gravity for each configuration was also checked and confirmed using XFLR5 software, which allows the modeling of the layout of components and structures in the form of mass points and masses distributed over the modeled solids. See Fig. 38.

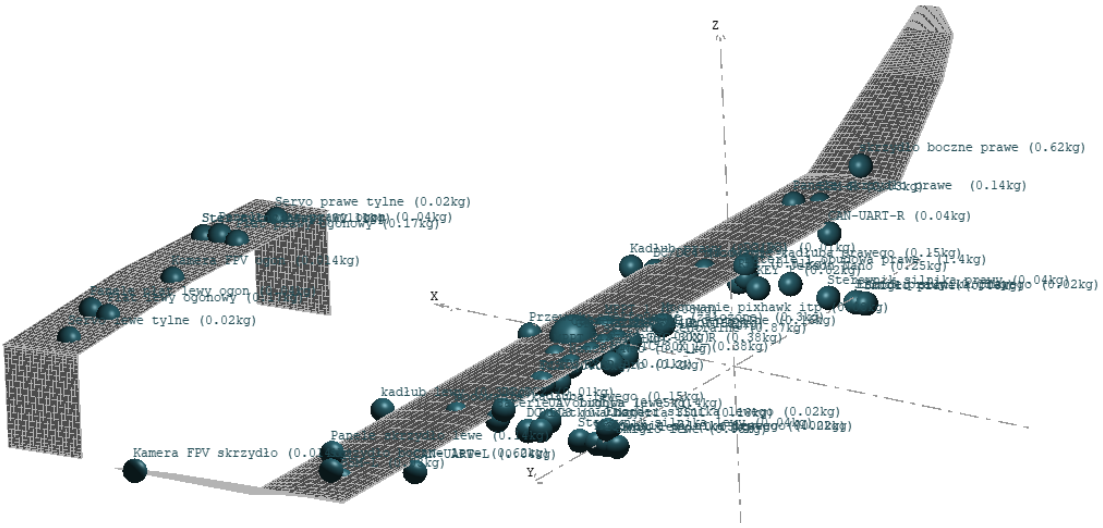

Fig. 38 Mapping of masses localization in XFLR5 software

4.4. Identification of forces and moments

The determination of the forces and moments acting on the test object takes into account the differences in tail configurations. This is caused by the different location of aerodynamic points for each of the configurations under study. The location of the aerodynamic centers was determined as a function of the distance from the origin of the adopted coordinate system along the fuselage axis "x" and along the perpendicular axis "z". The assumption made during the analysis was to determine the aerodynamic center position parameter for an angle of attack equal to 0 and the same flight speed. Due to the change in the position of the center of gravity for each configuration, the distance between these points was determined for each configuration. See Fig. 39.

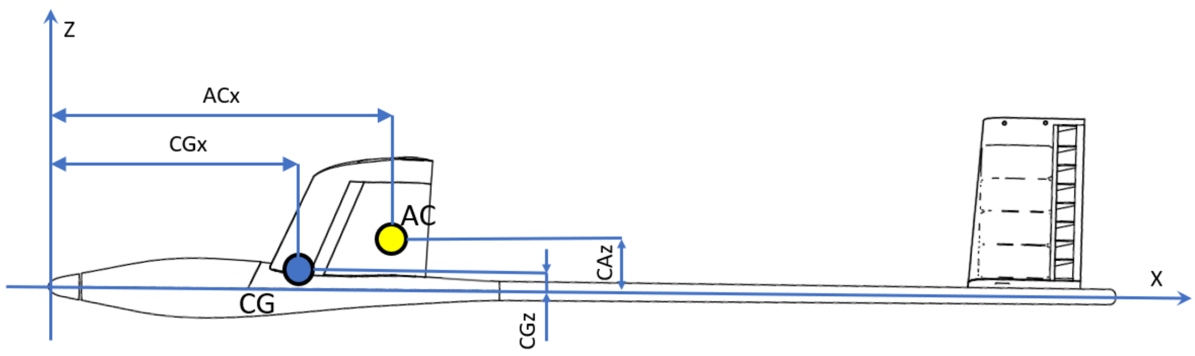

Fig. 39 AC and CG location in assumed coordinate system

As in the case of determining the position of the centers of gravity, a spreadsheet was developed to determine the forces and moments and their effect on the angle of attack in level flight for each of the configurations studied. The determination of forces was based on analytical calculations taking into account the parameters of the adopted aerodynamic profiles, airspeed and air density. During the calculations, the following values of the mentioned parameters were assumed:

- Flight speed,
- Air density,
- Airfoil used in the tail section.

The parameters of the forces themselves, which depend on the size of the airfoil, and their position relative to the adopted coordinate system, were specified as variable values. Due to the fixed configuration system of the main load-bearing airfoil, its parameters were determined and included in the calculations. Due to the possibility of a different angle of attack for each of the configurations considered, analyses were carried out for different angles of attack with a constant change of pitch.

Based on the data thus obtained, it is possible to determine the angle of stable horizontal flight for each of the configurations analyzed, assuming the rudder ailerons are placed in a neutral position. Analyses were carried out based on the system of static equilibrium equations. See Fig. 40.

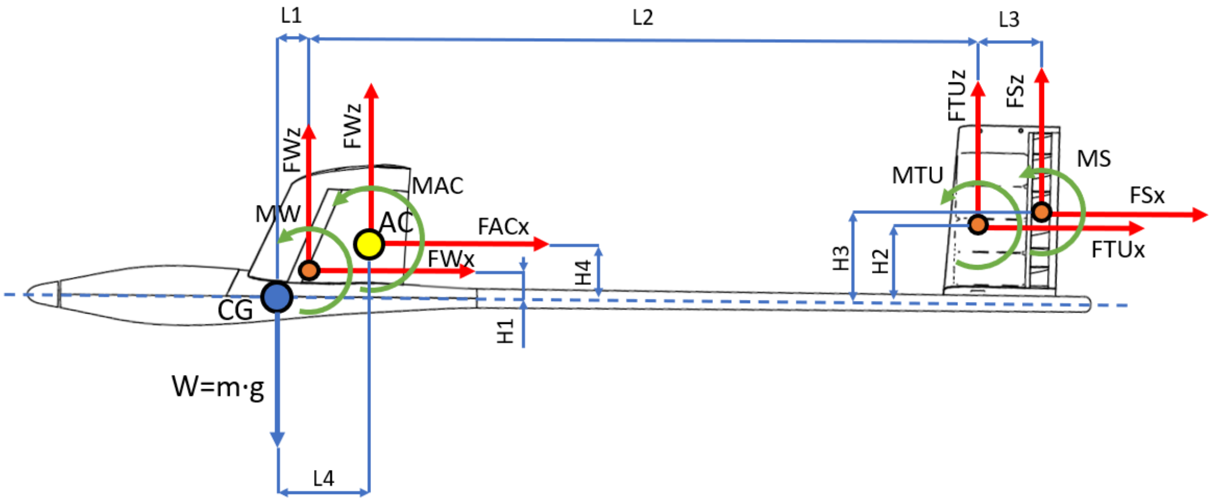

Fig. 40 Forces acting on Twin Stratos during flight

$$\sum[FiX = 0] \tag{37}$$

$$\sum[FiZ = 0] \tag{38}$$

$$\sum[MU = 0] \tag{39}$$

Where:

∑FiX – The sum of the forces acting relative to the X axis.
∑FiZ – The sum of the forces acting with respect to the Z axis.
∑MU – The sum of moments relative to the adopted system of coordinates.

During the analyses, the center of gravity position point was taken as a fixed point, connecting together the above equations. As a result to this procedure, it was possible to accurately determine the position of the Aerodynamic Center with respect to the "X" and "Z" axes.

4.5.Tail unit analyses

The purpose for the analyses is to change the shapes and design of the tail configurations themselves, the other components and shape of the drone, i.e. drives, wings, propellers and the like remain the same. The geometry is projected and the same aerodynamic profile was used in each of the tail configurations analyzed. The parameters are presented in subsection 4.2. The suspension angle of the airfoil is fixed, the assumed materials used in each of the proposed tail parts are fixed and consistent with the existing drone design. The approximation of the mass parameters was based on the geometry of the proposed configurations and the difference in length with the existing configuration.

Due to the influence of the tail section on the parameters presented in the above subsections (4.1-4.4), a summary of the key parameters of the tail section was made. They are presented in the table Tab 10 Aerodynamic parameters of the considered configurationsTab 10.

Tab 10 Aerodynamic parameters of the considered configurations

Configuration	I	II	III	IV	V
Angle of attack of horizontal flight *α* [˚]	4.30	4.29	2.87	3.50	3.30
Lift coefficient *CL*	0.96	0.96	0.90	0.89	0.87
Drag coefficient *CD*	0.038	0.038	0.034	0.034	0.033
Aerodynamic excellence *CL/CD*	25.44	25.48	26.40	26.37	26.40
Lift *L* [N]	112.83	112.75	105.73	104,14	101.85
Drag *D* [N]	4.43	4.43	4.01	3.95	3.86
Estimated mass of the UAV *m* [kg]	9.80	9.80	10.30	10.30	10.30
Estimated mass of the tail section m_{tu} [kg]	0.76	0.76	1.26	1.26	1.26

The tail versions were designed by projecting the geometry of the initial configuration. The models of the tested objects are shown in the table Tab 11.

Tab 11 Modelled tail configurations

Conf.	Front view	Side view	Top view
I			
II			
III			
IV			
V			

4.6.Stability analyses

Stability studies involve analyzing the forces and moments acting on each of the considered tail configurations in two programs, ANSYS CFX and XFLR5. To accurately determine the advantages and disadvantages of a given configuration, analyses were performed for extreme flight prarameters, since a given configuration may be stable in level flight, but unstable at higher flight speeds and angles of attack.

A study of the behavior of the analyzed object in the transverse plane, i.e., its lateral, roll, tilt stability, including aerodynamic components such as wings, vertical and horizontal stabilizers was conducted.

Unmanned aerial vehicles (UAVs) must meet safety requirements and flight mission conditions while maintaining adequate flight efficiency for specific applications. An important part of this process is static stability analysis and appropriate criteria for assessing this stability. As part of this process, an analysis of aerodynamic forces and moments acting on the UAV is carried out. In the future, the development of advanced analytical tools and evaluation methods will allow an even more precise approach to static stability issues in unmanned aviation.

Static stability refers to an aircraft's ability to return to a state of equilibrium after minor disturbances without external intervention. In the context of fixed-wing drones, this stability is crucial, as it determines their ability to maintain stable flight under various atmospheric and operational conditions. Based on the results obtained with advanced numerical modeling tools, in which the actual operating conditions of the UAV were mapped, and on the basis of a literature review, the static stability of various variants of the analyzed object was evaluated. Static stability evaluation criteria have been determined based on a literature review, for all configurations and their individual angles of attack of steady horizontal flight, for which the inclining moments are zero.

Static stability criteria (See Fig. 41).

- Evaluation criteria:
  - Pitching moment coefficient (*Cm*): Its variation as a function of the angle of attack.
  - Lift coefficient (*Cl*): Aerodynamic stability.
  - Drag coefficient (*Cd*): Aerodynamic optimization.
  - Aerodynamic center position (*AC*): Longitudinal stability.
  - Margin (*SM*): Adequate backup stability.

Evaluation of individual tail configurations

- Evaluation method:
  - A scale of 1 to 10 for each criterion.
  - Weighted average based on the relevance of each criterion.

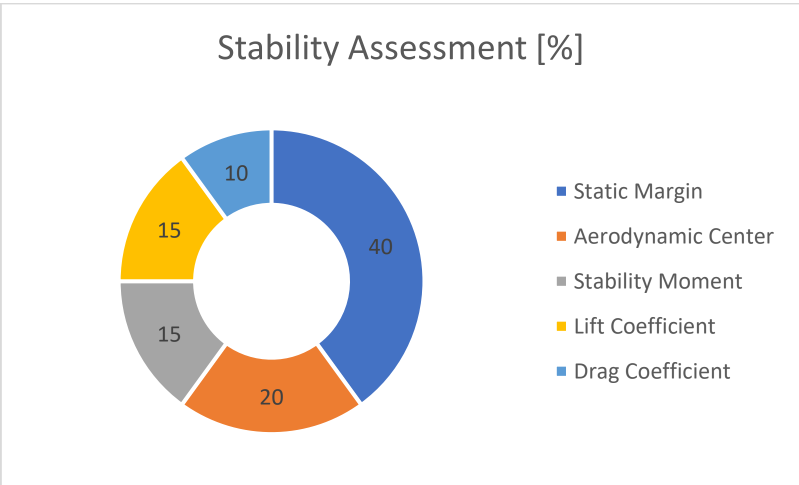

Fig. 41 Components of stability assessment

To evaluate the significance of static stability criteria for unmanned aerial vehicles (UAVs), percentage weights were allocated to represent the relative importance of each criterion. The total sum of the weights was normalized to 100% by:

- Stability Margin (*SM*): Adequate backup stability – 40% (Fig. 42)

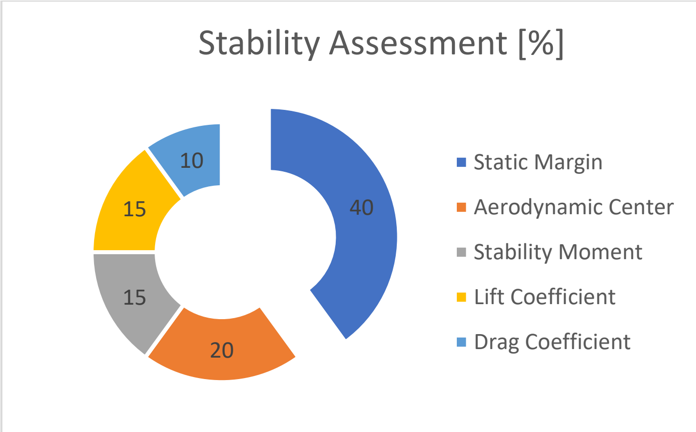

Fig. 42 Stability margin relative to stability assessment values

The stability margin (static margin) defines the distance between the center of gravity (CG) and the aerodynamic center (*AC*) as a percentage of the aerodynamic chord and is also important indicator of the static stability (Etkin and Reid 1996). Positive margin when *CG* is ahead of *AC* promotes longitudinal stability and automatic recovery from disturbance (Anderson, Aircraft Performance & Design 2012). A negative margin leads to instability, making it difficult to control the UAV. A low margin improves maneuverability, but can increase the risk of instability and stall. The high margin improves stability but reduces maneuverability (Hurt 1965). The optimal margin must balance stability with maneuverability, according to UAV operational specifications (Embry-Riddle Aeronautical University 2024).

- Central aerodynamic position (*AC*): Longitudinal stability – 20% (Fig. 43)

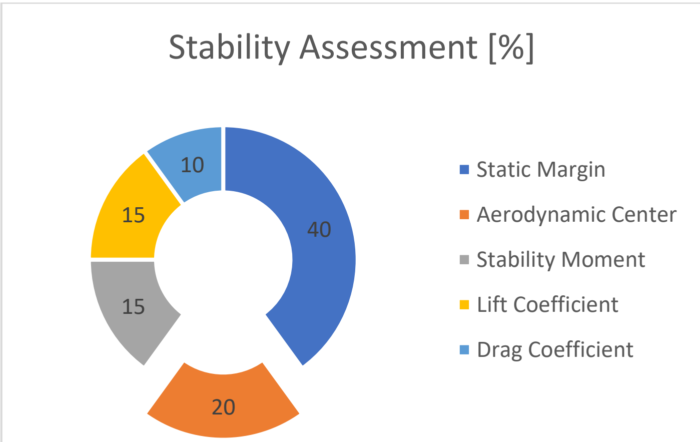

Fig. 43 Central aerodynamic position relative to stability assessment values

Proper aerodynamic positioning provides an essential measure for maintaining longitudinal flight stability (Nelson 1998). The aerodynamic center (*AC*) is the point on the wing profile where the leaning moment does not depend on the angle of attack, making it important for aircraft design. Longitudinal stability is achieved when the *AC* is in front of the center of gravity (*CG*), which generates a stabilizing moment that helps to maintain predictable flight. Moving the *AC* closer to the nose increases stability but can limit maneuverability (McCormic 1979). In addition, a higher *AC* is conducive to dynamic maneuvering, although it can cause stalling, requiring advanced control systems. The optimal *AC* position depends on the operational and design specifications to balance stability and maneuverability (Hurt 1965, Etkin and Reid 1996) .

- Pitching moment coefficient (*Cm*): Its variation as a function of angle of attack – 15% (Fig. 44)

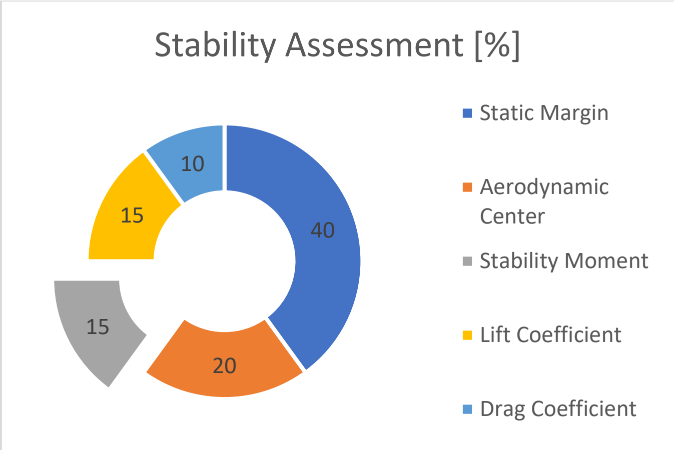

Fig. 44 Coefficient of pitching moment versus stability assessment value

The variability of the tilt torque as a function of the angle of attack affects the UAV's ability to return to equilibrium on its own after a disturbance, which is crucial for its stability and safety during flight maneuvers (Etkin and Reid 1996). The pitching moment coefficient (*Cm*) is an important parameter for determining the longitudinal stability of an aircraft, measuring the moment generated by aerodynamic forces around the center of gravity (Anderson, Fundamentals of Aerodynamics 2017). A positive Cm can lead to instability by increasing the angle of attack, while a negative *Cm* promotes automatic return to the original position, improving stability (Anderson, Aircraft Performance & Design 2012). However, too low *Cm* may limit maneuverability (McCormic 1979). Optimal *Cm* should be slightly negative to ensure stability without limiting the ability to maneuver quickly, which requires a precise design, balancing stability with maneuverability for optimal flight performance and safety (Hurt 1965, Anderson, Fundamentals of Aerodynamics 2017).

- Lift force coefficient (Cl): Aerodynamic stability – 15% (Fig. 45)

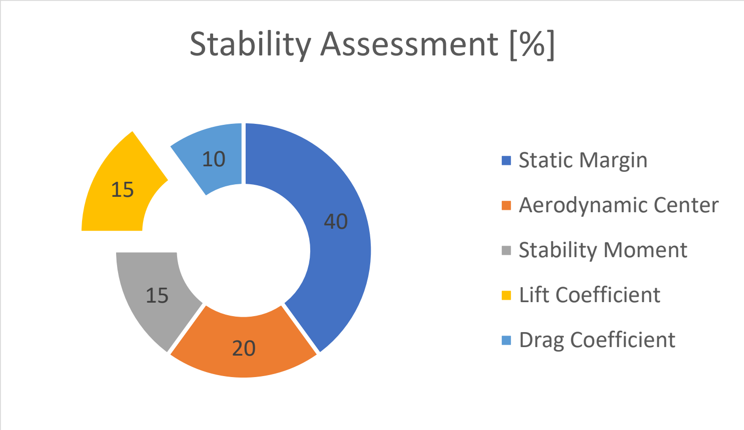

Fig. 45 Lift coefficient relative to stability assessment value

Aerodynamic stability, as measured by the lift coefficient, is crucial to flight efficiency and the UAV's ability to maintain altitude, especially during prolonged missions and in changing weather conditions (Anderson, Fundamentals of Aerodynamics 2017) . Higher lifting force brings numerous benefits, such as the ability to carry higher loads, which is important in transport and military aviation (Bertin and Cummings 2009). In addition, it allows takeoffs and landings on shorter runways for greater operational flexibility. Improved maneuverability at low speeds facilitates precision maneuvering, especially in difficult conditions. Higher lift also improves flight efficiency at higher altitudes, increasing range and reducing energy consumption, resulting in better energy efficiency. In addition, better stability in turbulence increases flight comfort and safety (Hurt 1965).

- longitudinal stability:

The higher lift force generated by the wings and control surfaces has a significant impact on the aircraft's longitudinal stability. The key factor here is the location of the center of lift force relative to the center of gravity. If the center of lift is too far from the center of gravity, this can lead to instability. To ensure longitudinal stability, it is necessary to properly balance the lifting force and precisely locate the center of gravity. As the literature indicates, proper aerodynamic design and mass placement are key to achieving longitudinal stability (Anderson, Aircraft Performance & Design 2012) (Anderson, Fundamentals of Aerodynamics 2017).

- lateral stability:

The lifting force generated by the wings significantly affects lateral stability. Wings with high lift force can contribute to lateral stability, which is beneficial in maintaining balance during lateral tilt. Increased lateral stability is particularly important during maneuvering and in turbulent conditions. Improving lateral stability through proper wing design is well documented in the literature (McCormic 1979).

- directional stability:

Directional stability is largely dependent on the lifting force generated by control surfaces such as the vertical stabilizer. Correct design of these surfaces is key to maintaining directional stability. Proper configuration of the vertical stabilizer helps prevent uncontrolled twisting or drifting, which is important for safe and stable flight. The literatures emphasize the importance of precise design in the context of directional stability (McCormic 1979) .

- Drag coefficient (*Cd*): Aerodynamic optimization – 10% (Fig. 46):

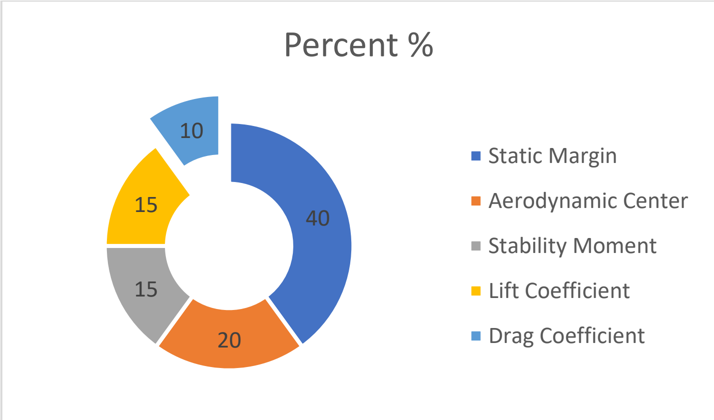

Fig. 46 Drag coefficient to stability assessment value

Aerodynamic optimization, measured by the drag coefficient, has a key impact on the UAV's energy efficiency. Lower drag improves energy consumption efficiency and increases flight time, which is important for missions that require a long stay in the air (Raymer 1992). Oppositely acting aerodynamic drag affects the UAV's performance, energy efficiency, and stability. This drag is divided into frontal drag and induced drag, with high induced drag associated with lift generation, which can lead to instability at low speeds, especially during take-off and landing (Bertin and Cummings 2009). Asymmetric frontal drag can interfere with directional stability, requiring constant control adjustments (Hurt 1965). Low aerodynamic drag reduces energy consumption and increases range (Raymer 1992, Anderson, Aircraft Performance & Design 2012), but can also lead to instability at low speeds and reduce control forces, making maneuvering difficult in difficult conditions (Hurt 1965). However, high induced drag can improve stability at low speeds, making takeoffs and landings easier. The optimal level of aerodynamic drag should balance energy efficiency with the required stability, especially at low speeds (Anderson, Introduction to Flight 2000). UAV design requires a trade-off between efficiency and stability, making aerodynamic drag management crucial to achieving optimal flight characteristics.

- Summary

The stability margin (*SM*) is considered the most important, as it directly affects the overall stability and safety of the UAV. Longitudinal stability (*AC*) and pitching moment variation (*Cm*) also have a significant impact on flight stability, while aerodynamic stability (*Cl*) and aerodynamic optimization (*Cd*) are key to the UAV's operational efficiency and performance. Each of these elements affects the UAV's flight efficiency, stability, and maneuverability. The optimal balance of these factors is essential to ensure safe, stable, and efficient UAV flight, especially on long-duration missions.

5. Preparing the computing environment to verify the methodology

All analyses conducted as part of this dissertation were performed on a single computing station to eliminate hardware-induced variations in the results. The analyses presented in this work utilized two software environments: ANSYS and XFLR5. ANSYS CFX is advanced software for the numerical analysis of fluid flows, heat and other physical phenomena. The methodology of the analyses carried out is presented in the chapter 5.1.

XFLR5 is an aerodynamic analysis and wing profile design software available for various operating systems. The methodology of the analyses carried out is presented in Section 5.2.

The developed analyses, regardless of the software used, were prepared following the scheme shown in the Fig. 47.

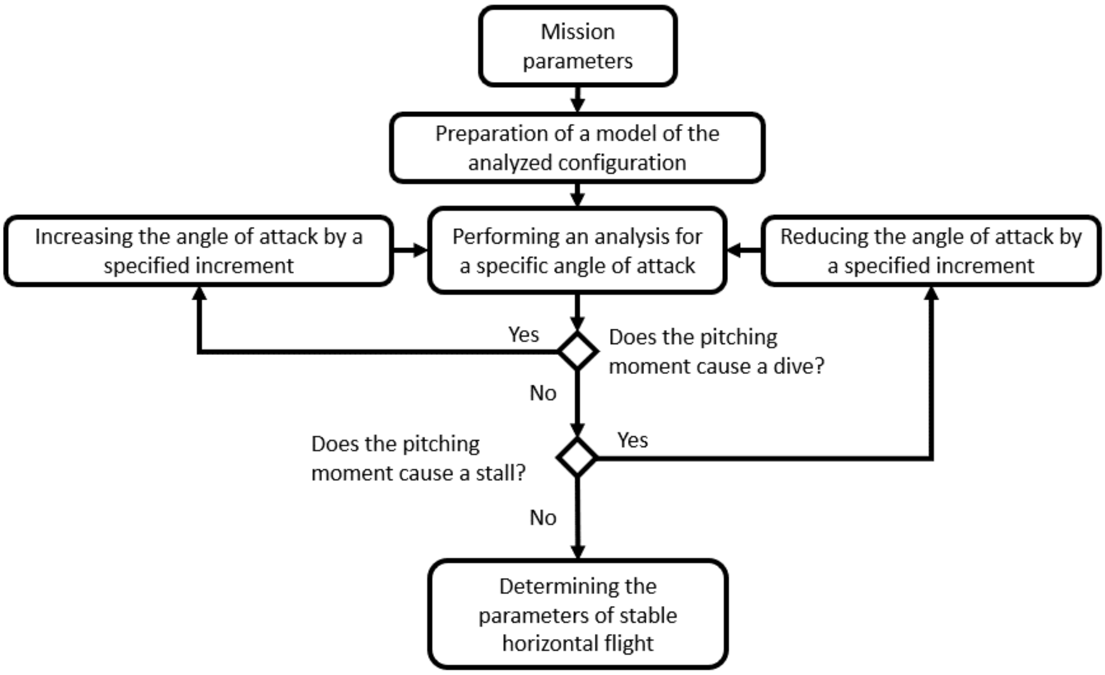

Fig. 47 Procedure for Conducting Numerical Analyses

The tests were conducted with constraints such as flight speed and angle of attack. The software was used to obtain lift and drag coefficients for the considered tail configurations mapped to the test object. The first, preliminary calculations were performed at the maximum values of horizontal flight speed for the UAV.

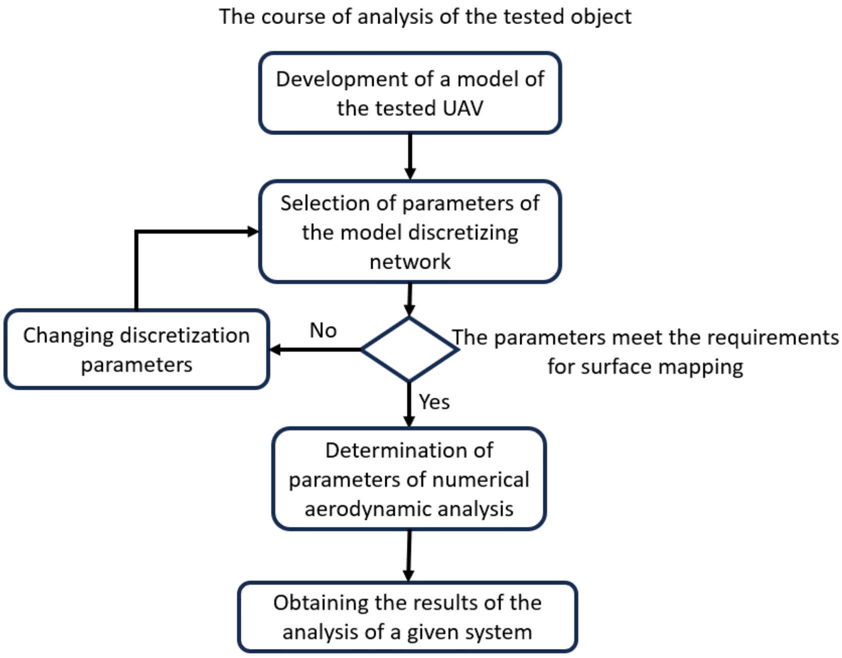

Fig. 48 Procedure for the Analysis Method of the Examined Object

Standardizing the method of preparation and execution of the analyses will enable consistent comparison of the results, irrespective of the computing environment utilized.

5.1. ANSYS simulation development

The analysis of the UAV Twin Stratos using ANSYS software followed the flowchart outlined in Chapter 5, as depicted in Fig. 48. During these analyses, the capability of conducting multiple independent simulations in parallel was utilized. This approach required the creation of models for the object under study, incorporating the various tail configurations and the surrounding environment. The models were subsequently discretized. Boundary conditions, including parameters for the system's inlet, impermeable walls, medium density, temperature, and system exit, were applied to the discrete models. The analyses performed in this manner produced results that were then used to assess flight stability. See Fig. 49.

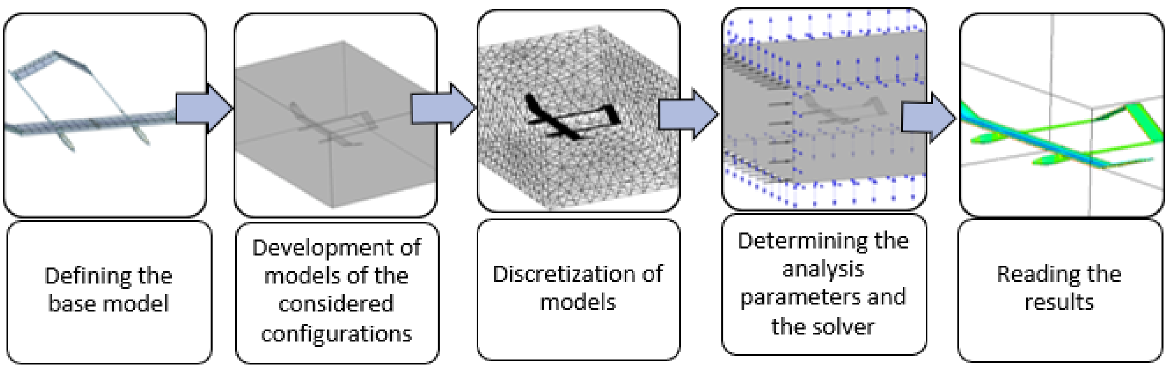

Fig. 49 Model preparation in the ANSYS environment

A detailed description of the steps presented is presented in the following subsections 5.1.1 - 5.1.4 The analyses were mainly conducted based on the Geometry and CFX modules, the block diagram used in ANSYS software is shown in the Fig. 50.

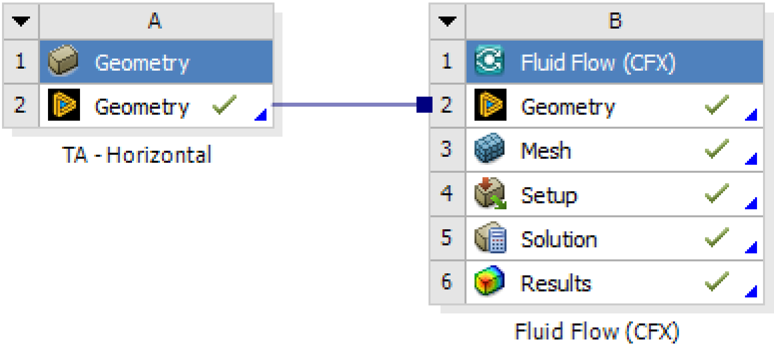

Fig. 50 ANSYS CFX module and geometry

Due to the multiplicity of configurations considered and the number of variable analysis parameters, the procedure scheme was simplified, which had a positive effect on the time of conducting the analyses themselves.

5.1.1. Preparation of simulation models

Based on a literature study of various tail systems found in wide-area aviation, five tail system configurations were selected for the Twin Stratos 1:7 object. The selection of options was guided by design assumptions that took into account the flight mission of the aforementioned UAV.

The development of the models of the tested tail configurations was carried out on the basis of the data and object model provided by Skytech Elab, taking into account the assumed geometric fixed parameters, which are presented in subsection 4.2. The specified object geometries allowed the generation of five solid models. See Tab 12.

Tab 12 Geometry models of analysed configurations

Configuration I	Configuration II	Configuration III
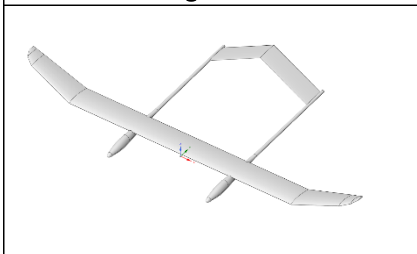	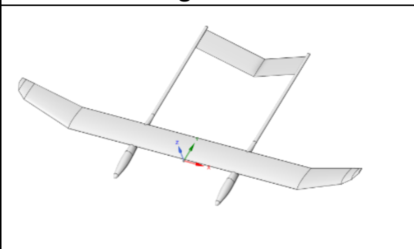	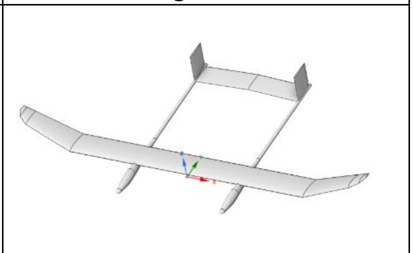
Configuration IV	Configuration V	
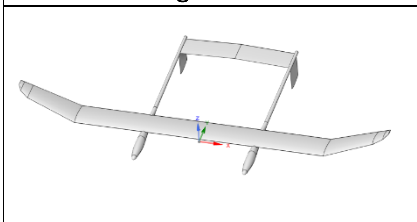	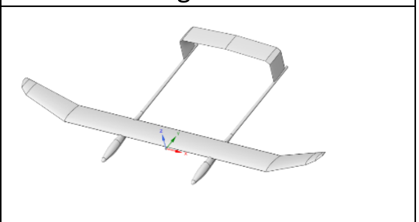	

The preparation of a model of the test environment is a key step in the conducted analysis for the ANSYS computational environment, due to its impact on further stages of the work. Numerical aerodynamic analyses conducted in the CFX environment require the development of a model of the medium, in the case of the above studies of air, surrounding the object under study. The development of the environment model was carried out with the "Geometry" module, using the "enclouser" option to cut the surface of the aircraft solid from the volume of the numerical wind tunnel model. See Fig. 51.

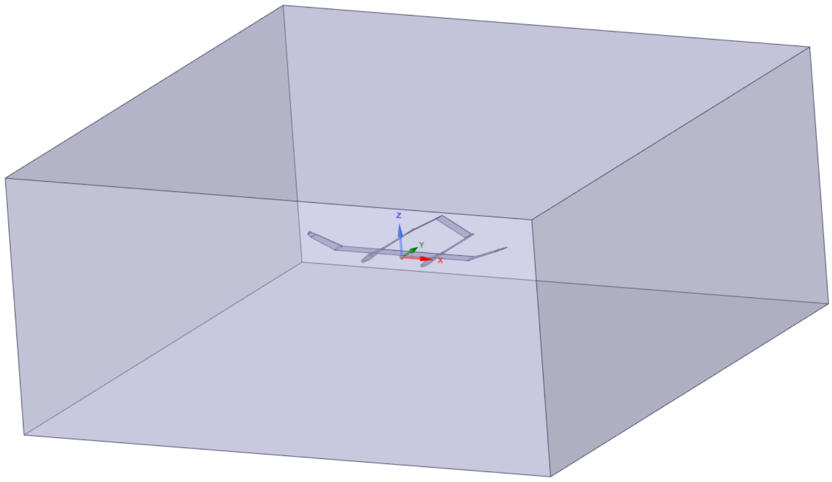

Fig. 51 Enclouser option visualization

Due to the conduct of comparative studies, the geometric dimensions of the modeled medium are specified. The use of this assumption makes it possible to reduce discrepancies in test results resulting from inconsistencies in the models. The dimensions of the described test system, along with the distances from the test object in the form of a UAV with a given tail configuration, are shown in the Fig. 52.

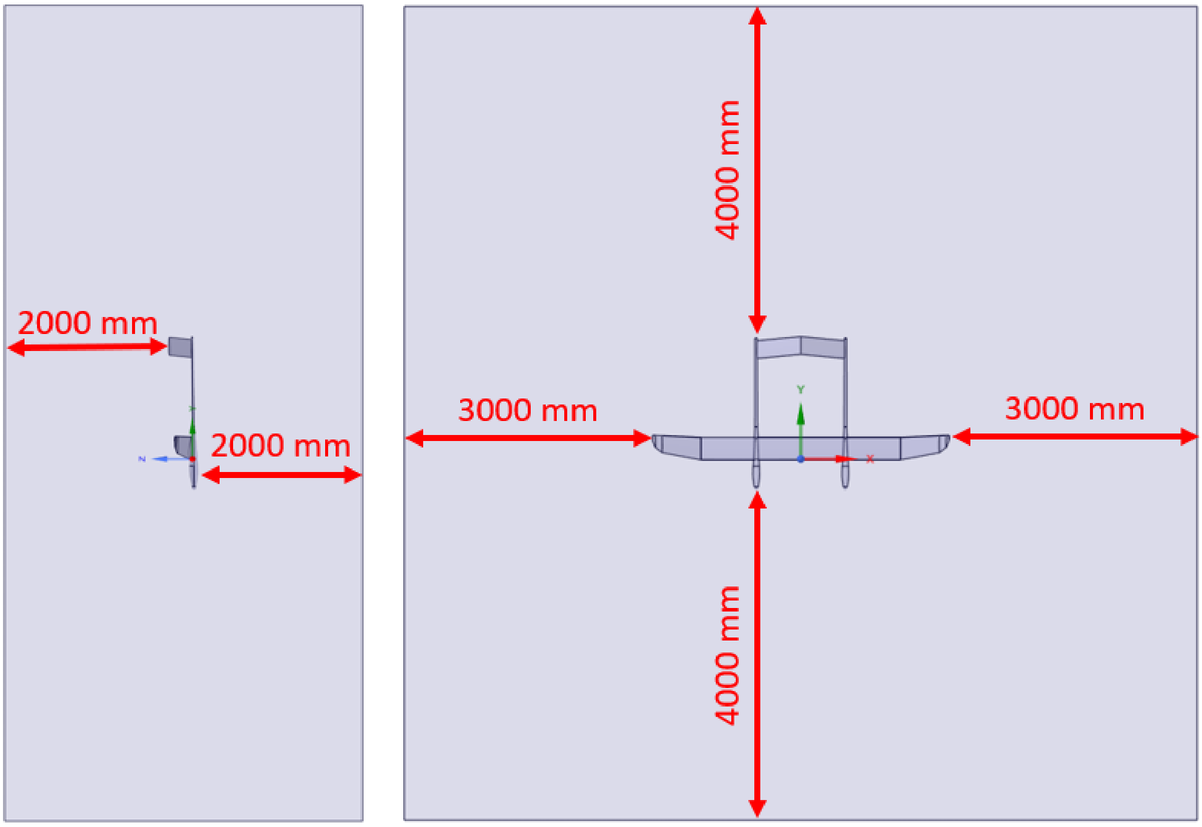

Fig. 52 Enclouser walls distances to analysed obiect

Taking this requirement into account, the previously developed models in the form of lumps of the objects under study were cut from the lumps of the virtual wind tunnel which was then discretized.

5.1.2. Discretization of models

Proper preparation of the models for numerical aerodynamic analyses required careful selection of discretization parameters, including element shape, size, and density at critical points in the model (Mańkowski, et al. 2021). Ten trials were conducted to appropriately size the elements, ensuring a sufficient number of analyses could be performed with the desired accuracy while maintaining the required analysis time. Since the focus was on the tail section, the initial determination of optimal discretization parameters for the front section allowed for the application of these parameters across all tail section models. However, any variations in the number of elements and nodes in the discrete models arose from differences in the geometries of the test objects, with an emphasis on preserving consistent discretization parameters across all models. The process for determining the relevant discretization parameters is illustrated in Fig. 53.

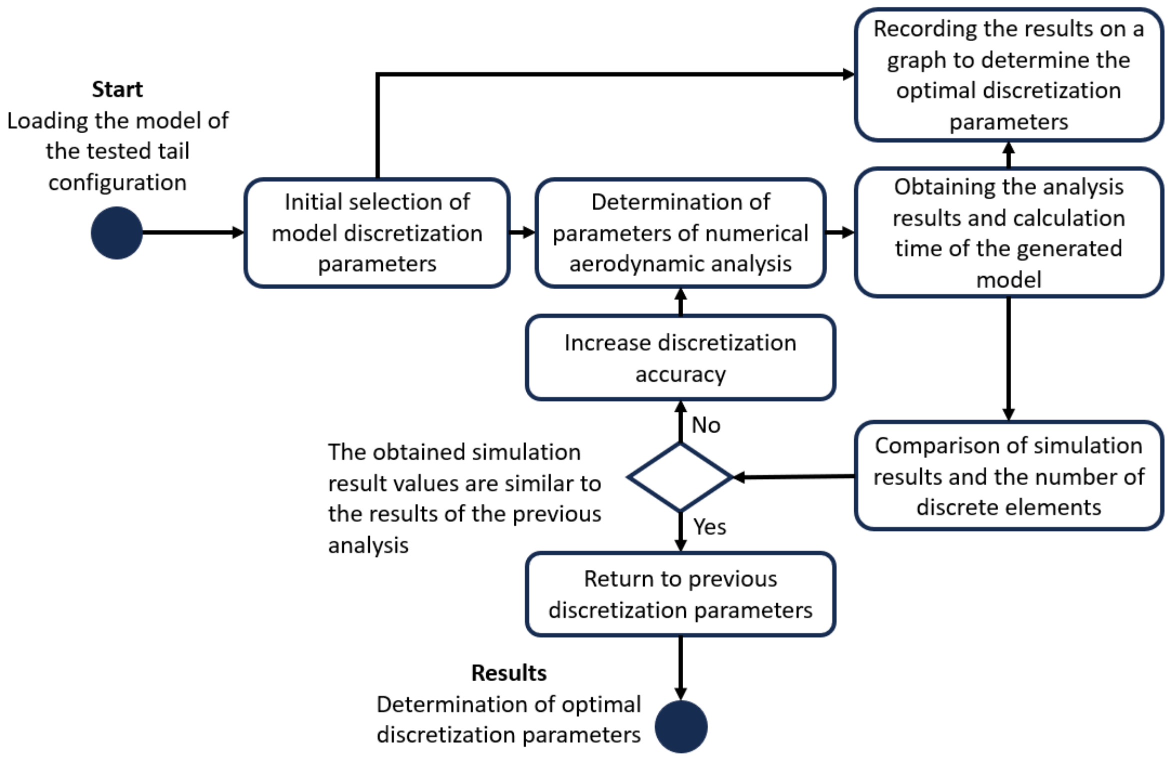

Fig. 53 Discretization Method of the Examined Object

In order to properly select the discretization parameters in the CFX module, it is necessary to consider the type of analysis to be performed, in this case it was an airflow analysis. Then, it is necessary to take into account the geometry of the aircraft under study and the boundary conditions (Mohamed Zouhir Dar Ramdane, Abidat and Hamel 2015, Suchocki, Lampart and Surwiło 2015). For flow analysis, it is important to consider a discrete model that will provide adequate resolution in flow-relevant areas such as separation zones, vortices, or areas of high velocity change. The model must provide sufficient element density to accurately reflect complex flow phenomena while maintaining computational efficiency (Mohamed Zouhir Dar Ramdane, Abidat and Hamel 2015). According to the developed procedure, one of the models developed for the tail concepts under consideration was loaded and discretized with the pre-developed parameters. See Fig. 54.

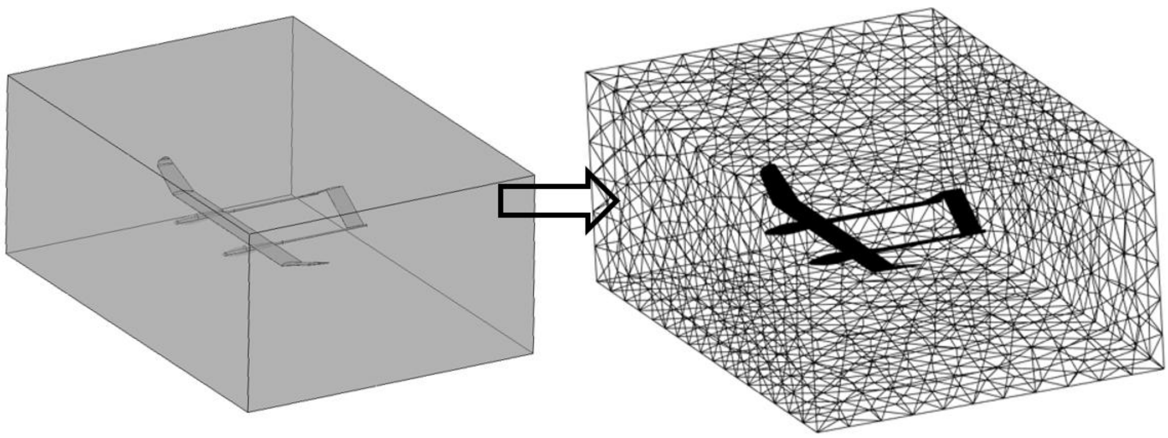

Fig. 54 Discretized model

Determination of the optimal discretization parameters requires following the presented task scheme. Because of this, it was necessary to conduct analyses of the discretized model taking into account the time of CFX analyses and the values of the results. Like any program that allows flow analysis, ANSYS CFX software generates results in a certain approximation to the real system. In order to determine a sufficient degree of approximation, a method based on comparing the results obtained was developed. In successive steps of comparing the obtained results, the number of discretization elements was increased over the entire surface of the test object by reducing the maximum length of their edges. See Fig. 55.

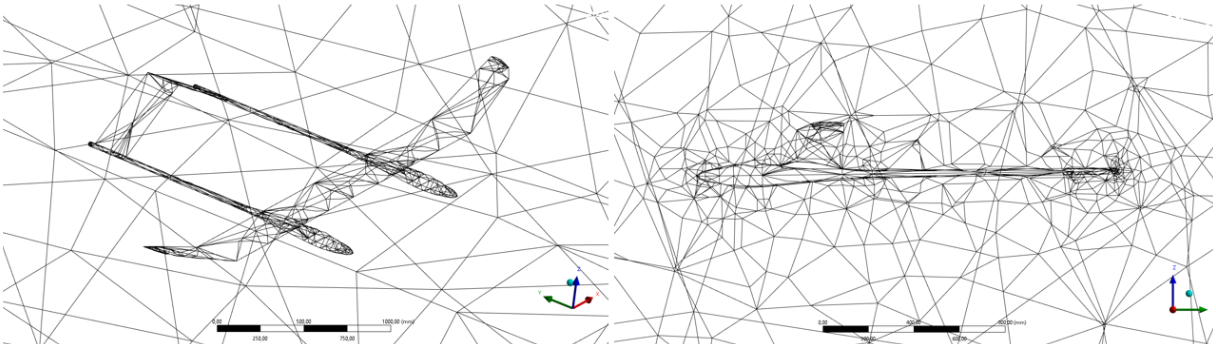

Fig. 55 Model discretized with preliminary parameters

Due to the significant increase in the time-consumption of conducting analyses with the increase in the number of discretization elements, the maximum length of the edges of the elements on the surface of the test object was reduced. Ultimately, the parameter was defined as 5 millimeters. Due to the large number of the study object's round surfaces, the parameter of the maximum approximate plane angle was also determined. It was specified as 2°. The discrete model generated using the described parameters is shown in the Fig. 56.

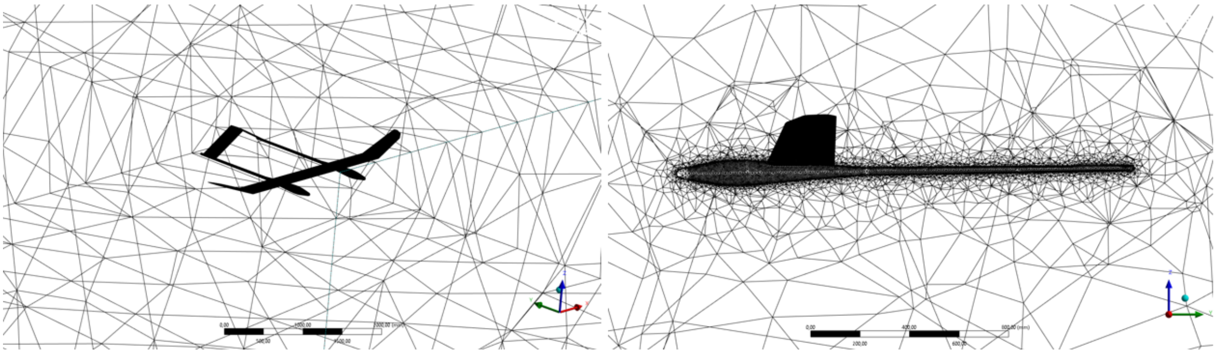

Fig. 56 Discretization based on surface curvature

In the next step, an attempt was made to increase the accuracy of the results obtained on the basis of a local increase in the number of elements. For this purpose, the trailing and leading edges were identified as critical locations under study for the flow. Incorrect discretization along these edges can cause a significant discrepancy in the results obtained. The compaction locations are shown in the Fig. 57.

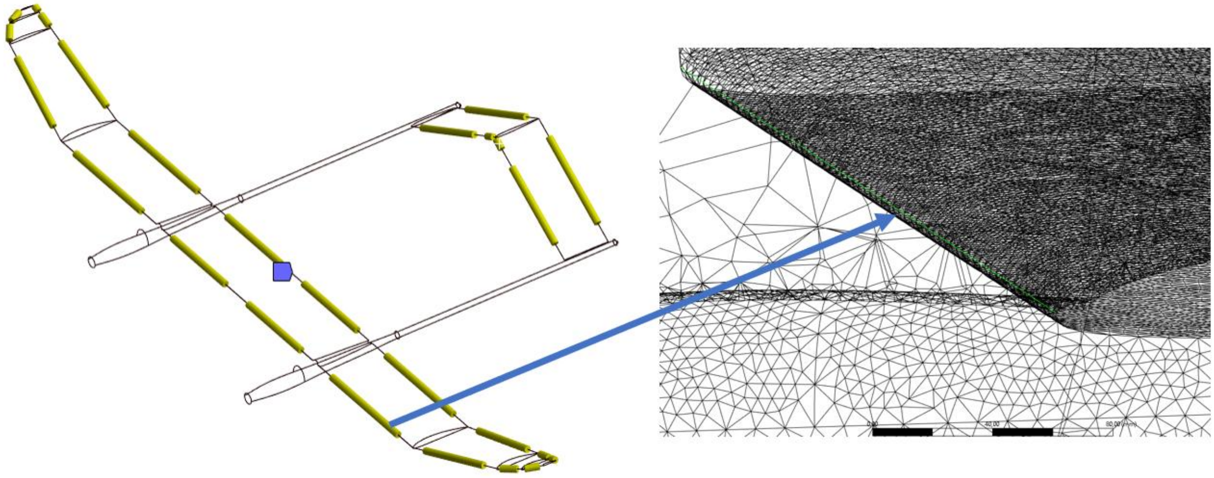

Fig. 57 Determination of edges that reduce the size of the discrete element

Taking into account the method of analysis and the fact that the solid of the test object is cut out of the volume of the medium that constitutes the test element, it was necessary to increase the accuracy of the discrete model of the medium in the wall layers of the test object in the direction of the outer walls of the modeled measurement system. For this procedure, the inflation option was used. It allows to thicken the near-wall layers and create more layers with specific parameters. Analyses related to the dependence of the results obtained and the calculation time allowed to determine the inflation parameters. The near-wall layer was defined at a distance of 0.2 mm from the test object and each subsequent layer was increased by 1.2. In this way, 20 layers were defined around the entire test object. The discretization using the inflation option is shown in the Fig. 58.

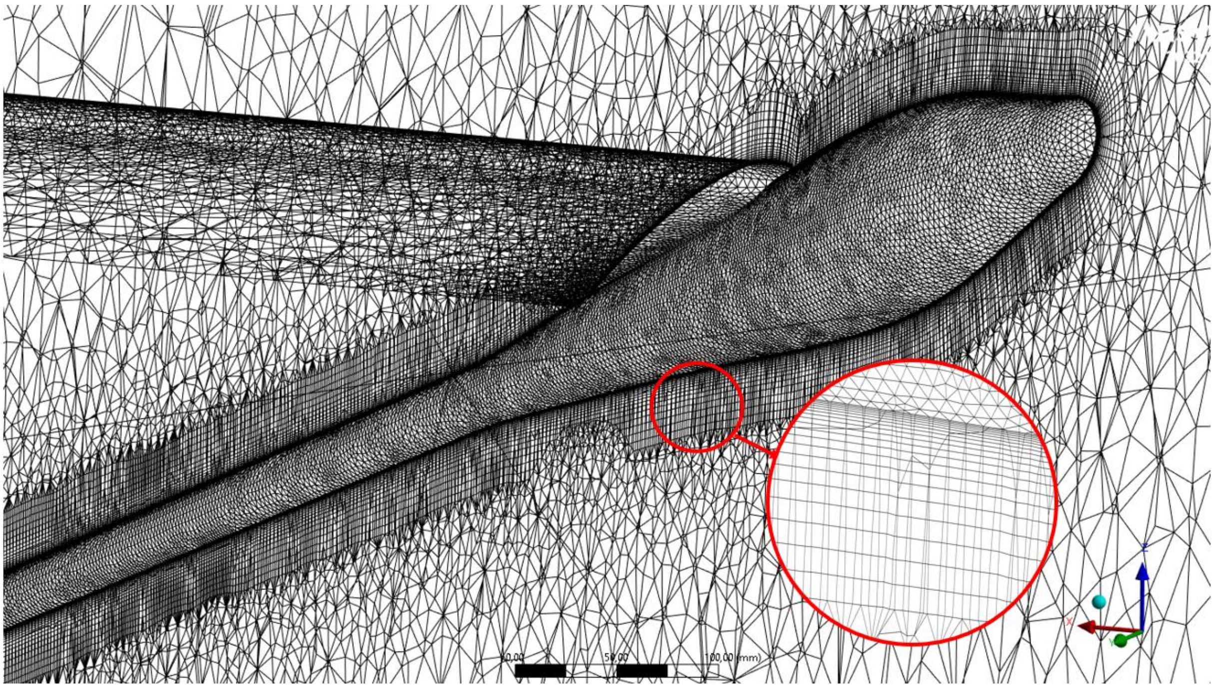

Fig. 58 Specification of Parameters for the Applied Inflation Option

The developed discrete model parameters used for all tail configurations considered, the number of elements and discretizing nodes are shown in Tables Tab 13 and Tab 14.

Tab 13 Discretization parameters

Parameter	Value
Mesh Defeaturing size	5 mm
Curvature Min Size	5 mm
Curvature Normal Angle	2°
Smoothing	Medium
Inflation Option	First Layer Thickness
First Layer Height	0.2 mm
Maximum Layers	20
Growth Rate	1.2

Discrete models prepared on the basis of the above analysis were used in further stages of the analysis.

Tab 14 Obtained parameters of the discrete model

Configuration	I	II	III	IV	V
Number of discretization elements	4,066,697	3,854,331	4,015,891	3,909,853	3,941,412
Number of nodes of the discretization network	1,481,905	1,437,132	1,480,479	1,436,033	1,462,367

5.1.3. Determining simulation parameters and selecting a solver

Analyses conducted in the ANSYS CFX environment require defining the parameters of the study area, the medium in which the analyses are conducted, and selecting a solver based on the appropriate computational hypothesis for the object under study. Knowledge of the critical flight parameters determined from the flight envelope made it possible to determine the flow parameters inside the medium corresponding to the planned mission. They were determined according to the conditions prevailing at a flight altitude of 1,000 meters above sea level and a temperature of 25°C. The adopted parameters are shown in Table Tab 15.

Tab 15 Flight parameters adopted for comparative analyses

Analysis type	Flight speed $[m/s]$	Angle of Attack	Altitude [m]	Air density $[kg/m^3]$	Temperature [°C]
Critical condition 1	19	14	1000	1.12	25
Critical condition 2	22	-5	1000	1.12	25
Critical condition 3	35	0	1000	1.12	25
horizontal flight	14.5	Based on configuration	1000	1.12	25

To identify the appropriate computational solver for the object, an analysis of the maximum Reynolds numbers within the measurement system was conducted. This analysis was based on parameters defined by the profile shape and the chord length at specific section. The properties of the airfoils were determined from the Airfoil Tools (Airfoil Tools 2023) airfoil parameter database. Due to the significant discrepancy in the lengths of the chord profiles of the analyzed wing, the above-described parameter was determined for the key points of the main lifting wing and the tail section. These points are shown in Fig. 59. The results of the analysis carried out are shown in Tab 16.

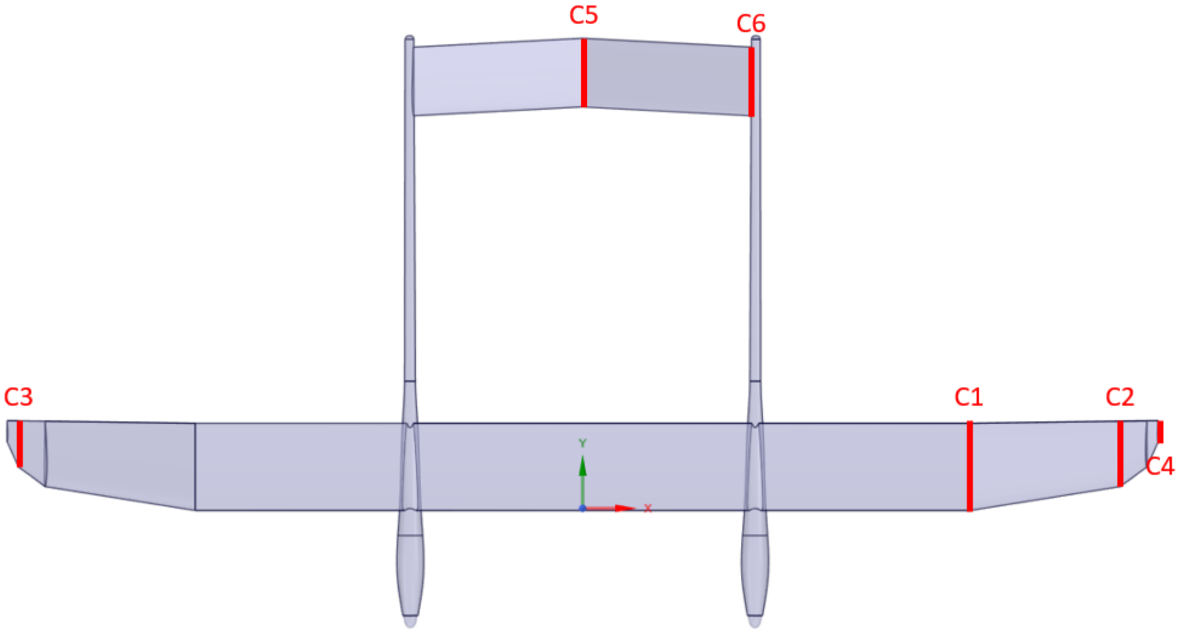

Fig. 59 Representation of the position of the chords for which the Reynolds number was determined

Tab 16 Values of specific Reynolds numbers (Airfoil Tools 2023)

Aerodynamc chord	Chord Length [mm]	Re value
C1	273	672 556
C2	205	505 033
C3	145	357 218
C4	66	162 596
C5	215	497 982
C6	215	497 982

Taking into account the results obtained and the literature research on the issue of selecting a suitable computational model for turbulence analyses, K-Epsilon was determined as a suitable model for the analyzed object. The previously adopted parameters were also determined. See Fig. 60.

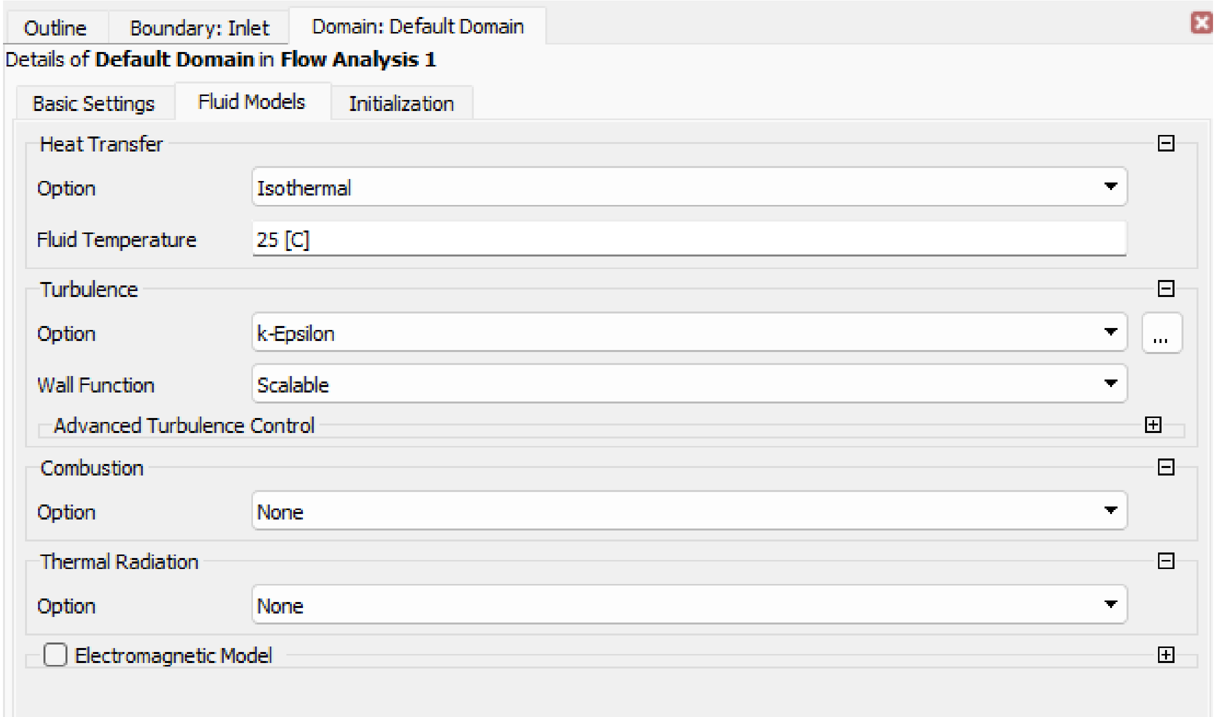

Fig. 60 The applied mathematical model adopted during the analyses

Then, based on the flight mission and Critical Point readings from the flight envelope, three critical flight variants were determined, they are ascent, level flight and descent, and one steady-state flight condition corresponding to the main flight stage during the assumed mission. The parameters for which the analyses were carried out are shown in Table Tab 15.

The specified parameters were consistently applied across all the tail configurations considered. The subsequent step involved defining the parameters of the numerical measurement system. This process required constraining the degrees of freedom in the wind tunnel by establishing the inlet wall, where velocity parameters are specified, and the outlet, where the exit pressure was set to 0 [Pa].

Due to the flow parameters determined during the preparation of the analyses, the type of flow at the inlet surface was assumed to be subsonic, and the amount of turbulence occurring was determined to be normal, according to studies on the adopted computational environment. See Fig. 61.

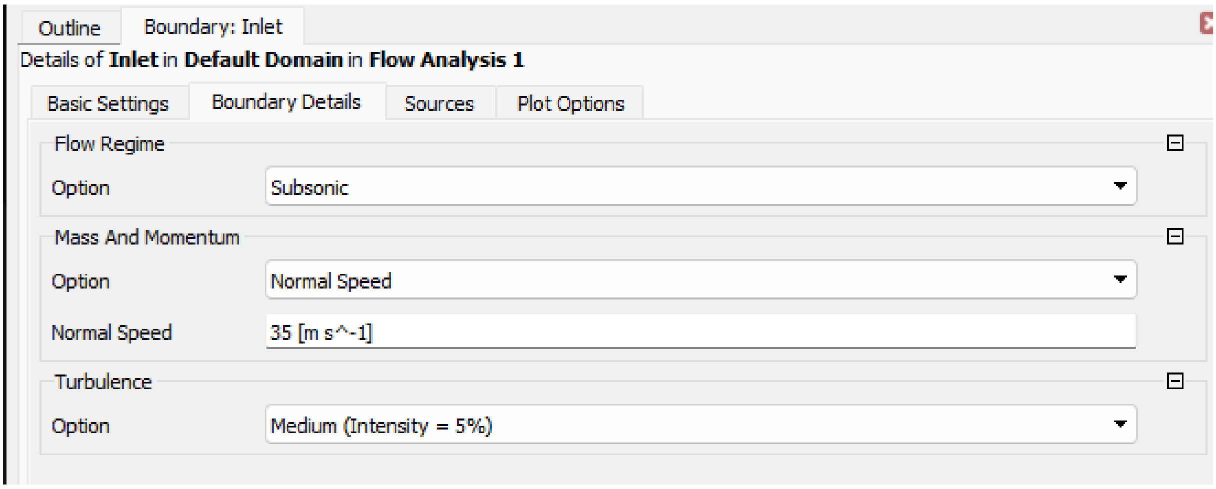

Fig. 61 Determination of airspeed parameters for the modeled wind tunnel

The side surfaces of the modeled test system were defined as permeable walls with constant pressure. The use of this procedure helps prevent local pressure increases at the boundary of the test system caused by the presence of the test object. The parameters are shown in the Fig. 62.

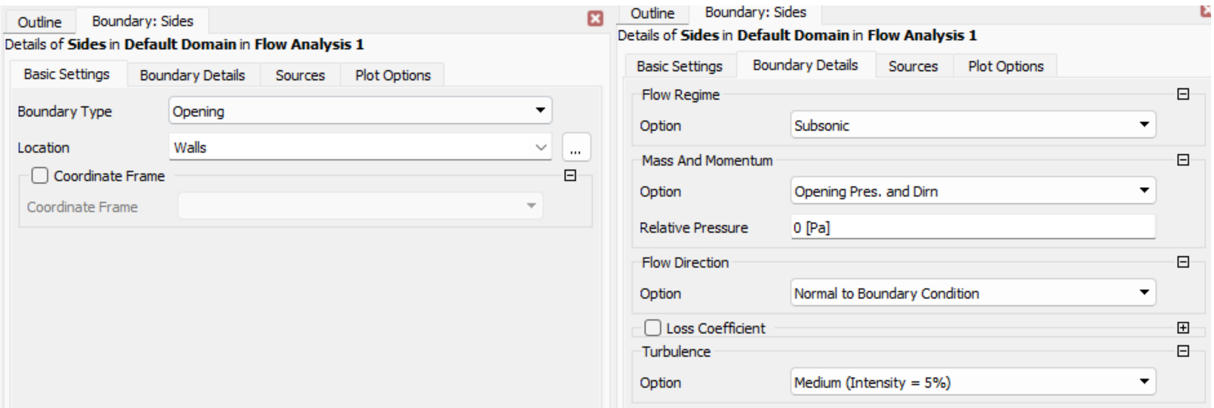

Fig. 62 Determination of the sidewall parameters of the modeled measurement system

The last parameter specified inside the "setup" module is the type of surface of the test object as an impenetrable wall. The final prepared measurement system is shown in the Fig. 63.

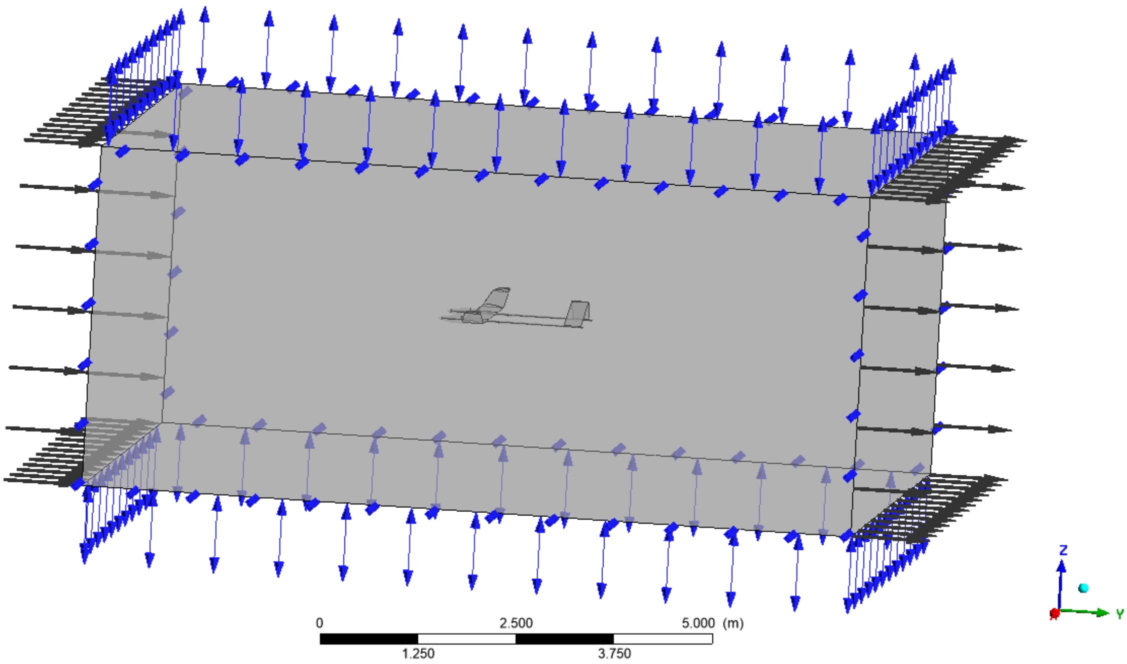

Fig. 63 The measurement tunnel model prepared in ANSYS software with the assumed boundary conditions

The measurement system parameters were established in this manner for each tail configuration model and for all flight states considered. Consequently, all the previously described steps were incorporated into the systems under analysis. This approach necessitates the creation of a distinct solid representing the designated measurement system, modeled as a virtual wind tunnel, with the test object sectioned at the appropriate angle corresponding to each examined angle of attack.

5.1.4. Simulation run

Due to the conduct of comparative analyses and the need to limit the values of variables, each analysis was prepared and run on a single computer. Due to this fact, the influence of hardware parameters on the results obtained was ignored. As part of running the analysis, it is necessary to determine the number of processor cores used during the analysis, determine the type of processor used, graphics processing unit (GPU) or computing processor (CPU). The parameters selected for each of the configurations presented are shown in the visualization. See Fig. 64.

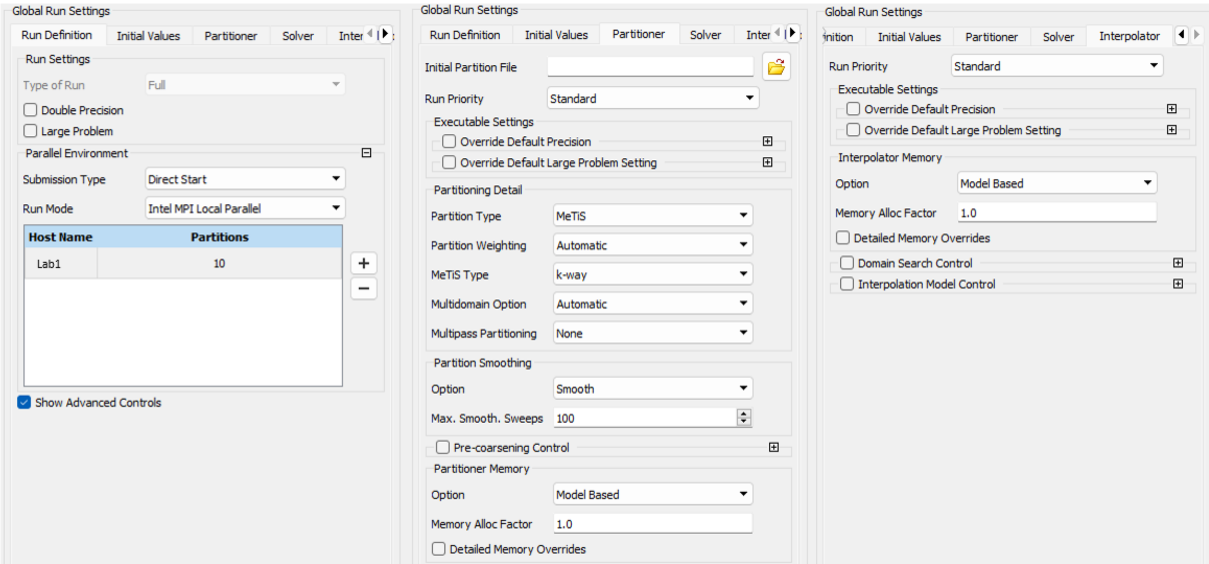

Fig. 64 Parameters for running the conducted analyses

Once initiated, the analysis proceeds for a predetermined number of iterations, known as approximations, or continues until the error value reaches a specified threshold or lower. The progression of error magnitude across successive iterations is illustrated in Fig. 65.

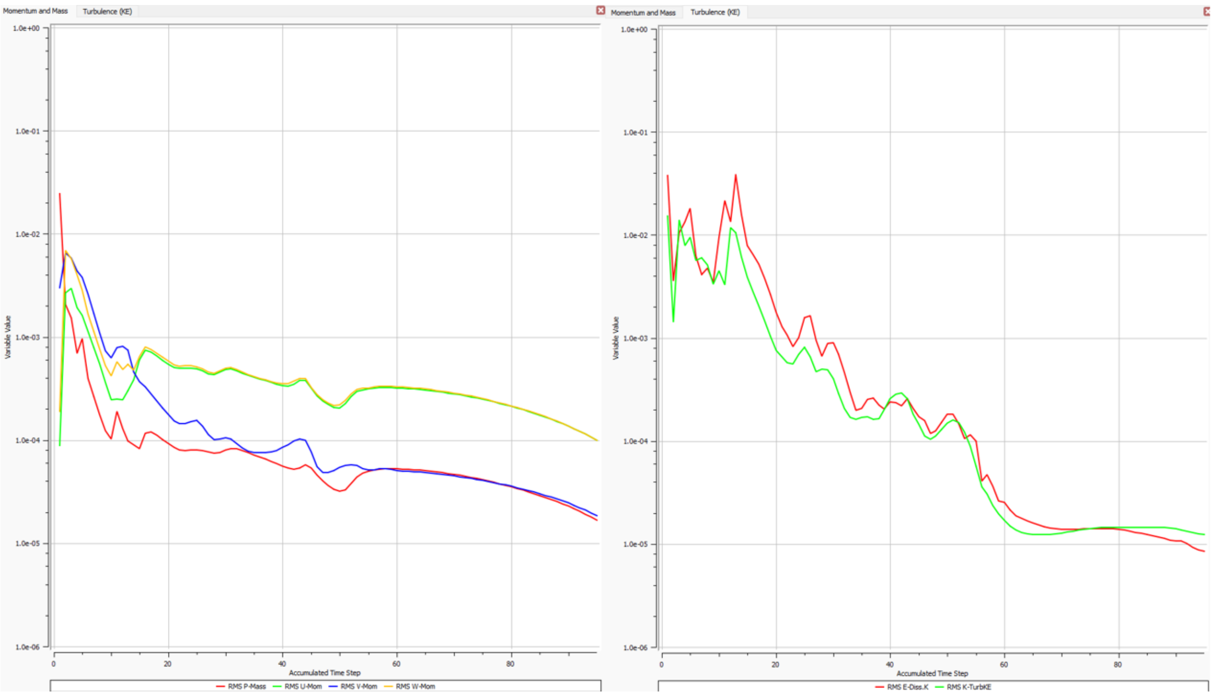

Fig. 65 Graphs of error magnitude against successive iterations of ANSYS software

The results obtained through this process can be further processed and presented in graphical form, numerical data, or as the values of specific parameters of interest. These parameters include maximum pressure, the resultant force along a defined axis, or the pitching moment relative to a particular point within the given coordinate system.

5.1.5. Method of results interpretation

The analysis results are automatically initiated by displaying a pressure distribution map on the object (Fig. 66). This feature allows for the assessment of the accuracy of the obtained results. Understanding the physical phenomena related to the airflow around the wing, which contribute to lift generation, indicates lower pressure above the wing surface and higher pressure below it. This results in a distinguishable pressure distribution across the wing surfaces. Typically, increased pressure can also be observed along the leading edge and forward surfaces of the fuselage, due to the aerodynamic drag generated by these surfaces. Deviations from this expected distribution, or elevated pressures in unanticipated regions, may signal an error in the analysis setup or the results obtained.

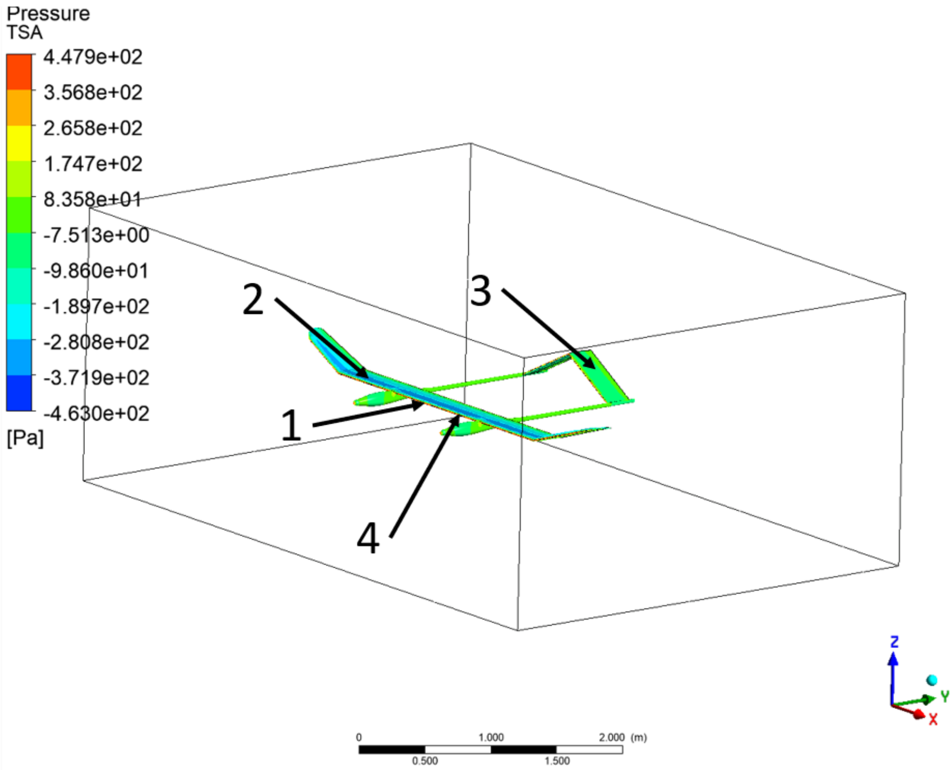

Fig. 66 Pressure distribution on the surface of the test object

Where: 1- high pressure associated with aerodynamic drag, 2- low pressure band as a component of the lifting force, 3- pressure distribution close to the medium in which the analysis is conducted, visualizes the small aerodynamic drag caused by the side surfaces, 4- high pressure band as another component of the lifting force generated by the flow of the medium around the main support plane.

The analyses conducted in the above work focused on parameters related to flight stability. Due to this fact, values such as aerodynamic drag, generated lifting force and inclining moment relative to a given point in three planes were read. In order to obtain the above values, it is necessary to introduce the functions necessary to read them.

force_y()@TS

force_z()@TS

The parameters thus obtained were used to conduct comparative analyses of the tail configurations studied.

5.2.XFLR5 simulation development

XFLR5 is a tool for analyzing airframes, wings and aircraft (XFLR5 2023). The tool allows for direct and inverse XFoil analysis, and the ability to design and analyze wings based on lift line theory, vortex mesh method and 3D panel method. Wing modeling in the XFoil module is designed for two-dimensional anlaysis of the wing profile itself and the tail unit (Fig. 67).

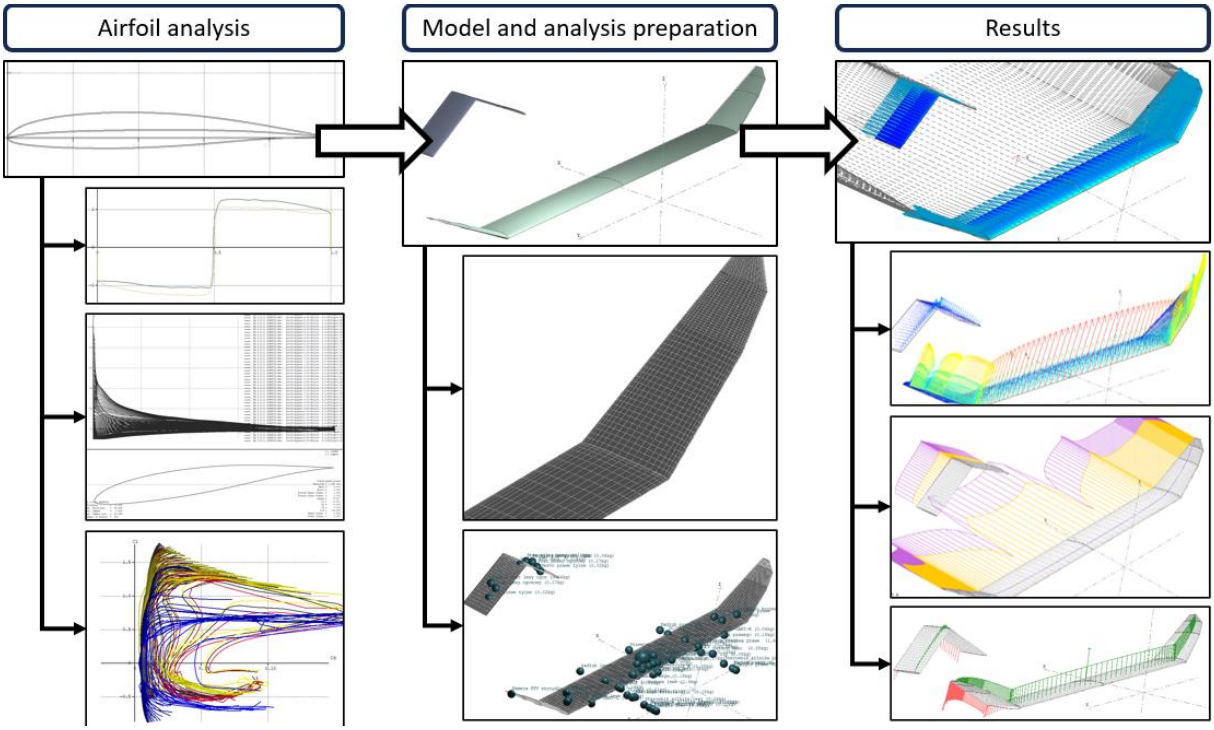

Fig. 67 XFLR5 analysis options

5.2.1. Analysis methods in the XFLR5 environment

Based on the literature review in Chapter 3.4.2 on the program and the instructions on the vendor's website, it is possible to identify applications for the following methods:

- Lifting Line Theory (LLT)
- Vortex Lattice Method (VLM)
- 3D Panel Method

In summary, the aforementioned methods differ primarily in their applications, complexity, and the accuracy with which they are able to represent actual aerodynamic flow. The 3D Panel Method was selected for further analysis, it offers the highest accuracy for modeling complex aerodynamic configurations. Due to the complexity of the analysis itself, it was necessary to determine the points describing each of the selected airfoils, and to conduct tests on the distribution of forces on the selected airfoils depending on the Reynolds number considered.

5.2.2. Preparation of simulation models

Using the XFoil direct analasys module, the aerodynamic profiles used to map the airfoil and tail for the subject of research were modeled. The aerodynamic profile adopted based on the assumptions presented in Chapter 2 was mapped in the XFLR5 environment. See Fig. 68. The aerodynamic profiles thus mapped were discretized to increase the speed of analysis while maintaining adequate accuracy of the obtained results.

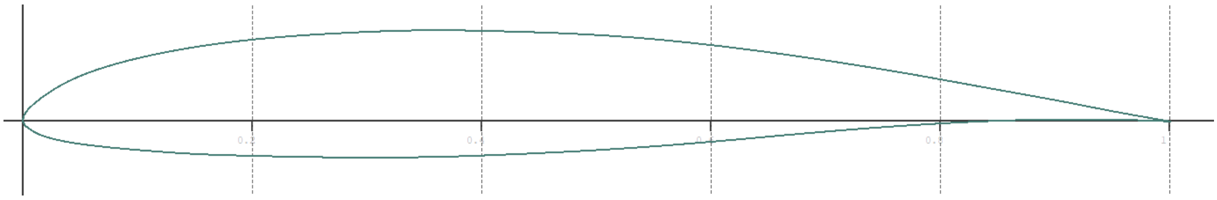

Fig. 68 XFLR5 wing profile readed from excel file

The mapped profile was then pre-discretized to increase the accuracy of the analysis results. The discretized model was used to determine the parameters of the profile's load carrying capacity, aerodynamic drag and inclining moment. Increasing the accuracy of the discretization points is done automatically and the compaction itself usually occurs in the vicinity of the leading edge and trailing edge. Each of the airfoils considered was divided into two hundred shape mapping elements. An example of the distribution of points describing the curvature of one of the analyzed airfoils is shown in the Fig. 69.

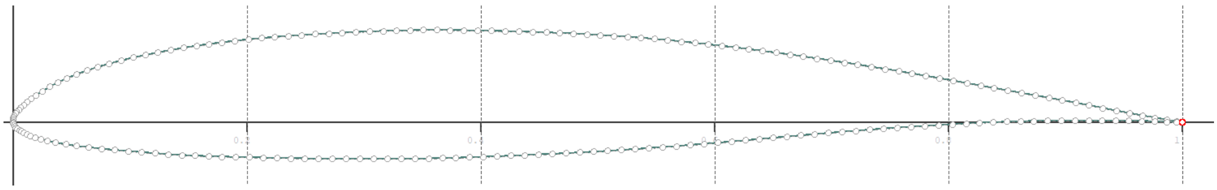

Fig. 69 Profile element modiffication

In this way, analyses were prepared for each of the aerodynamic profiles used in the model. Due to the fact that the analyses were conducted on the global model of the tail configuration under study, each of the profiles considered was analyzed in an identical range of Reynolds numbers. This procedure avoided measurement errors associated with the different considered flow velocities affected by the specified Reynolds numbers. An example of the result of the analysis of one of the airfoils for a specific angle of attack is shown in visualizations Fig. 70 and Fig. 71.

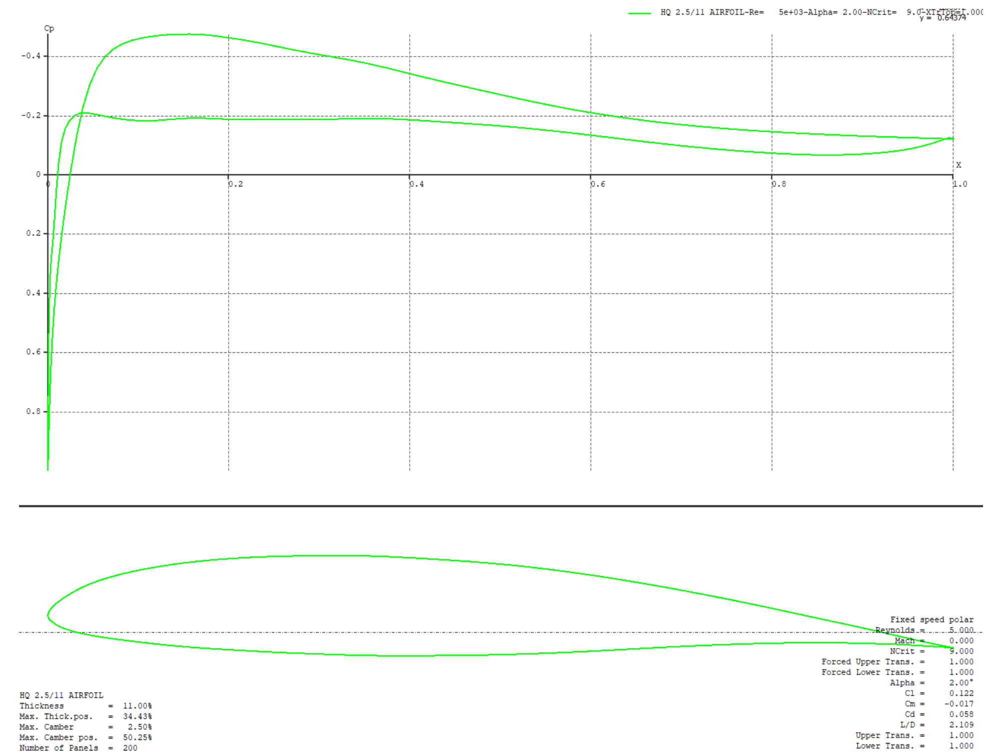

Fig. 70 Wing profile example in Xfoil software

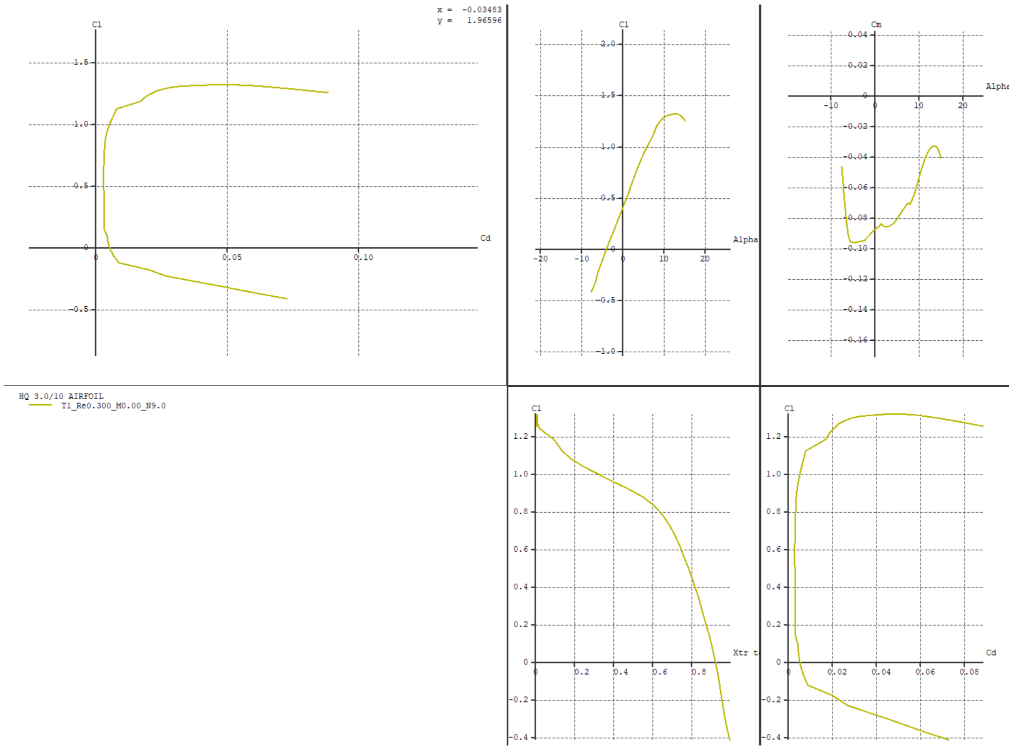

Fig. 71 Xfoil analysis result example

Each of the profiles was considered in the Reynolds number range from 5,000 to 10,000,000. Due to the multiplicity of the analyses carried out, the Reynolds number jump was not determined linearly and was related to the length of the individual chords of the lobes of the object under consideration at the point of the jump in their size. The method of determining the count parameters is shown in the Fig. 72.

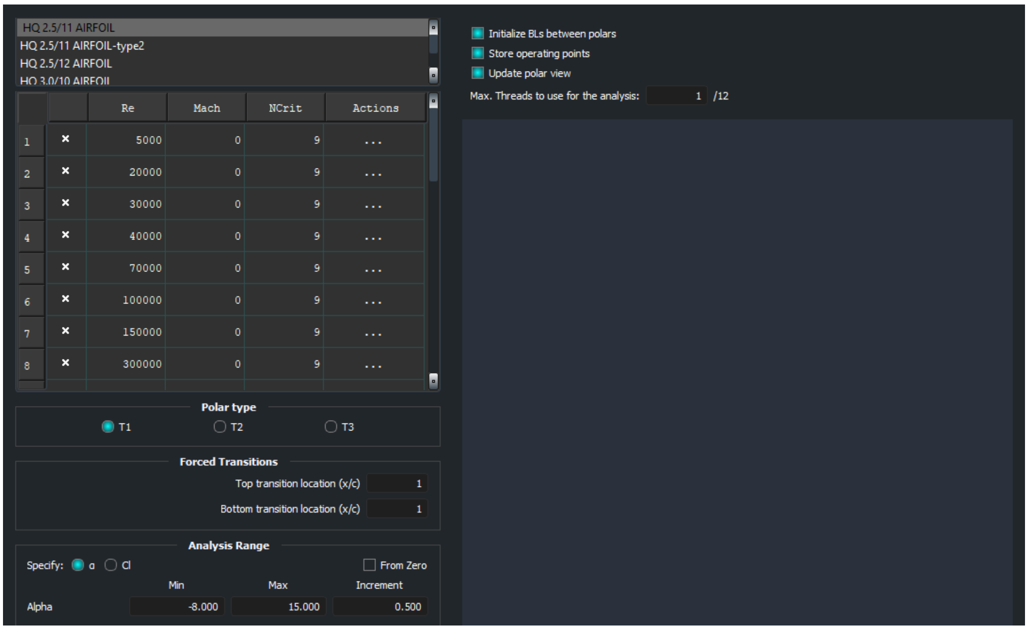

Fig. 72 Reynolds number based analysis for each of used wing profile

The analysis conducted for a large number of profiles, Reynolds numbers considered, and angles of attack ranging from -8˚ to 15˚, with increments of 0.5˚, requires the preparation of a combined analysis using the "Bach Analysis" function. The waveforms of the analyzed parameters are shown in the Fig. 73.

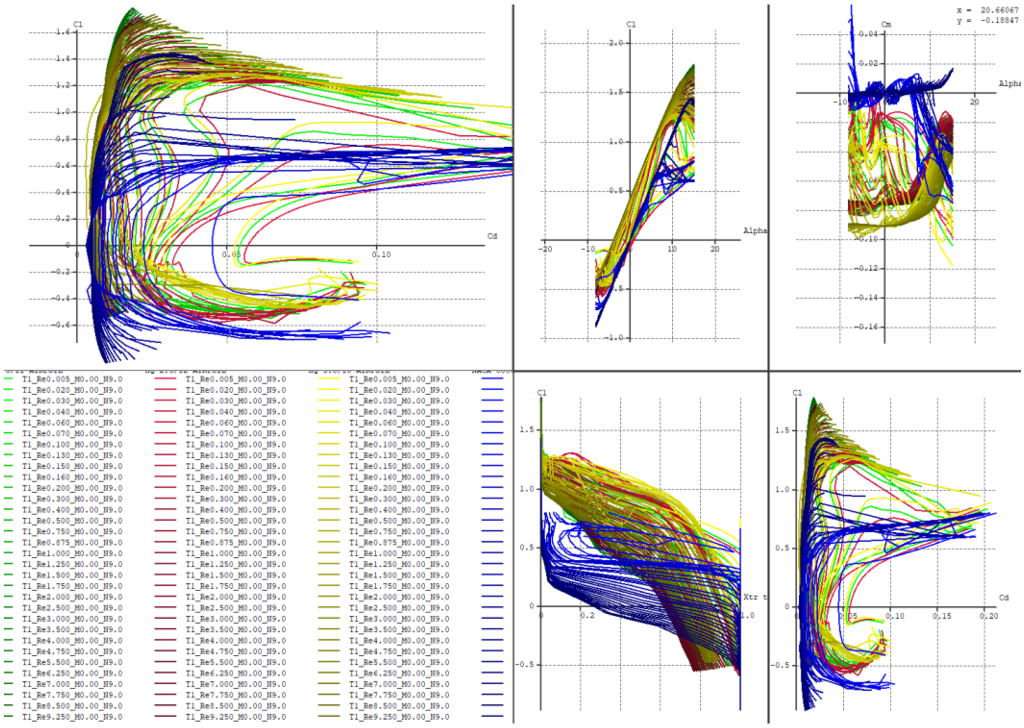

Fig. 73 Prepared Reynolds number analysis results

The next stage of the model preparation was the transition from the "Wing and Plane design" module, in which models of the objects under study are built on the basis of predetermined aerodynamic profiles, taking into account the distance from the origin of the adopted coordinate system. Due to the impossibility of mapping fuselages in the models, and thus considering their impact on the studied object, it was decided to omit these elements. Taking this limitation into account, the models were prepared using only the "Main wing" and "Elevator" elements. See Fig. 74.

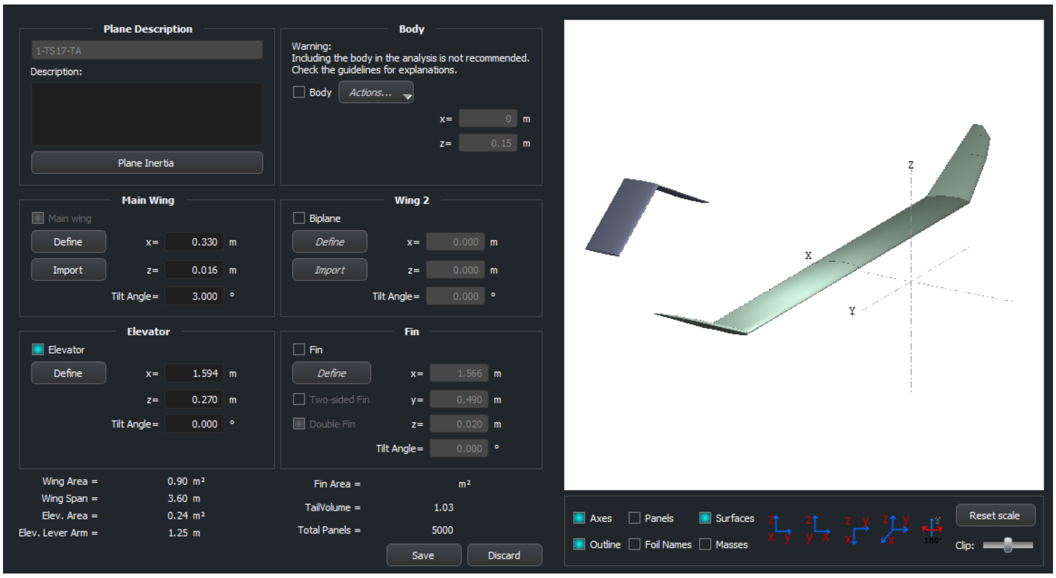

Fig. 74 Model prepared in XFLR5 enviroment

The mapping of the tail part was performed using the "Elevator" option thanks to the ability to specify the surface at a certain angle to the plane of symmetry of the object under study. During modeling, the adopted aerodynamic profile and its location in the coordinate system of the tail section are determined. See Fig. 75. The tail section is then placed in the global coordinate system of the object under study.

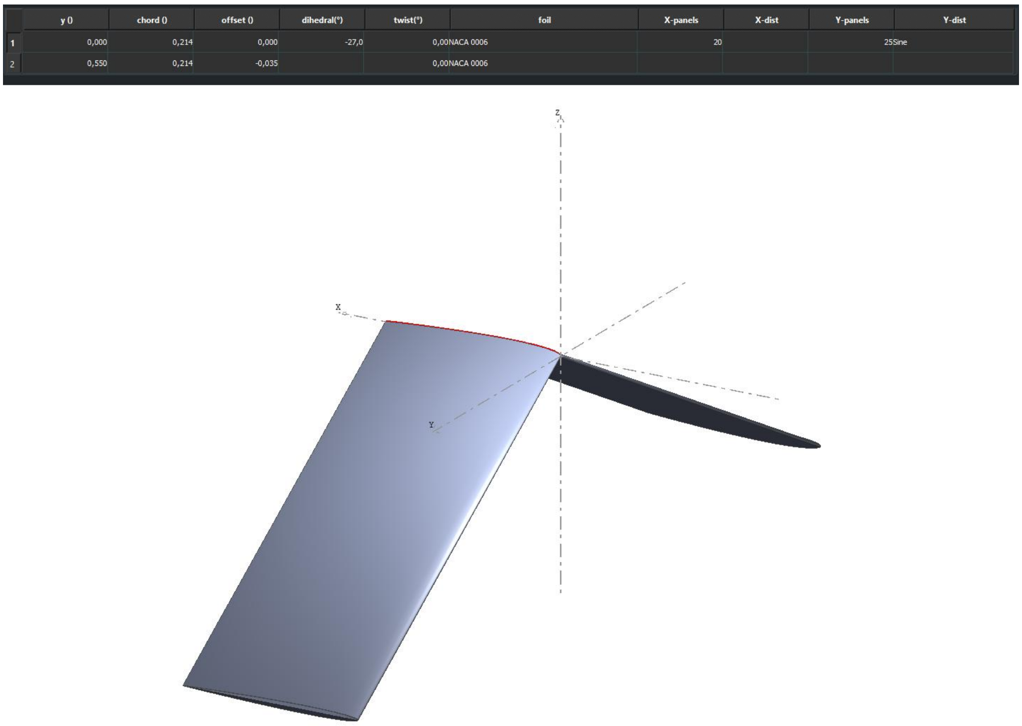

	y ()	chord ()	offset ()	dihedral(°)	twist(°)	foil	X-panels	X-dist	Y-panels	Y-dist
1	0,000	0,214	0,000	-27,0	0,00	NACA 0006	20		25	Sine
2	0,550	0,214	-0,035		0,00	NACA 0006				

Fig. 75 Tail unit model prepared in XFLR5 enviroment

Due to the analysis assumptions outlined in subsection 4.6, the control surfaces were not mapped in the model. Flight stability analyses developed in the XFLR5 environment require determining the position of the center of gravity of the analyzed object. Taking into account the capabilities of the adopted environment, the determination of the position of the center of gravity was done by determining the assumed masses of all components and their position relative to a specified coordinate system. The method of proceeding and the method of determining the location of the center of gravity in a given environment converges with the analytical methods presented in subsection 4.3. Parameters are determined in the "Wing and plane design" module using the "Define Inertia" option. See Fig. 76.

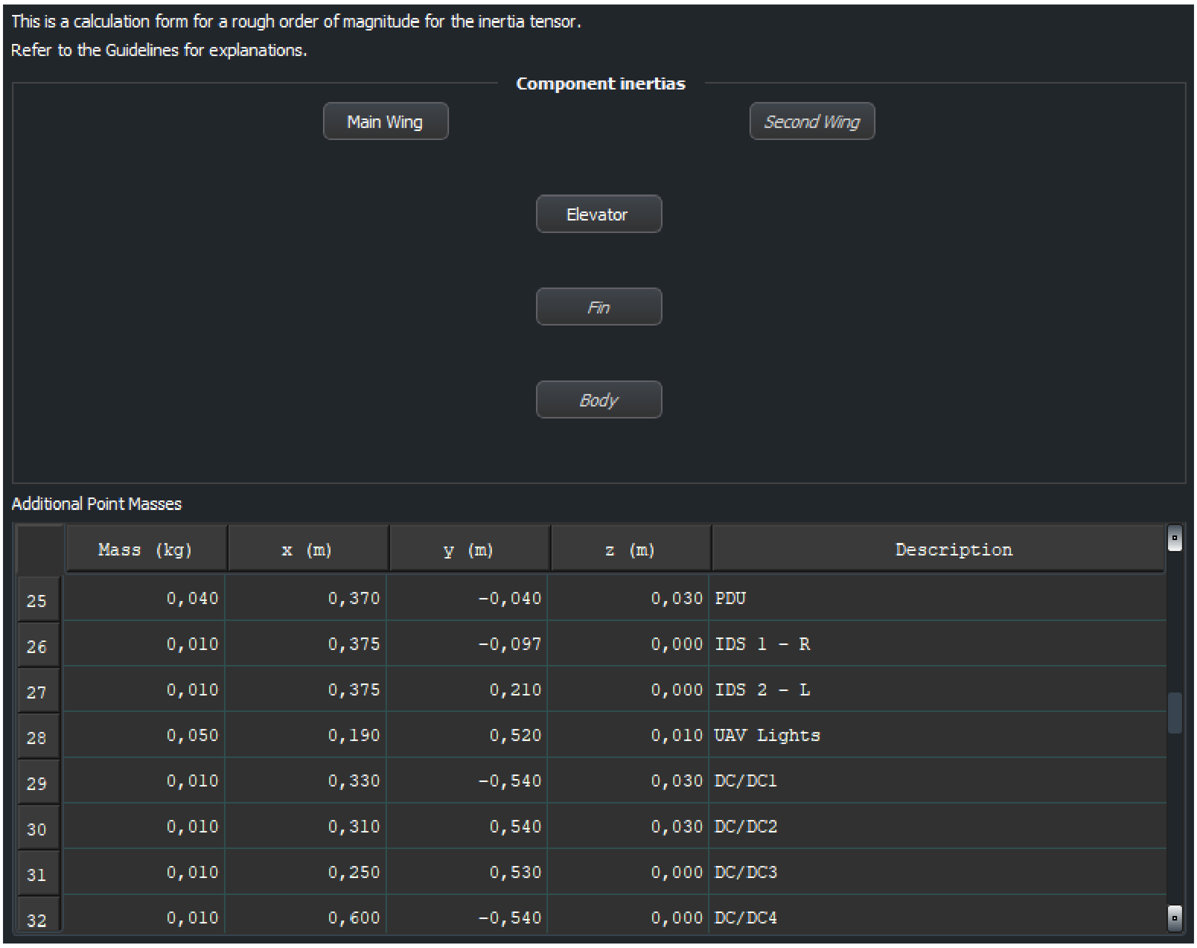

Fig. 76 Mass points modelled in XFLR5

The impossibility of mapping the structure inside the object under study and the type of materials used made it necessary to determine the masses and positions of the centers of gravity of elements such as wings, fuselages and the tail section. After mapping all the elements of the object under consideration, information such as the total mass of the object, the position of the center of gravity in the adopted coordinate system, moments of inertia of the object under study is obtained. The parameters are calculated automatically and presented in Fig. 77.

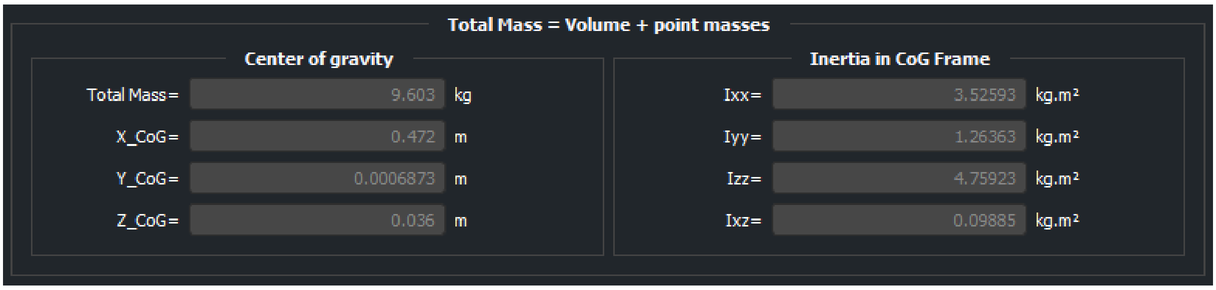

Fig. 77 CG position and airplane weight calculated in XFLR5

The correctness of the adopted distribution of electronic components can be determined from the visualization launched in the "Wing and plane design" module. By enabling the "Masses" option in the specified coordinate system, the points defining the components described in the previous steps of the analysis are visualized. An example representation of the mass distribution of the analyzed object is shown in the Fig. 78.

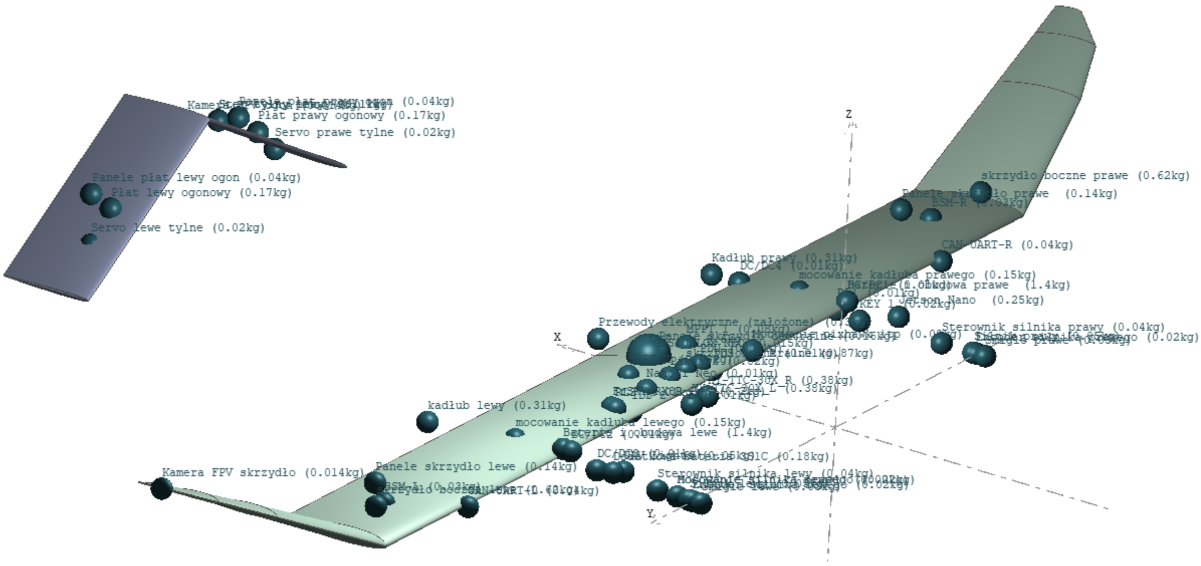

Fig. 78 All mass points addet to XFLR5 model

The model thus prepared was finally checked for mass distribution and compared with technical drawings of the test object. As a result, an adequate representation was found. The model was then discretized.

5.2.3. Discretization of models

Discretization of models prepared in the XFLR5 environment is performed using the 3D Panel Method. Discretization of models using this method allows for accurate aerodynamic analysis, and involves dividing the aircraft surface into smaller segments, called panels, which are analyzed separately. The panels are protocoque in shape and form the discretized geometry of the UAV.

The density of the discretization mesh is adjusted manually, adjusting the number of panels along and across each section of the model to increase the accuracy of calculations in areas under consideration, such as tail surfaces or wings. Visualizations of the change in density of the wing discretization elements are shown in visualization Fig. 79.

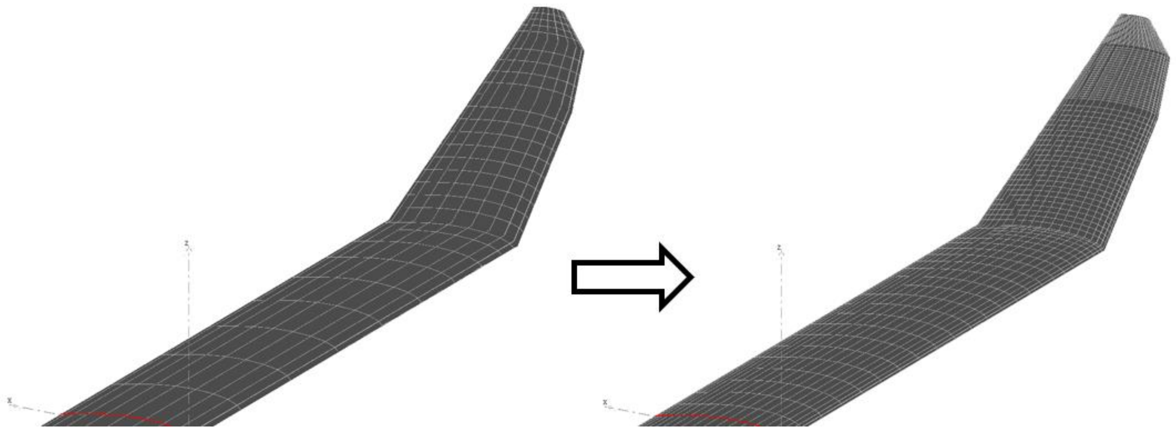

Fig. 79 Model discretization in XFLR5

Due to the XFLR5 environment and the way models are built, it is not possible to condense the number of discretization elements at specific locations on the flap along the chord. The distribution of components is invariably symmetrical, as is the shape of the discretizing elements.

The determination of the correctness of the discretization parameters of the model of the object under study was carried out in a manner consistent with the methodology for analysis conducted in the ANSYS environment presented in the subsection 5.1.2.

When preparing the object for numerical analyses, the change of the tail section was taken into account as the only variable. Due to this, the model of the main lifting flap was invariant and its discretization parameters were fixed. The discretization parameters of the tail section were determined to be constant along the tail section chevron, while due to different configurations they were variable based on the length of the airfoil from the plane of symmetry taking into account the displacement along the height of the tail section. An example of the distribution of tail section discretization elements is shown in the Fig. 80.

	y ()	chord ()	offset ()	dihedral(°)	twist(°)	foil	X-panels	X-dist	Y-panels	
1	0,000	0,214	0,000	-27,0	0,00	NACA 0006	20		25	Sine
2	0,550	0,214	-0,035		0,00	NACA 0006				

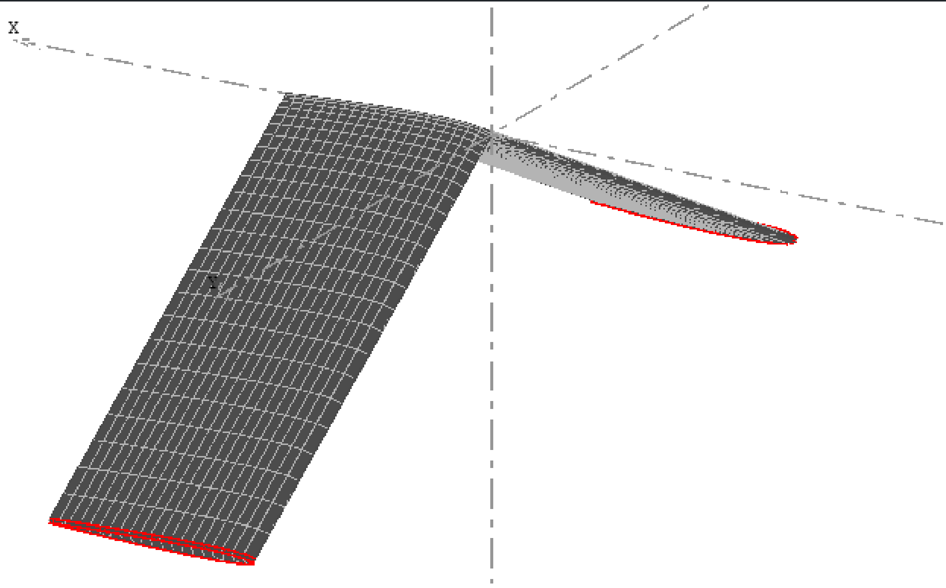

Fig. 80 Tail unit mesh covered model

The final object prepared for analysis is shown in the Fig. 81.

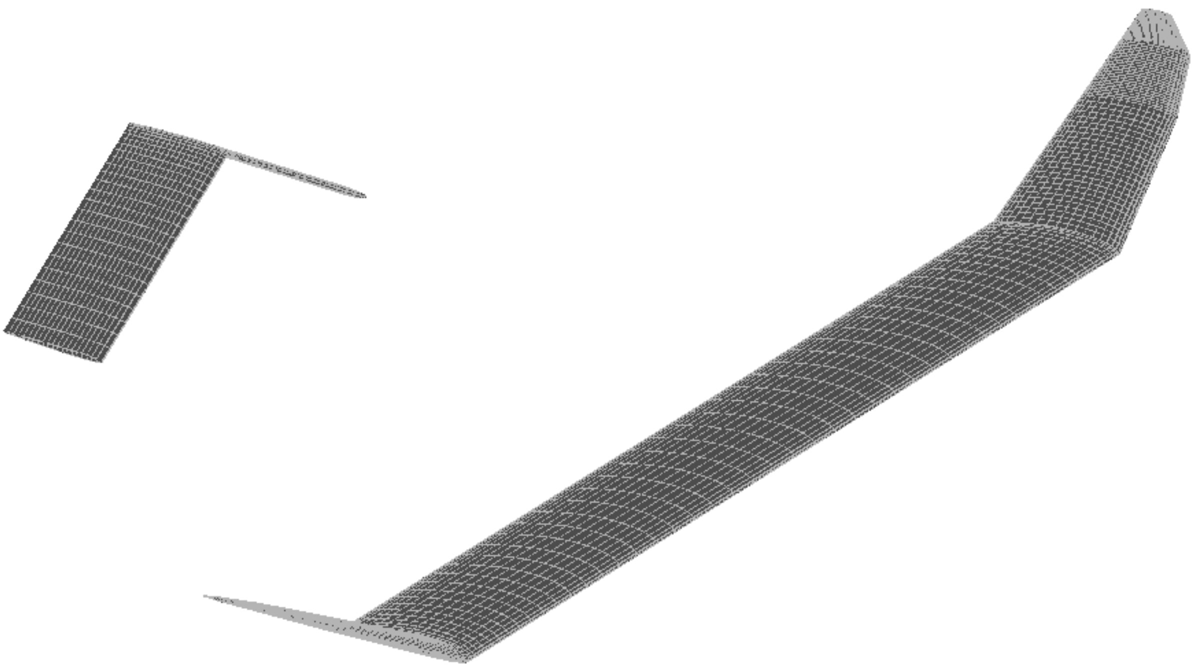

Fig. 81 XFLR5 3D model prepared for analysis

5.2.4. Determining simulation parameters and selecting a solver

The simulation parameters were determined according to the assumptions presented in subsection 5.1.3. The XFLR5 environment requires specifying the parameters of the medium in which the mapped geometry is studied. These are parameters such as temperature and flight altitude. Based on these parameters, the software determines other necessary parameters of the medium for analysis. Regardless of the type of analysis being conducted, the software requires that these parameters be determined. Examples of these parameters are shown in the Fig. 82.

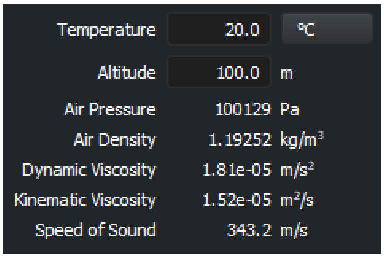

Fig. 82 Air parameters imput for XFLR5

The next step in the selection of simulation parameters is to determine the type of analysis to be conducted depending on the parameter being sought. During the analyses, the assumption of constant airspeed and variable angles of attack (Type 1 analysis) and angular inclination with respect to the direction of flight (Type 2 analysis) was made. See Fig. 83.

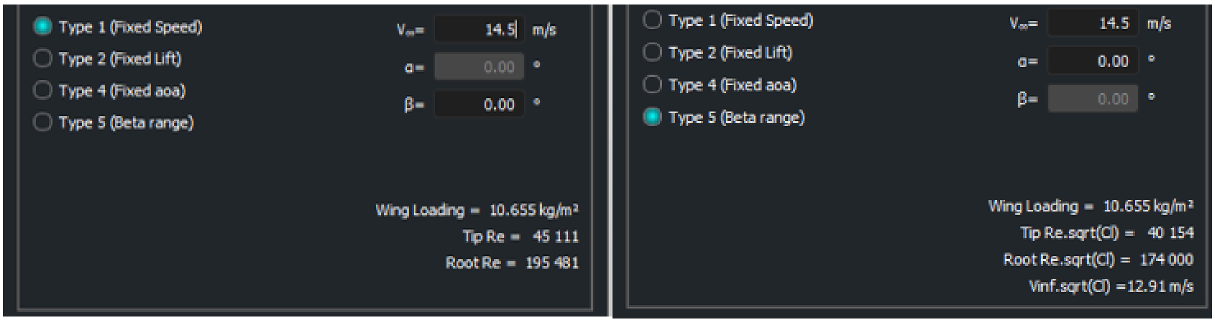

Fig. 83 Airflow parameters

Depending on the type of analysis selected, it is possible to specify the analysis model. Guidelines for selecting this parameter are presented in Section 3.4.2. The software also recommends the use of particular functions for the parameters adopted at earlier stages. The selection window for the described function is shown in the Fig. 84.

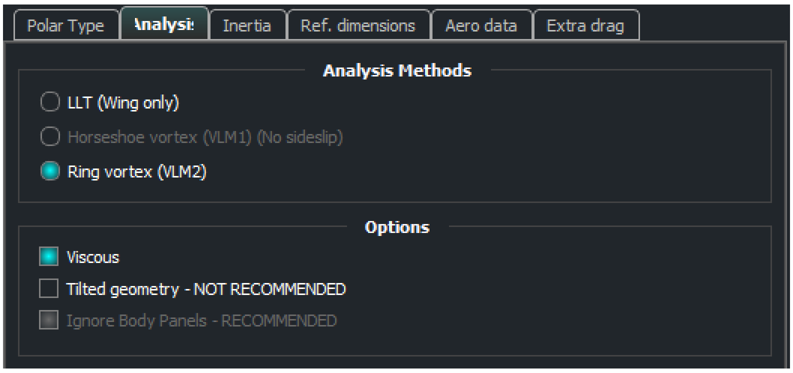

Fig. 84 XFLR solver used for analysis

Using the "Define analysis (advanced users)" function, it is possible to set all the parameters relating to the simulation in one place. Using this option allows to run functions normally unavailable for given analyses. The selection window is shown in the Fig. 85.

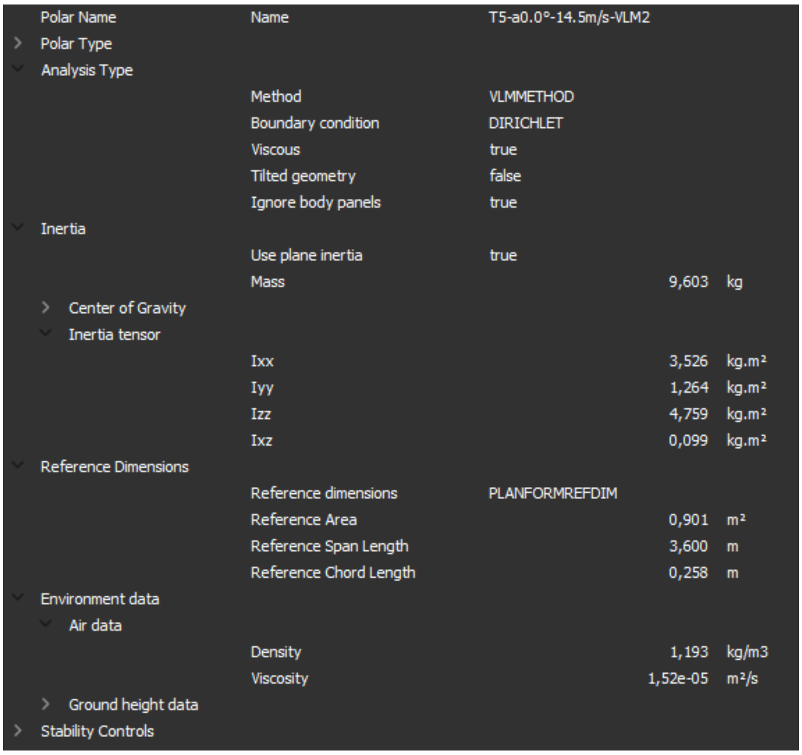

Fig. 85 Extended options used for analysis in XFLR5 enviroment

The analysis prepared in this manner is integrated into the model as a potential computational scenario.

5.2.5. Simulation run

The software allows specifying multiple analyses on a single prepared model. Due to the comparative type of analyses carried out, analyses in line with those carried out in the ANSYS environment were prepared first. According to the requirements of the individual analyses, the extreme parameters for the sequential test and the pitch value are then determined. As in the case of the analysis with variable angle of attack, the minimum angle (including negative ones), the maximum positive angle and the pitch of the change in angle of attack are determined. See Fig. 86.

Fig. 86 Pitching analysis based on alpha angle change

The running analysis loads the initially specified geometric and mass parameters of the model, the parameters of the medium and the variables, and then performs the specified calculations. The method of starting up and obtaining results is shown in the Fig. 87.

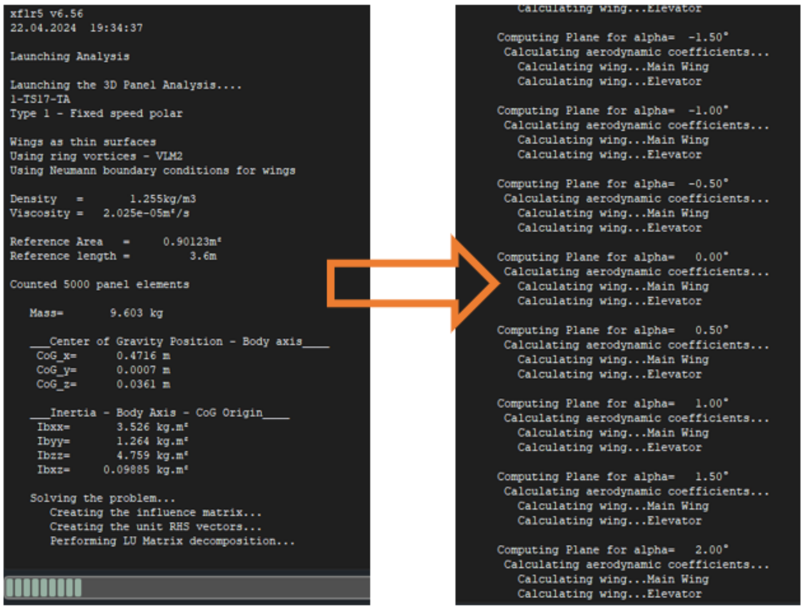

Fig. 87 XFLR5 calculations screens

5.2.6. Method of results interpretation

The analyses were conducted guided by the stability of horizontal flight. To this end, a series of tests were performed for an assumed flight speed and a variable angle of attack of the test object with the tail configurations considered. The planned outcome of the study was to determine the angle of horizontal flight for each configuration under the specified flight conditions. This made it possible to conduct comparative studies against the ANSYS computing environment.

The assumption of stable horizontal flight is the overlap of the position of CG and CA points in the defined coordinate system. With this assumption, the angles of attack of horizontal flight are determined. The angles of stable horizontal flight can also be read from the Cm/Alpha plot, where the point of intersection of the plot with the vertical axis (Cm) determines the angle for which the tilting moment of the analyzed object is zero. This ensures that the object under study is longitudinally stable. Example graphs for UAV analysis are shown in the Fig. 88.

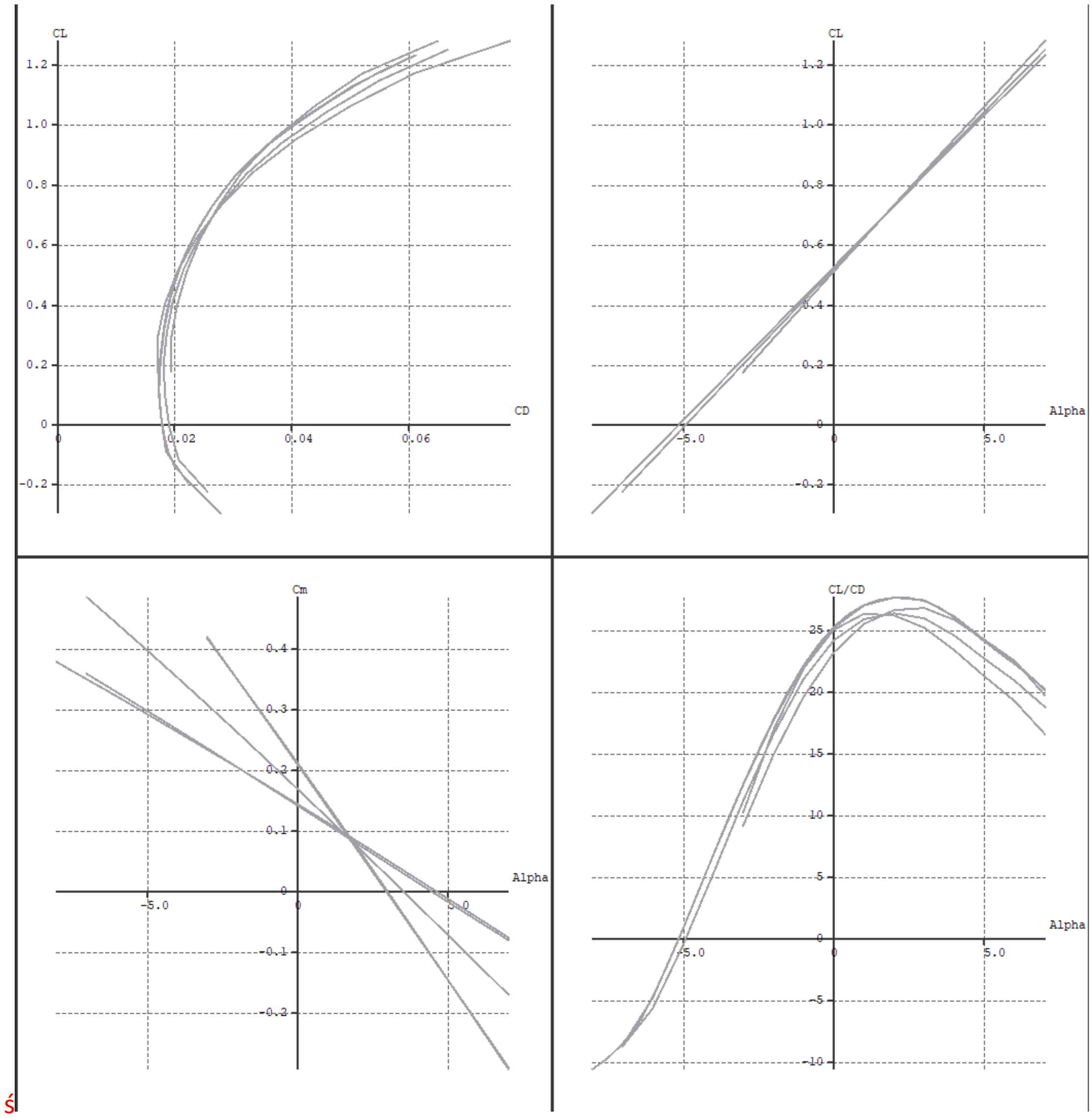

Fig. 88 XFLR5 result graphs

The XFLR5 environment allows reading many parameters of the object under study. They are presented in the form of graphs as in the above visualization, tables of results generated by the program, in which specific parameters are placed for given flight conditions, or graphical, such as maps of pressure distribution, forces generated on each of the analyzed nodes of the discrete model or aerodynamic drag. Some of the visualized parameters are shown in the graphic Fig. 89.

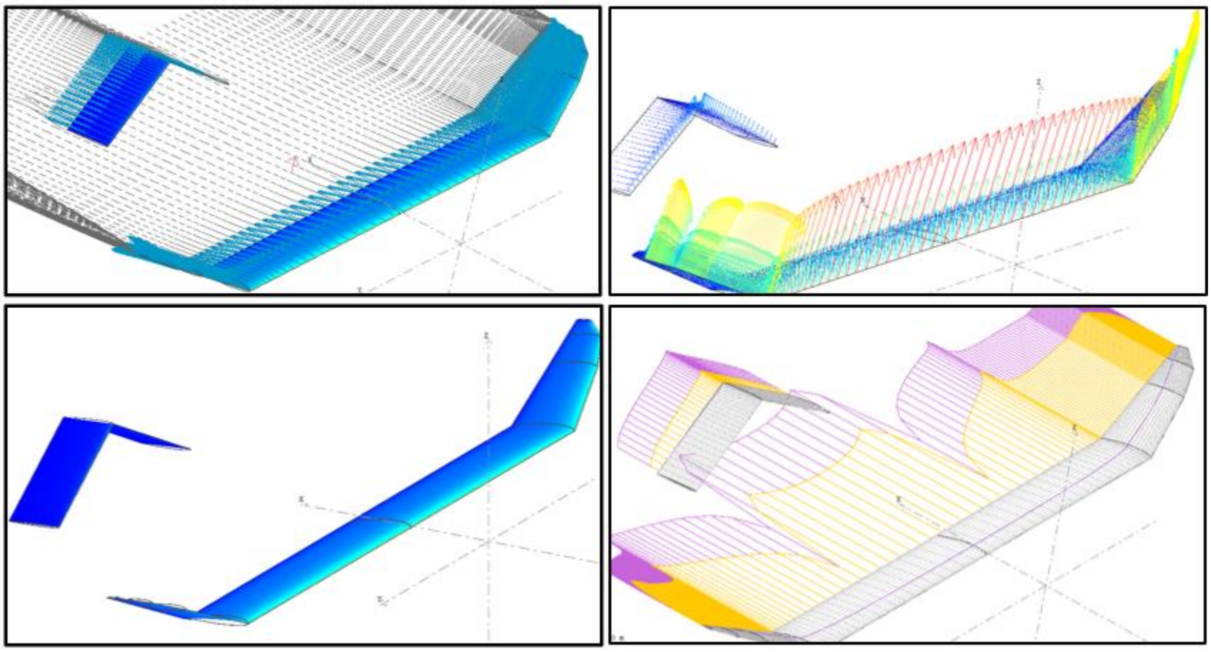

Fig. 89 XFLR5 3d model analysis results visualizations

Based on the analyses conducted for all models of the object under study, a set of angles of attack was determined for which the objects in question were in equilibrium. This angle of attack and velocity were then entered into the ANSYS environment to prepare comparative studies with the XFLR5 environment.

5.3. Analytical study

The first step of the analytical study was the collection of data obtained during flight tests. Aerodynamic parameters were determined based on certain parameters, such as flight speed, wind speed and direction, the empty weight of the object during test flights, the type of propulsion system used and the like. The parameters are shown in the table (Tab 17). With this procedure, an iteration of the numerical models was performed and the software whose results were closest to the data obtained during the test was determined.

The key parameters read during the tests are the following for the analysis to be carried out:

- Flight parameters: speed, altitude, angle of attack, glide angle,
- Sensor readings: forces and moments acting on aircraft, control responses,
- Aircraft reactions to disturbances: how the aircraft reacts to changing weather conditions, steering maneuvers.

The collected data was subsequently analyzed using the equations of flight dynamics. The equations of motion were derived to identify the forces and moments acting on the UAV, while static stability was assessed by examining angles of attack, sideslip, and their disturbance responses. Based on test data provided by the pilot-operator, Dr. Eng. Wawrzyniec Panfil, the lift coefficient (*CL*), drag coefficient (*CD*), and moment coefficient (*CM*) were calculated.

Tab 17 Test flight parameters

Stratos 1-7	Test 1	Test 2	Test 3	Test 4	Test 5	Unit
Flight speed	20	14	14,6	15	16	m/s
wind speed	3-4	3-7	3-7	3-7	3-7	m/s
wind direction relative to the drone	0 E	45 (SW)	45 (SW)	45 (SW)	45 (SW)	-
drone mass	10.75	10.75	10.75	10.75	10.75	Kg
size of propeller	16x6.1	16x6.1	16x6.1	16x6.1	16x6.1	Inch
propeller speed	-	-	-	-	-	rev/s
angle of attack of the drone	11	8	7	7-8		°
takeoff speed	16	13-14	13	13		m/s

The tests were conducted while flying in a well-defined direction. This made it possible to determine the direction of the wind relative to the test object. The layout of the analyzed UAV in relation to the world directions was determined in the Fig. 90.

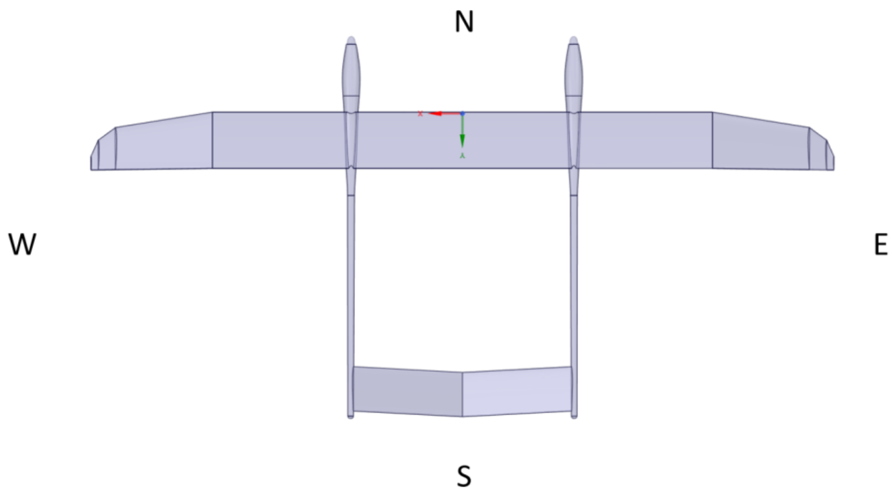

Fig. 90 Test flight direction

The parameters necessary for the comparative analysis were determined based on the calculation methodology and equations presented in Section 3.4.1. The results of the analyses performed are presented in Chapter 6.2.

6. Results of analyzes carried out according to the developed methodology

The analysis methodology is presented in Chapter 5. The developed methodology was prepared in order to determine the optimal environment for comparative studies of the considered tail units to determine the statistical error of the conducted research, to numerically determine the optimal tail configuration for the assumed mission, to evaluate the stability on the basis of the pilot's evaluation and the Harper-Cooper test completed by him, and to comparative studies with the real demonstrator of the tested object. The compilation of parameters obtained on the basis of the developed methodology makes it possible to determine the correctness and convergence of the conducted analyses. The compilation of results in a transparent manner requires a separation into individual stages of work. They are presented and described in the following subsections. The first subsection presents the results of the analyses conducted to determine the optimal CFD software to be used in further stages of work.

6.1. Comparative studies of computational environments and result discrepancies

The analysis consisted of comparing XFLR5 and ANSYS results for critical flight conditions and determining the discrepancy of the results obtained depending on the used computing environment. The methodology is presented in the visualization Fig. 91.

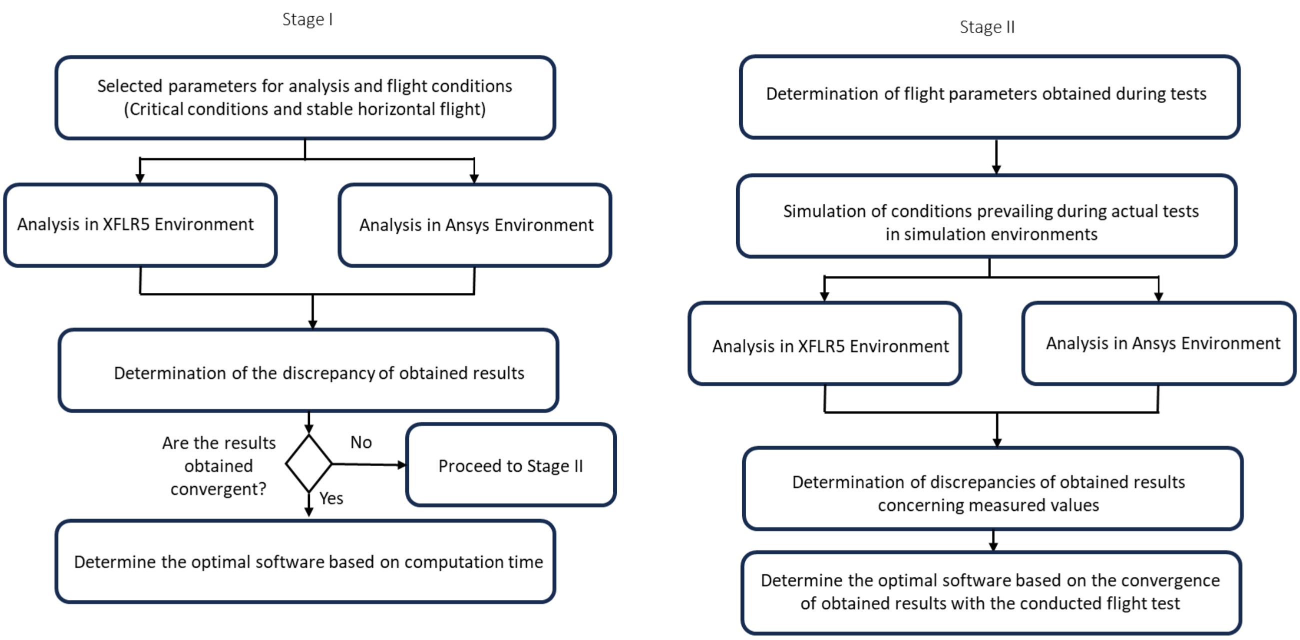

Fig. 91 Determination of the optimal software for the conducted analysis

Determination of a suitable computational environment made by comparing results for equally specified flight parameters. The flight parameters for which the analyses were conducted were determined for three critical states and one stable state of horizontal flight. The parameters of the conducted analyses are shown in the table Tab 18.

Tab 18 Analysis parameters

Analysis name	Critical condition I	Critical condition II	Critical condition III	Stable Flight
Flight Speed $[m/s]$	35	19	-5	14.5
Angle of Attack [°]	0	14.25	22	Dependend of configuration
Air Density $[kg/m^3]$	1.12	1.12	1.12	1.12
Air Temperature [°C]	25	25	25	25

Analysis for horizontal flight of each configuration required determining the angle of attack for which the pitching moment of the analyzed configuration along the wingspan is equal to zero. The results of the neutral angle of attack are presented in Tab 19.

Tab 19 Neutral AoA for anaysed tail unit configurations

Tail unit configuration	I	II	III	IV	V
Angle of Attack [°]	4.30	4.29	2.87	3.50	3.30

The discretization parameters of the analyzed models, were determined based on the methodology presented in Chapter 5. Preparing the computing environment to verify the methodology. A summary of the obtained results for the considered configurations is presented in the tables Tab 20 – Tab 23.

Tab 20 Critical condition I analysis results

Critical condition I									
Software	ANSYS			XFLR5			Delta		
Tail unit configuration	Lift [N]	Drag [N]	L/D	Lift [N]	Drag [N]	L/D	Lift [%]	Drag [%]	L/D [%]
I	348.72	22.81	15.29	365.56	4.49	81.45	-4.65	27.08	-81.23
II	351.41	22.86	15.38	365.48	4.57	79.96	-3.85	28.50	-80.77
III	346.04	23.84	14.52	357.39	4.93	72.48	-3.18	56.74	-79.97
IV	345.42	23.67	14.59	358.36	4.88	73.39	-3.61	55.72	-80.12
V	349.10	23.89	14.91	357.96	4.61	77.60	-2.48	36.05	-80.79

Tab 21 Critical condition II analysis results

Critical condition II									
Software	ANSYS			XFLR5			Delta		
Tail unit configuration	Lift [N]	Drag [N]	L/D	Lift [N]	Drag [N]	L/D	Lift [%]	Drag [%]	L/D [%]
I	282.52	49.12	5.75	393.21	17.95	21.90	-28.15	173.65	-99.54
II	277.17	49.85	5.56	398.04	17.78	22.38	-30.37	180.37	-99.46
III	288.40	49.31	5.85	416.23	15.21	27.36	-30.71	224.19	-98.79
IV	278.75	48.27	5.78	417.12	15.20	27.44	-33.17	217.57	-98.10
V	276.80	51.13	5.41	415.35	17.56	23.65	-33.36	191.17	-98.44

Tab 22 Critical condition III analysis results

Critical condition III									
Software	ANSYS			XFLR5			Delta		
Tail unit configuration	Lift [N]	Drag [N]	L/D	Lift [N]	Drag [N]	L/D	Lift [%]	Drag [%]	L/D [%]
I	-0.94	9.38	0.10	3.40	0.41	8.27	-127.65	2187.80	-98.79
II	1.12	9.08	0.12	2.25	0.48	4.69	-50.22	1791.67	-97.44
III	-3.16	9.63	0.33	-10.35	0.59	17.51	-69.47	1532.20	-98.12
IV	-5.20	9.91	0.52	-10.29	0.59	17.40	-49.47	1579.66	-97.01
V	-3.61	9.78	0.37	-9.96	0.51	19.68	-63.76	1817.65	-98.12

Tab 23 Stable flight analysis results

Stable Flight									
Software	ANSYS			XFLR5			Delta		
Tail unit configuration	Lift [N]	Drag [N]	L/D	Lift [N]	Drag [N]	L/D	Lift [%]	Drag [%]	L/D [%]
I	112.83	4.43	25.44	109.60	6.86	15.98	2.95	35.40	59.30
II	112.75	4.43	25.48	108.29	6.98	15.51	4.12	36.60	64.20
III	105.73	4.01	26.4	107.89	6.54	16.50	2.00	38.80	60.00
IV	104.14	3.95	26.37	101.73	6.09	16.69	2.37	35.20	58.00
V	101.85	3.86	26.40	97.00	5.71	16.99	5.00	32.40	55.40

Due to significant discrepancies in the results obtained for considered flight conditions, a decision was made to prepare additional test for the flight parameters occurring during tests of an existing demonstrator equipped with a Type A tail configuration. According to the graphic of Fig. 91. this analysis has been referred to as "Stage II" and is aimed at determining the optimal software to determine the stability parameters of the test object considering different tail configurations. The results of the analysis are presented in the following subsection.

6.2. Comparative analysis of numerical results and experimental data

In order to determine the correctness and convergence of the real results and those obtained during numerical analysis, a decision was made to map the existing test object according to its geometry, the positions of its centers of gravity and additional external instrumentation. The flight test object is shown in the Fig. 92.

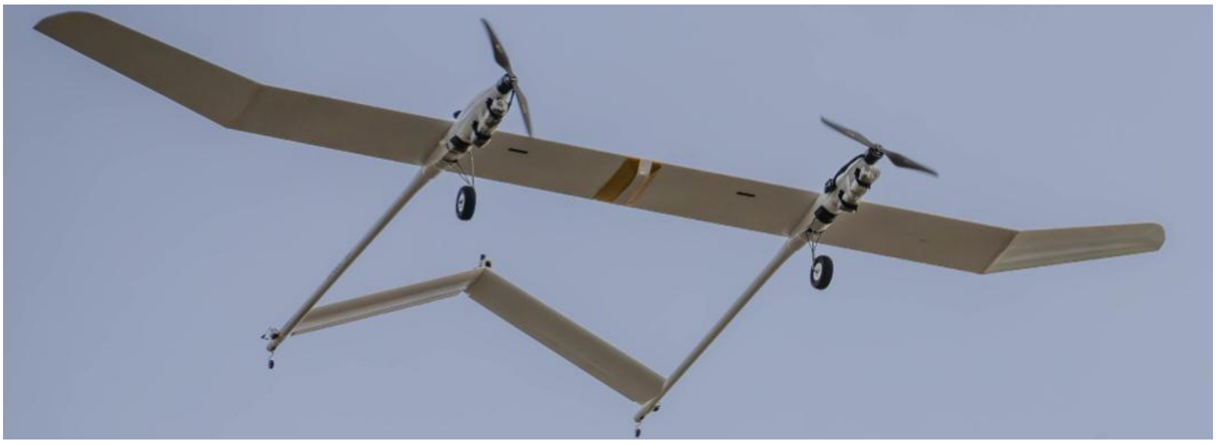

Fig. 92 Tested TS17 (Polnor Leader 2019)

The analysis was carried out by preparing numerical flight tests using both the computing environments, XFLR5 and ANSYS. Due to the lack of values for direct data on aerodynamic drag and lift force generated by the object during flight, it is necessary to determine the parameters analytically using data obtained during the tests. The data of the configuration on which the tests were conducted are shown in Tab 24.

Tab 24 Tested configuration parameters

TS17 Flight test configuration parameters		
Propeller dimensions	16.0 x 6.1	Inch
TS17 mass	10.75	kg
Main wing area	0.901	m^2
Wing span	3.6	m
Tail unit configuration	A	-
Tail unit area	0.258	m^2
One motor power	1800	W

The parameters obtained during the conducted flights are shown in Tab 25. Based on the presented parameters, the values of lift force, aerodynamic drag and leaning moments were approximated for three selected trials during the conducted tests. The wind direction during the tests is shown in the Fig. 93.

Tab 25 Flight parameters of TS17 demonstrator reached during test

TS17 test	Test 1	Test 2	Test 3
Flight Speed $[m/s]$	14	14.6	15
Wind speed$[m/s]$	5	5	5
Wind direction relative to UAV, See Fig 93	45 (SW)	45 (SW)	45 (SW)
Power consumed by motor [W]	190	182	200
Electric current [A]	8.45	8.1	8.9
Angle of attack [°]	8	7	7.5
Flight altitude [m]	200	200	200
Air density $[kg/m^3]$	1.201	1.201	1.201

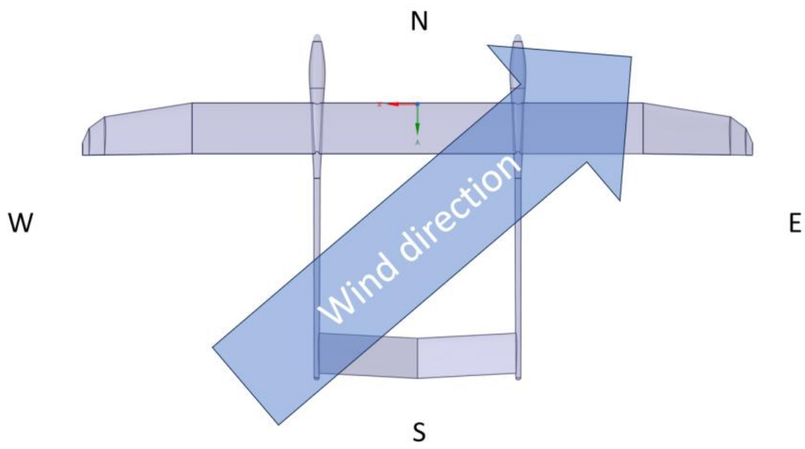

Fig. 93 Wind direction

Based on the values of the parameters determined and the system of preserved equilibrium in flight of the aircraft, the following parameters of lift force and aerodynamic drag of the test object were determined. The results are shown in Tab 26.

Tab 26 Flight parameters calculated in base of flight tests

TS17 test	Test 1	Test 2	Test 3
Estimated propeller revolutions [*rmp*]	5085	5013	5173
Estimated Static Thrust [*g*]	1814	1761	1879
Assumed Lift Coefficient CL [-]	1.2613	1.2194	1.2402
Lift [*N*]	133.61	140.48	150.81
Drag [*N*]	12.78	12.41	13.20
Lift to Drag ratio (Efficiency) [-]	10.45	11.32	11.43

Those parameters obtained during the flights and knowing the flight parameters such as speed and direction of flight, wind speed, engine rotation and angle of attack during horizontal flight, it is possible to implicate the parameters in the two considered computational environments and prepare numerical aerodynamic analyses. Based on the data and results, a comparison of the parameters of lift force, aerodynamic drag and pitching moments of the analyzed object were prepare. The results of the comparison are presented in the tables Tab 27 to Tab 29.

Tab 27 Comparison of results obtained in computational environments compared to the I flight test

Test 1 results comparison			
	TS17 Test 1	XFLR5	ANSYS CFX
Lift [N]	133.61	145.73	140.02
Drag [N]	12.78	4.73	10.70
Lift to Drag ratio [-]	10.45	30.79	13.09

Tab 28 Comparison of results obtained in computational environments compared to the II flight test

Test 2 results comparison			
	TS17 Test 1	XFLR5	ANSYS CFX
Lift [N]	140.48	146.26	142.16
Drag [N]	12.41	4.39	10.53
Lift to Drag ratio [-]	11.32	33.35	13.50

Tab 29 Comparison of results obtained in computational environments compared to the III flight test

Test 3 results comparison			
	TS17 Test 1	XFLR5	ANSYS CFX
Lift [N]	150.81	160.83	154.98
Drag [N]	13.20	5.04	11.44
Lift to Drag ratio [-]	11.43	31.89	13.55

Based on the comparison shown in the tables (Tab 27 to Tab 29), it is possible to conclude that there is a negligible discrepancy between the results of the ANSYS environment analyses compared to the data obtained during the test flights. Confirming and thus taking into account the parameters obtained during numerical analyses and knowing the results of the pilot's evaluation, it is possible to unambiguously determine the optimal of the tail unit configurations considered in terms of flight stability according to the given computational environment, for the adopted mission.

6.3. Numerical stability analyses of the considered tail configurations

Stability analyses were conducted using ANSYS software. Stability was determined for three possible degrees of motion of the analyzed object. These are Pitch Yaw and Roll rotations. The analyzed rotation angles are shown in the Fig. 94.

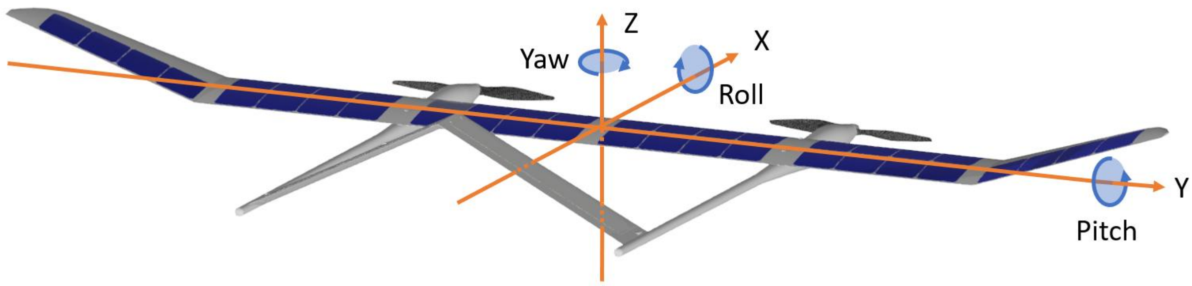

Fig. 94 Analysis assumed movement directions

Due to the type of prepared analysis, it was necessary to use grooves to determine the parameters sought for each of the study case. The point relative to which the described parameters were determined, was moved to a location consistent with that presented in subsection 4.3. Step was prepared for determined center of gravity for each configuration. The relocated reference point for one of the configurations considered is shown in the graphic Fig. 95. The equations used are shown below.

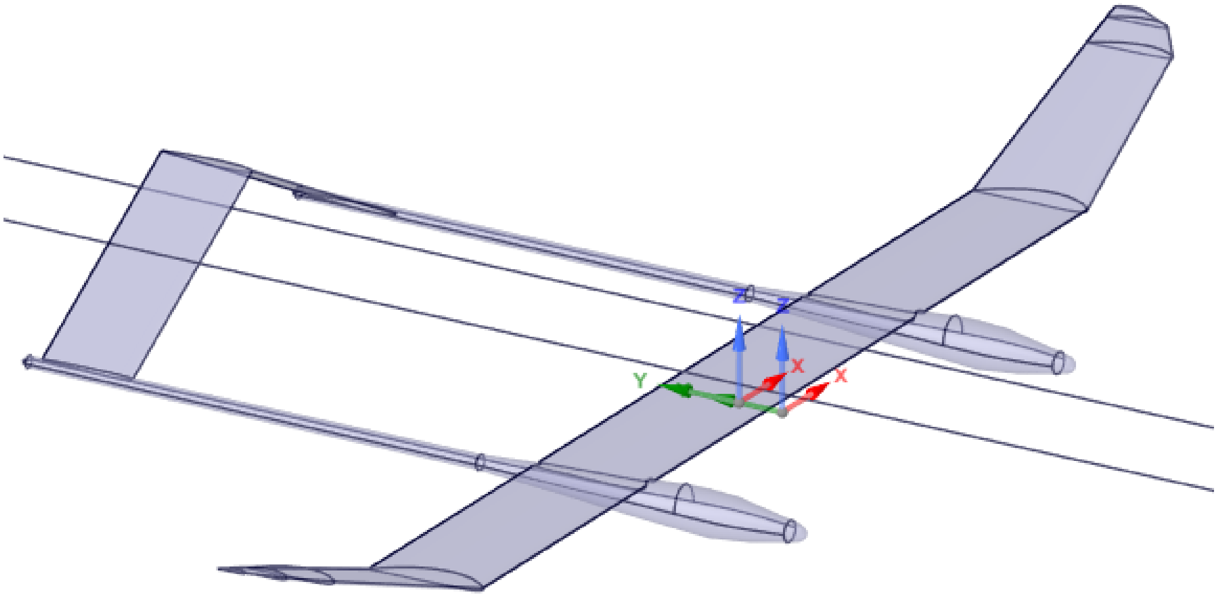

Fig. 95 Transferring the position of the origin of the coordinate system to the center of gravity

Equations defining the parameters to be compared, used in the ANSYS environment:

Lift=force_z()@TS17

Drag=force_y()@TS17

Pitching moment=-torque_x()@TS17

Yaw moment=torque_z()@TS17

Roll moment=torque_y()@TS17

Where:

force_z, y, x – determine the forces occurring in the directions of the given axes according to the phrases defined earlier in the ANSYS environment.

torque_z, y, x – determine the skew moments with respect to the given axes according to the left-handed system previously defined in the ANSYS environment.

In order to correctly describe the values of the variables, the tilt angles of the test object were described as *Θ* - the angle with respect to the X axis, *ψ* - the angle with respect to the Z axis and *φ* - the angle with respect to the Y axis (Rogalski, Nowak and Wałek 2015).

The analyses were carried out for the fixed parameters adopted for each of the tail configurations considered. The adopted parameters of the conducted analyses are shown in Tab. 30.

Tab 30 Extreme parameters adopted for each analysis.

Analysis type	Pitch Analysis - Θ	Yaw Analysis - ψ	Roll Analysis - ϕ
Min AoA [°]	-6	0	0
Max AoA [°]	16	50	20
AoA change step [°]	2	5	2

On the basis of the prepared research, the results of certain aerodynamic parameters were obtained from which it is possible to determine the stability of flight in function of the described angles. Based on the obtained results and comparisons, the plots of lift force against angle of attack for each of the considered tail configurations were determined. The results obtained for the considered configurations were summarized and divided according to the type of considered analysis.

6.3.1. Pitch analysis results

Based on the graphs shown (Fig. 96 - Fig. 101), each configuration was evaluated for aerodynamic stability, analyzing the dependence of lift, drag, and aerodynamic moments on pitch angle (*Θ*).

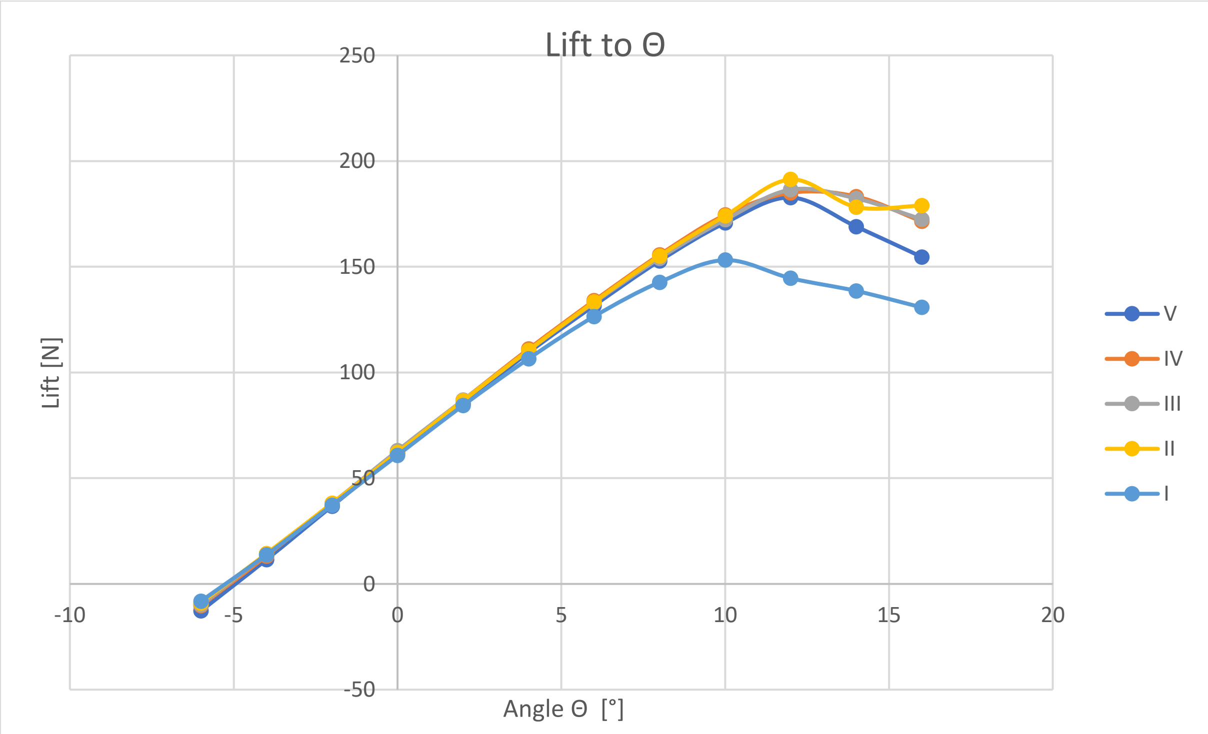

Fig. 96 Lift to Θ for considerred configurations

The graph Fig. 96. shows the dependence of the lifting force on the angle of inclination. A stable configuration should provide a predictable increase in lift force as the angle Θ increases until the jet is detached. When analyzing the results, the main considerations were the value of the lifting force and the linearity of the graph.

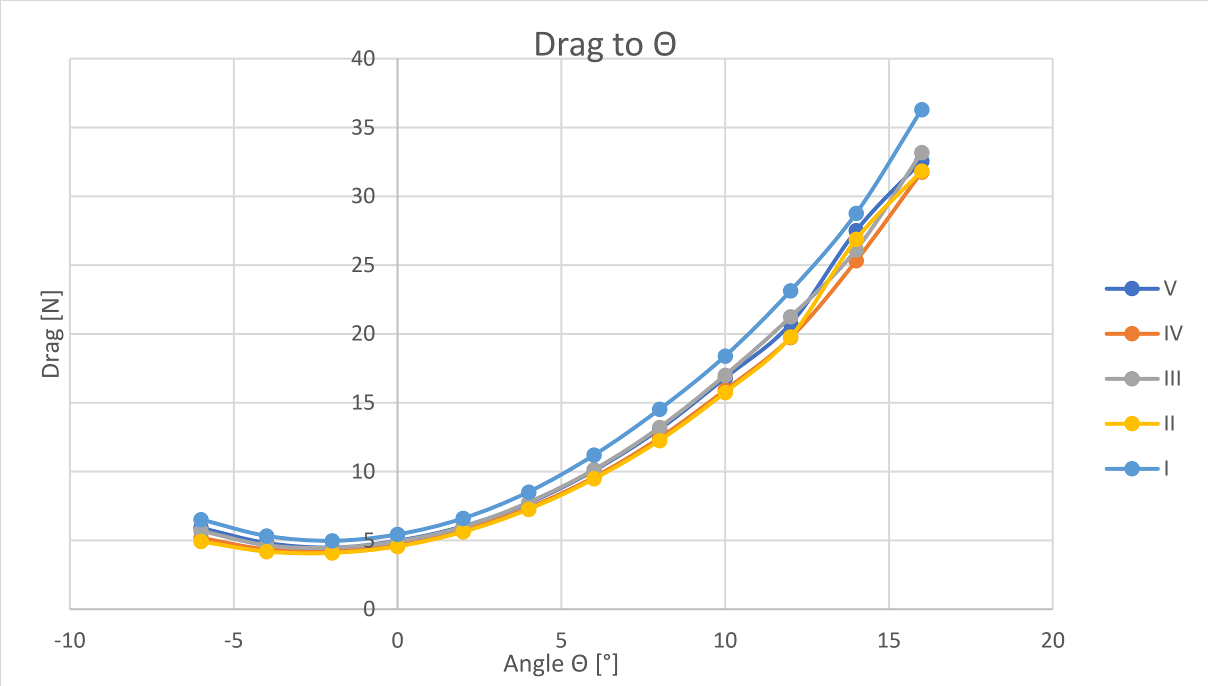

Fig. 97 Drag force to Θ for considerred configurations

Aerodynamic drag as a function of pitch angle *Θ* is shown in the Fig. 97. Low drag at high lift force is desirable because it provides greater aerodynamic efficiency. The configuration rating was influenced by the lowest value of drag with respect to pitch angle.

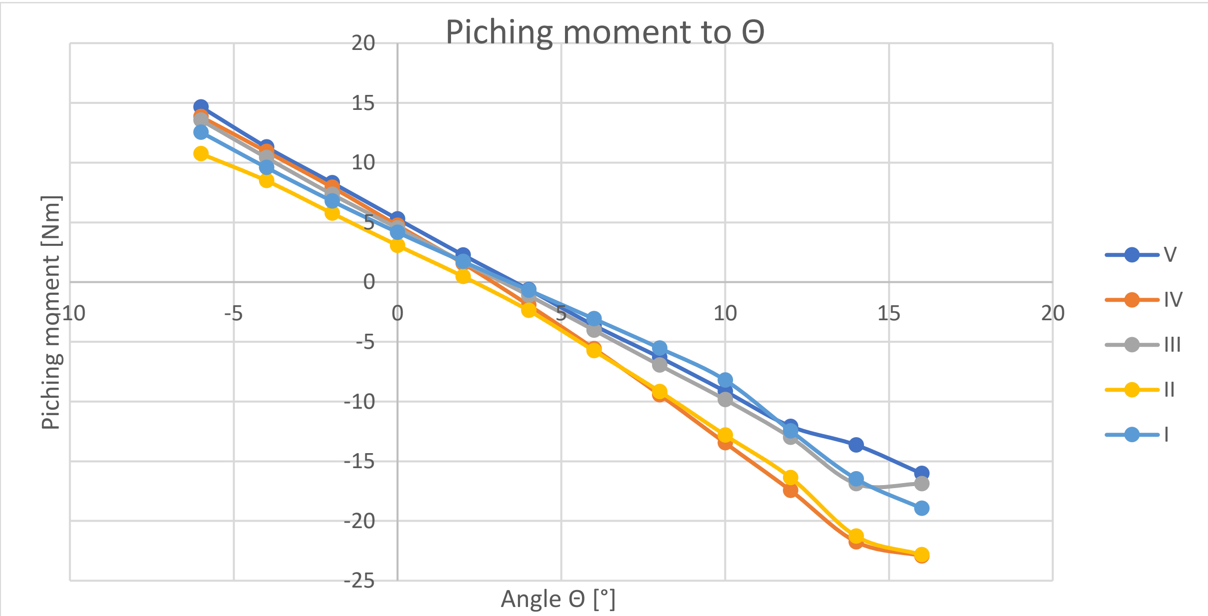

Fig. 98 Pitching moment to Θ for considerred configurations

The results presented (Fig. 98) show the tilting moment (pitching) as a function of pitch angle *Θ*. Stability requires that the moment decreases as the angle increases, signaling a tendency to return to equilibrium. When evaluating the results, consideration was also given to maintaining the linearity of the graph with respect to pitch angle.

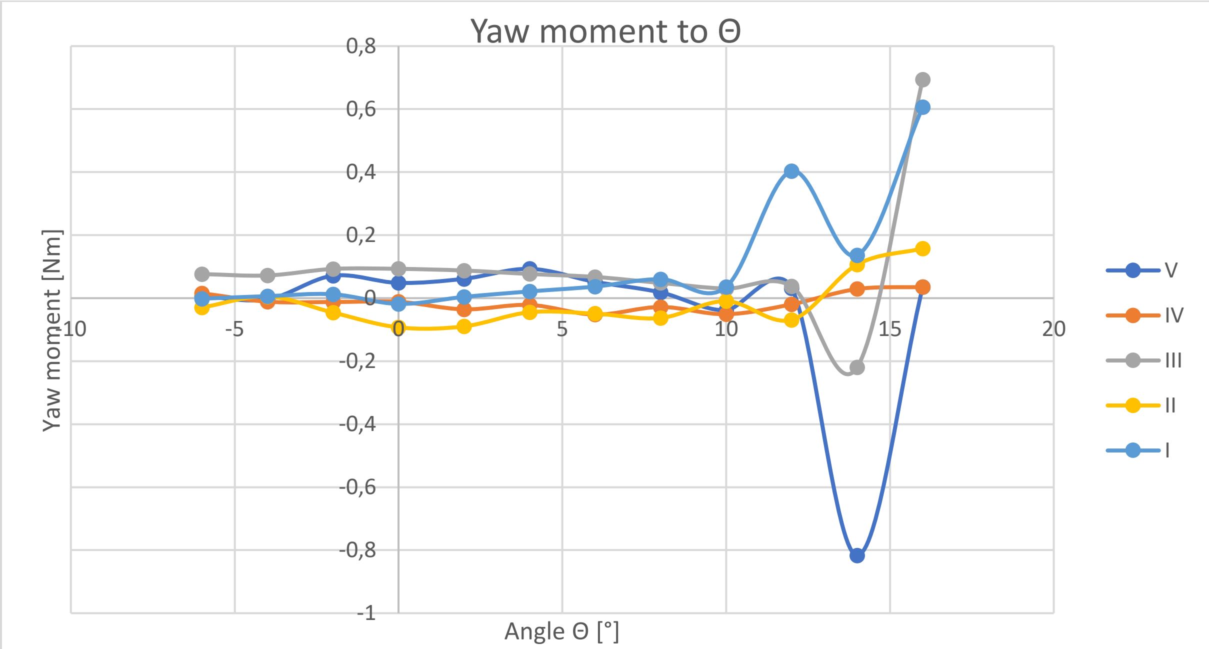

Fig. 99 Yaw moment to Θ for considerred configurations

The graph (Fig. 99) shows the yawing moment (yawing) as a function of the angle *Θ*. Indications of good directional stability are low and stable values without abrupt changes.

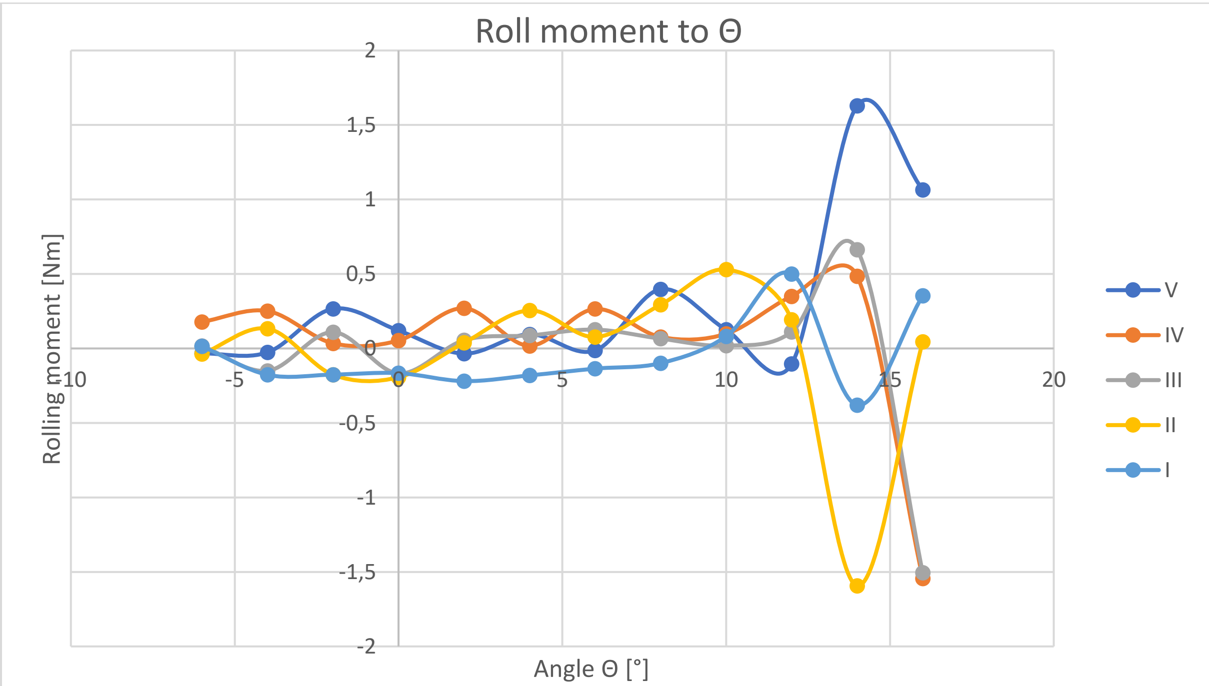

Fig. 100 Roll moment to Θ for considerred configurations

The graph Fig. 100 illustrates the tilting (rolling) moment as a function of angle *Θ*. The stable configuration is characterized by moderate changes in moment, without sharp fluctuations.

6.3.2. Yaw analysis Results

Based on the charts presented, each configuration was analyzed for aerodynamic stability, considered the lateral angle (β) and aerodynamic moments (pitching, yawing and rolling).

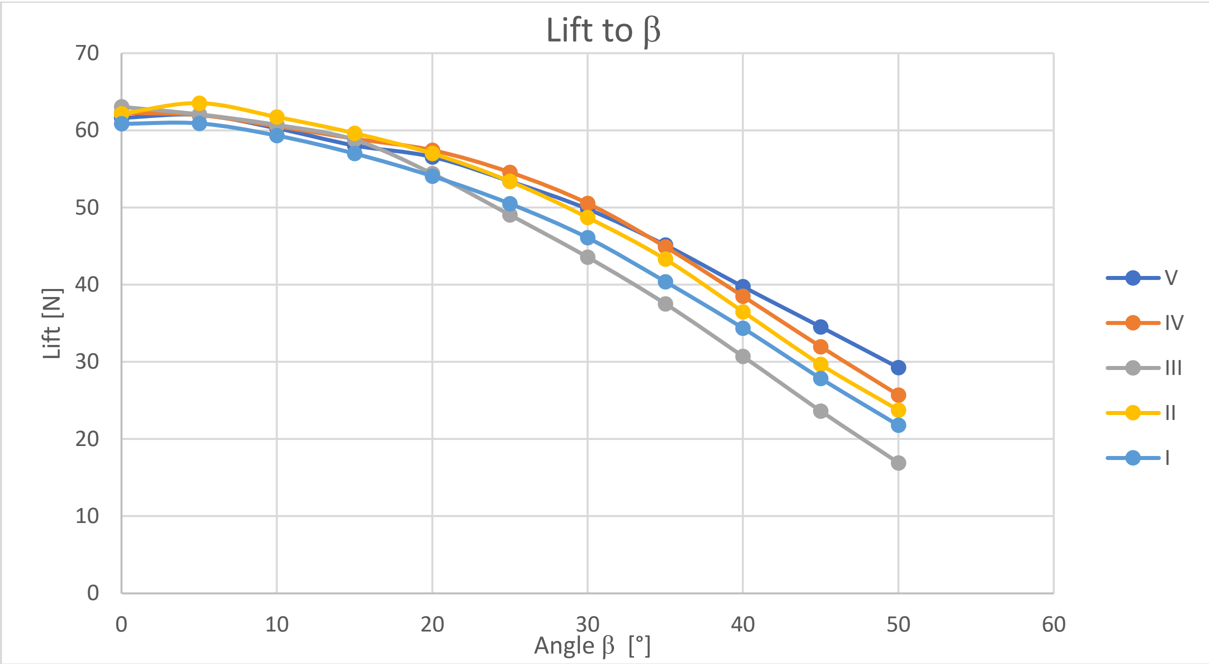

Fig. 101 Lift force to β for considerred configurations

The graph Fig. 101 shows the dependence of the lifting force on the lateral angle β. A stable configuration should show a steady decrease in lifting force as the angle β increases.

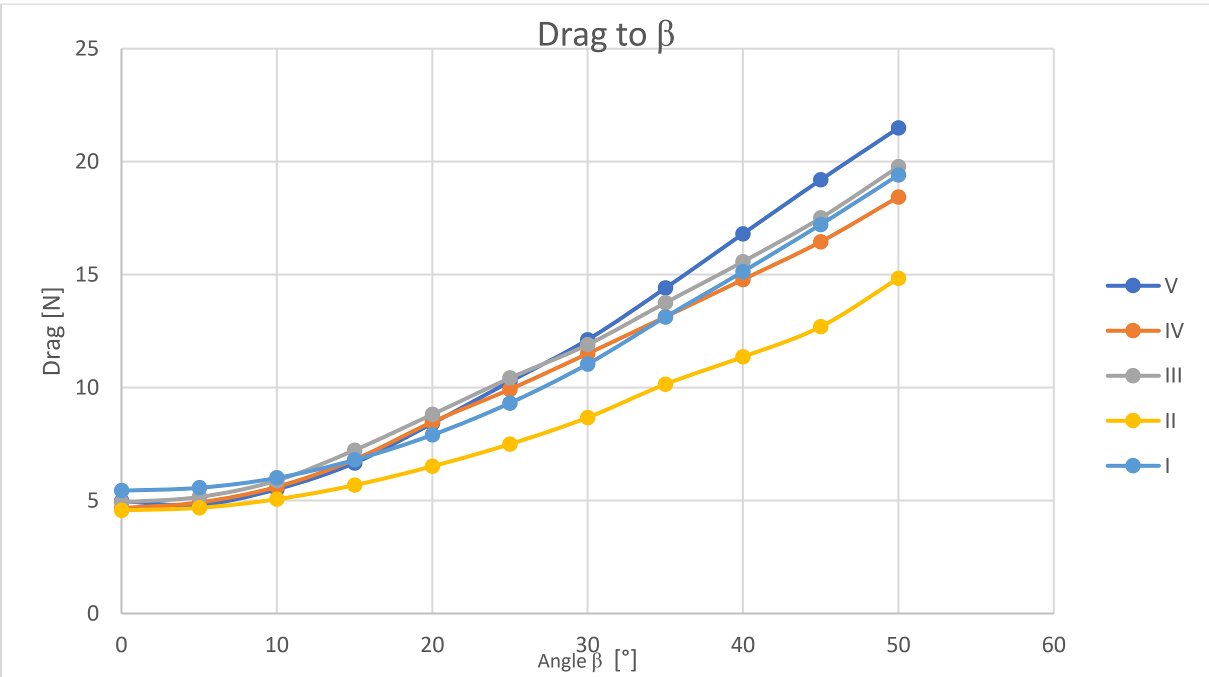

Fig. 102 Drag force to β for considerred configurations

The graph Fig. 102 shows the aerodynamic drag as a function of the lateral angle β. For stability and aerodynamic efficiency, a lower value of drag is preferred with increasing angle β.

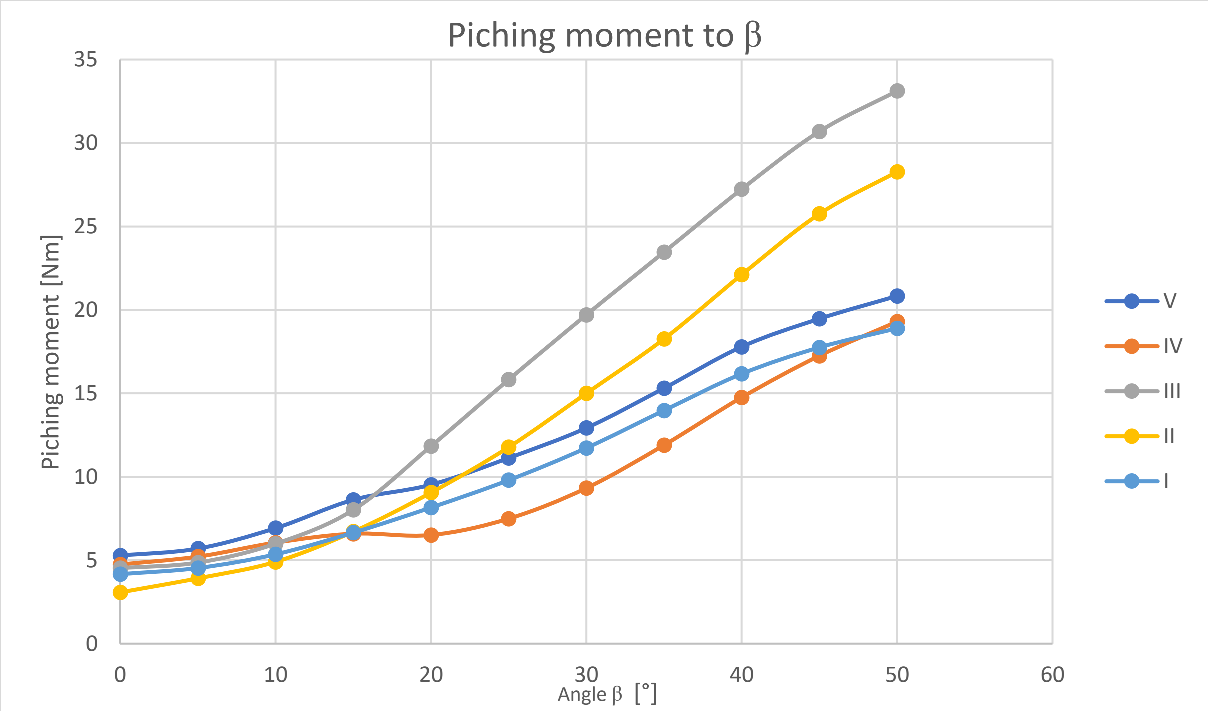

Fig. 103 Pitching moment to β for considerred configurations

Graphic Fig. 103 shows the tilting moment as a function of angle β. For stability, a relatively flat characteristic with no sudden increases is desirable.

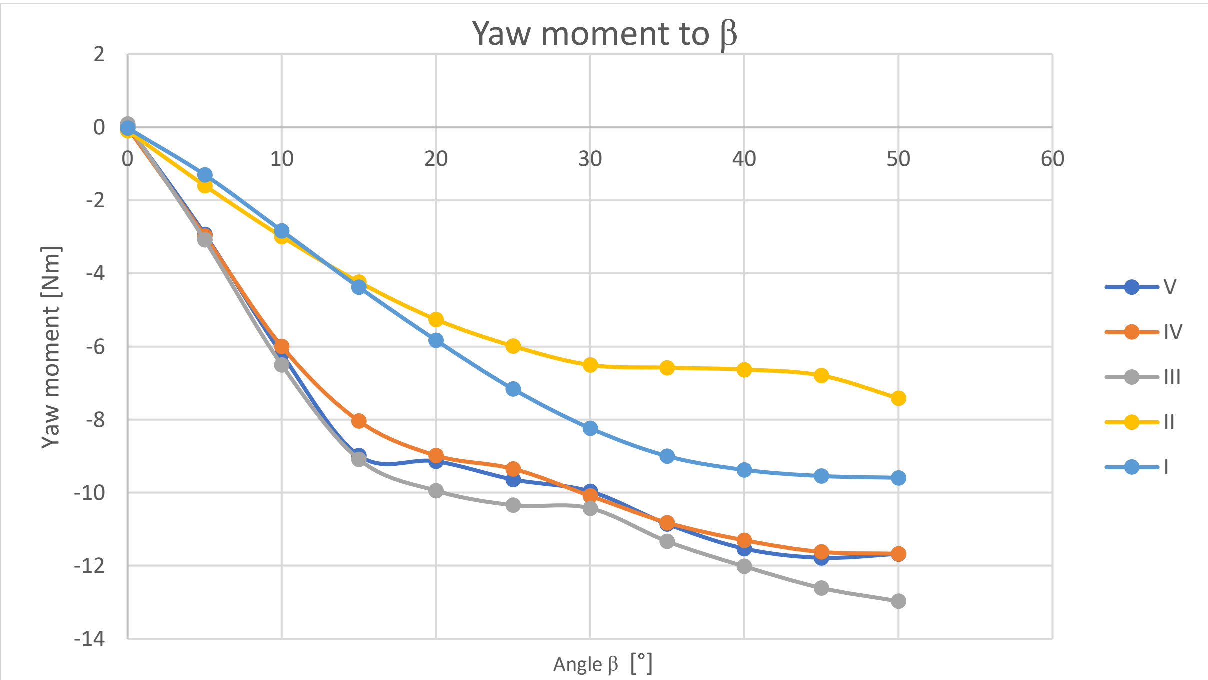

Fig. 104 Yaw moment to β for considerred configurations

The graph shown in the Fig. 104 yawing moment (yawing). A smooth and stable waveform without abrupt changes is a sign of good directional stability.

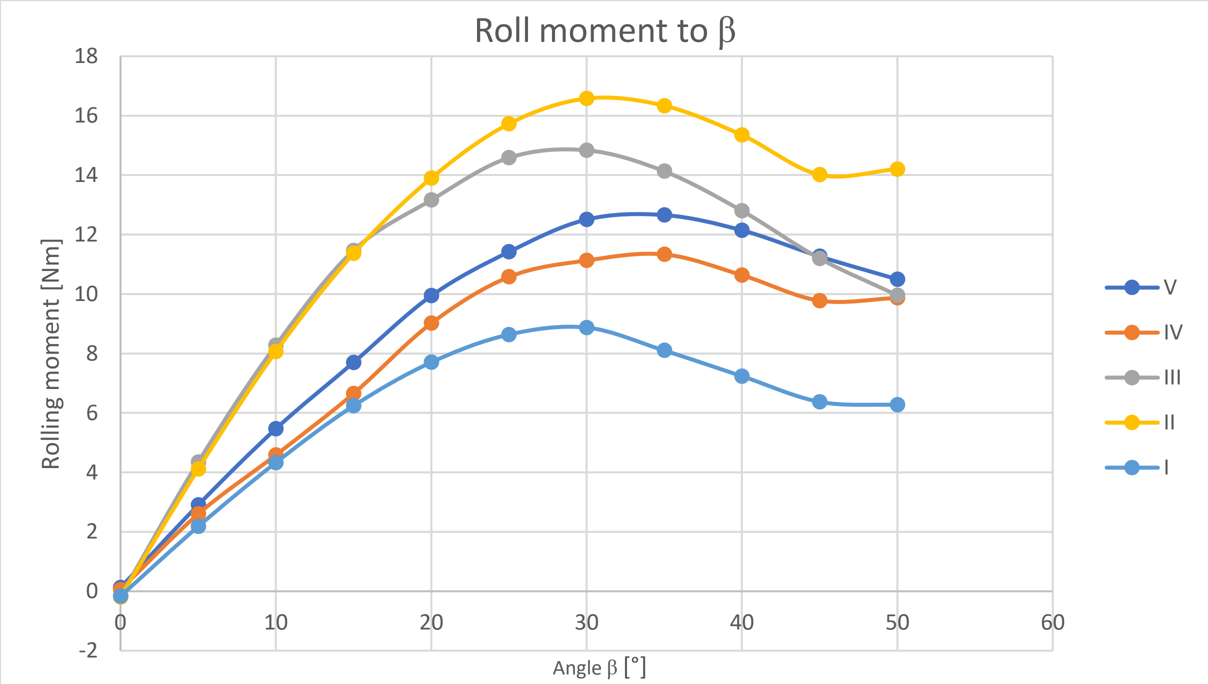

Fig. 105 Roll moment to β for considerred configurations

The graph Fig. 105 shows the tilting (rolling) moment as a function of the lateral angle β. The stable configuration shows moderate and predictable changes in the.

6.3.3. Roll analysis Results

Based on the presented plots of lift, drag and aerodynamic moments (pitching, yawing and rolling) as a function of roll angle (φ), it was analyzed which configuration shows the best aerodynamic stability.

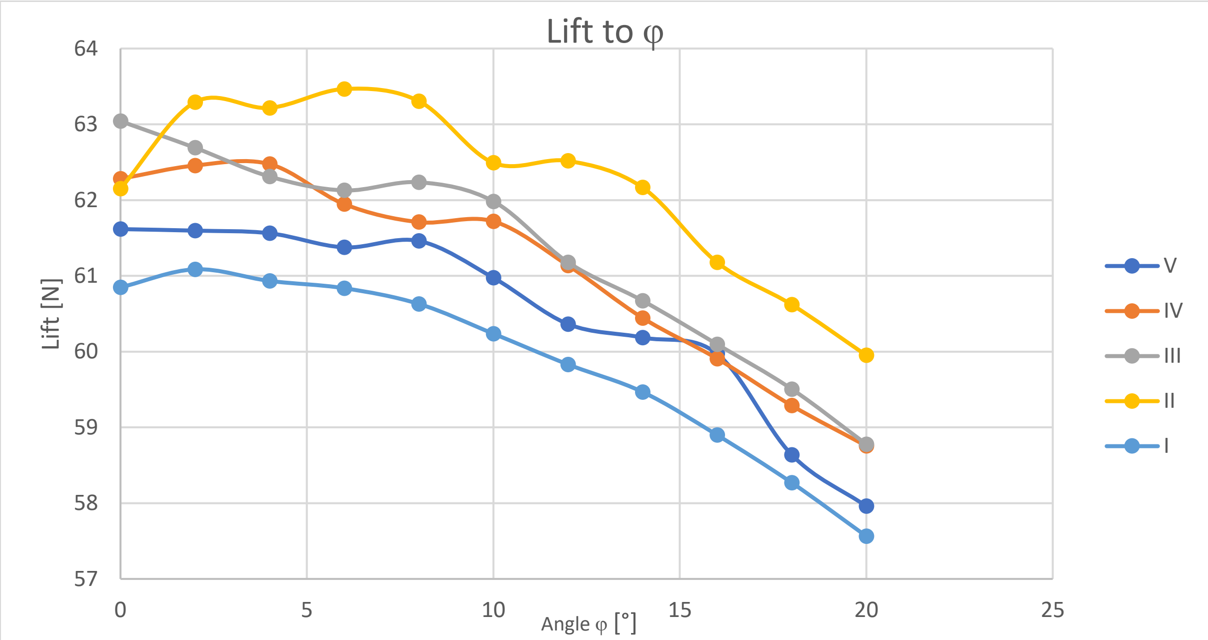

Fig. 106 Lift force to φ for considerred configurations

The graph Fig. 106 shows the dependence of the lifting force on the roll angle. A stable configuration should maintain a high lifting force with moderate changes as the angle φ increases.

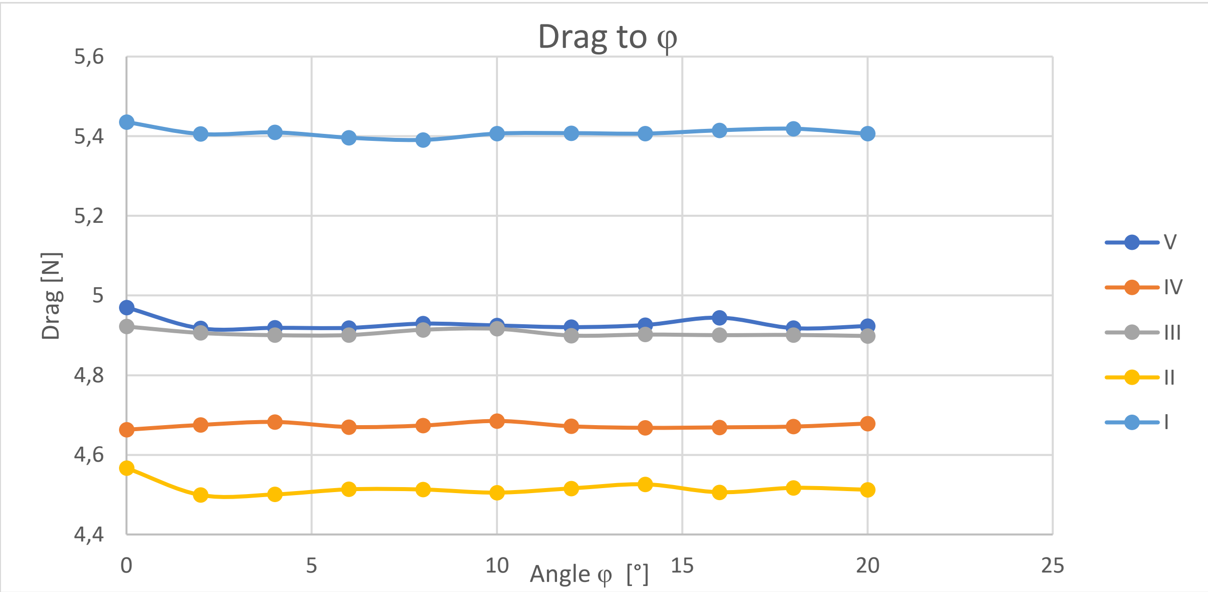

Fig. 107 Drag force to φ for considerred configurations

The graph Fig. 107 illustrates aerodynamic drag as a function of angle φ. Lower drag with increasing angle is advantageous because it indicates better aerodynamic efficiency.

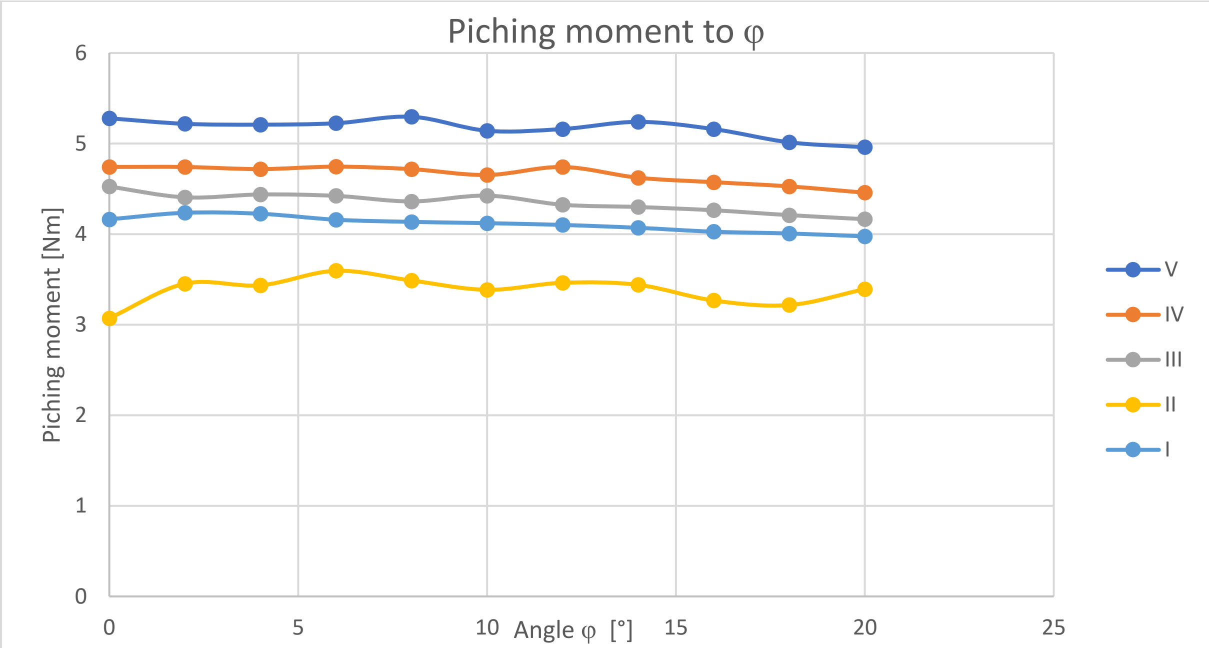

Fig. 108 Pitching moment to φ for considerred configurations

Visualization Fig. 108 shows the tilting moment as a function of the angle *φ*. Aerodynamic stability requires that the pitching moment be relatively constant and devoid of abrupt changes.

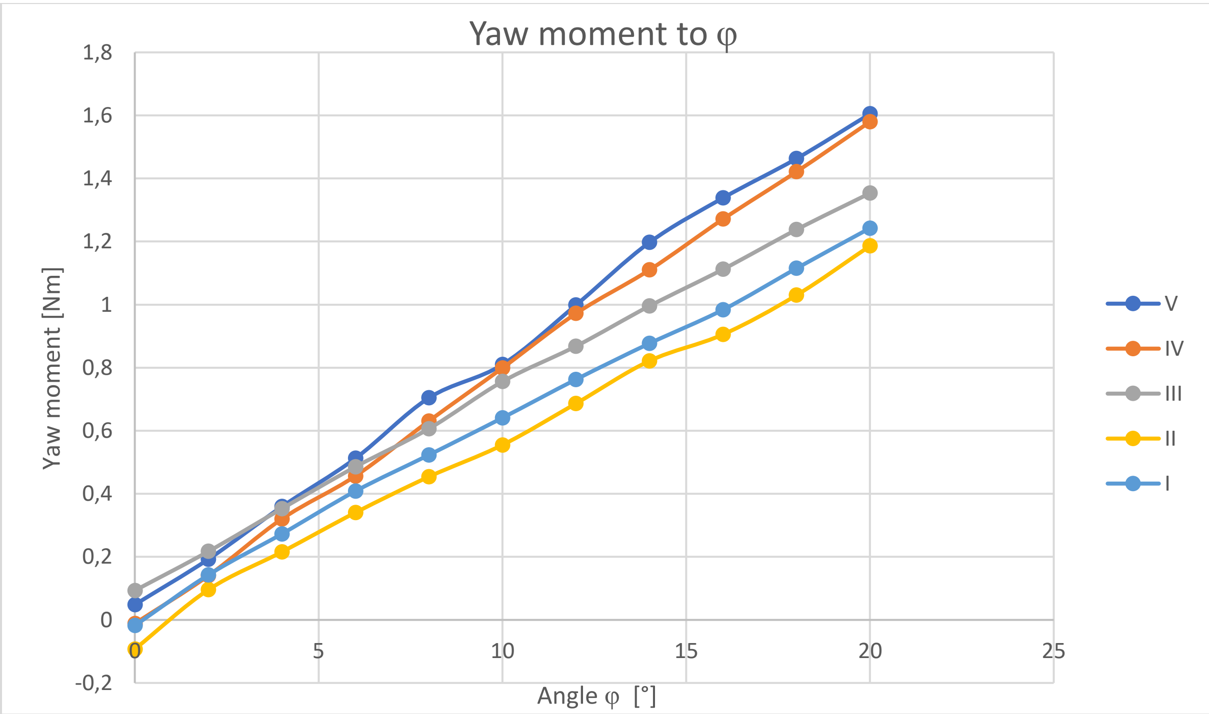

Fig. 109 Yaw moment to φ for considerred configurations

The chart Fig. 109 shows the yawing moment (yawing). A stable moment waveform with no sudden increases or decreases is desirable for directional stability.

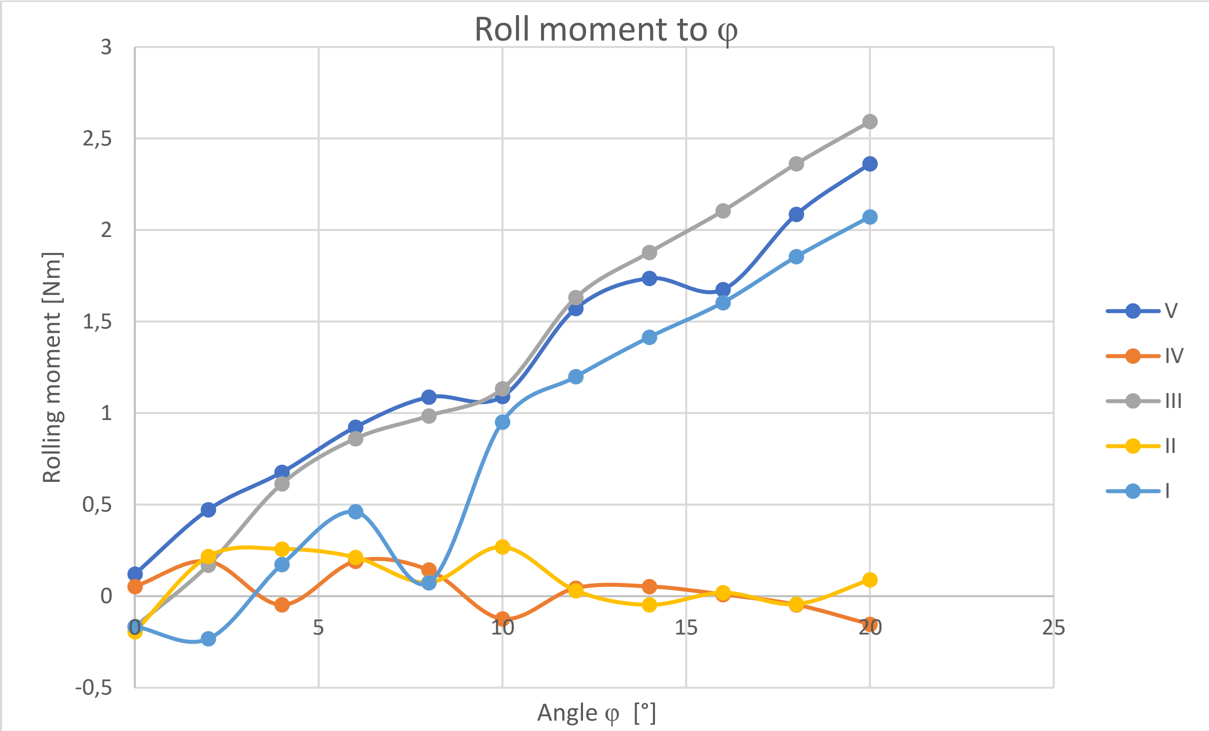

Fig. 110 Roll moment to φ for considerred configurations

The visualization Fig. 110 shows the tilting (rolling) moment as a function of the angle φ. A stable configuration should show moderate torque values with smaller fluctuations.

6.3.4. Presentation of the results in the form of an adopted table and scoring system

Based on the analysis results presented above, a table (Tab 31) was prepared, listing all the stability parameters of the considered tail configurations. Subsequently, the parameters were determined in a scoring manner, allowing to statistically summarize the results and determine the optimal configuration from among the considered tail parts, due to numerical analyses in the ANSYS environment. Ratings were determined based on the values obtained during a specific test and the stability of the effect of the change on the values obtained. A value of 1 was assigned to the configuration with the worst performance for a given test and a rating of 5 to the configuration with the best performance. The discrepancy of values was not considered, only the order of the results of the configurations.

Tab 31 Scoring of tail configurations based on conducted analyses

Configuration	I	II	III	IV	V
Lift to Θ	1	5	4	3	2
Drag to Θ	1	3	4	5	2
Pitching moment to Θ	5	1	3	2	4
Yawing moment to Θ	3	4	1	5	2
Rolling moment to Θ	5	1	3	4	2
Sum for $\boldsymbol{\Theta}$	**15**	**14**	**15**	**19**	**12**
Lift to β	2	3	1	4	5
Drag to β	3	5	2	4	1
Pitching moment to β	5	2	1	4	3
Yawing moment to β	5	3	2	4	1
Rolling moment to β	5	1	2	4	3
Sum for β	**20**	**14**	**8**	**20**	**13**
Lift to φ	2	1	5	4	3
Drag to φ	1	5	3	4	2
Pitching moment to φ	4	1	3	5	2
Yawing moment to φ	4	5	3	2	1
Rolling moment to φ	3	2	5	1	4
Sum for $\boldsymbol{\varphi}$	**14**	**14**	**19**	**16**	**12**
Sum of all points	49	42	42	55	37

Based on the results obtained, tail configuration I - configuration A - was adopted as the optimal configuration in terms of flight stability. Due to the limitations associated with the landing method of the test object (on the belly), configurations obtaining more points were discarded due to the need to permanently install an additional landing gear system. At angles φ, configuration I exhibits stable prone moment values, which promotes good lateral stability. This is beneficial in situations requiring moderate maneuvering without abrupt changes in orientation. Configuration I maintains relatively stable pitching moment values at all angles, which promotes predictable flight behavior and can facilitate control of vertical orientation. Compared to other configurations, the configuration I has less torque fluctuation (especially roll and yaw), which may indicate stability and ease of control in conditions without extreme maneuvers.

The Twin Stratos UAV in its optimum configuration is shown in the Fig. 111. The next stage of the analyses is the evaluation of the case study by a pilot - an aviation specialist.

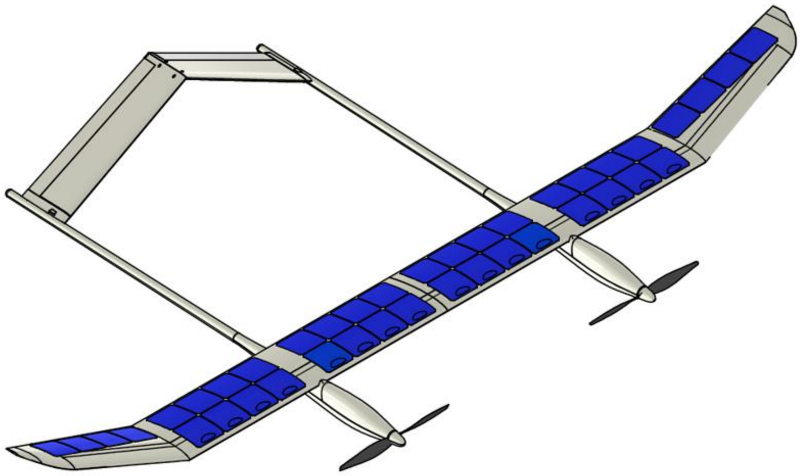

Fig. 111 The optimal tail configuration, according to the analysis, for the studied object

The parameters shown in Tab 32 were determined based on the relationships presented in subsection 4.6.

Tab 32 Table summarizing the results of the static stability parameter evaluation based on data from ANSYS for steady-level flight according to the criteria from Section 4.6 Stability Analyses

Configuration	I	II	III	IV	V
Static margin [%]					
Value	-27.52	-27.13	-43.02	-34.5	-43.02
Marking	8	10	4	6	4
Average	32	40	16	24	16
Aerodynamic center location [m]					
Value	0.40	0.40	0.37	0.39	0.37
Marking	10	10	6	8	6
Average	20	20	12	16	12
Stability moment [Nm]					
Value	0.14	0.14	0.21	0.17	0.21
Marking	10	10	6	8	6
Average	15	15	9	12	9
Lift coefficient [-]					
Value	1.07	1.07	0.99	0.99	0.97
Marking	10	10	8	8	6
Average	15	15	12	12	7
Drag coefficient [-]					
Value	0.042	0.042	0.038	0.037	0.036
Marking	4	4	6	8	10
Average	4	4	6	8	10
Weighted average					
	8.6	9.4	5.5	7.2	5.4

Assumed the type of landing of the Twin Stratos aircraft, which is a belly landing, it should be added as an criterion for evaluating the considered tail configurations. Based on the analysis of the results presented in the table, evaluating the considered tail configurations in terms of their static stability and aerodynamic optimization, the following conclusions can be made about the efficiency and optimality of the various configurations.

Configuration 2 received the highest weighted average score of 9.4, making it the most favorable choice in the context of all analyzed criteria (Tab 32). The high scores for stability margin (SM), location of central aerodynamic position (AC), stability moment (Cm), lift coefficient (Cl) and drag coefficient (Cd) indicate that this configuration offers an optimal balance between static stability and aerodynamic efficiency. Particularly high scores in stability margin and tilt moment stability suggest that the configuration provides an adequate reserve of stability necessary for safe aircraft operation. The configuration prevents fuselage landing.

Configuration 1 ranks second with a rating of 8.6 (Tab 32). The high scores for lift coefficient (Cl) and stability margin (SM) indicate good aerodynamic stability. However, lower scores in other criteria, such as drag coefficient (Cd), indicate that despite its generally satisfactory characteristics, this configuration may present worse parameters compared to Configuration 2, especially in terms of minimizing aerodynamic drag. This configuration is suitable for fuselage landings.

Configuration 5 stands out as having the highest rating in terms of drag coefficient (Cd), suggesting the best aerodynamic optimization of all the configurations analyzed (Tab 32). Although its overall score is 5.4, which places it in a lower position, its clear advantage in the context of aerodynamic drag reduction may make it preferable in cases where drag minimization is crucial. However, its lower scores in other criteria, such as stability margin (SM) and stability moment (Cm), suggest that it may require compromises in terms of static stability. The configuration allows for a fuselage landing.

Configuration 4 received a weighted average rating of 7.2 (Tab 32), suggesting that it is a configuration that offers a moderate balance between stability and aerodynamic efficiency. Ratings in terms of lift coefficient (Cl) and stability moment (Cm) indicate satisfactory performance, although lower compared to configurations 2 and 1. It can be considered in scenarios where a balance is required between different aspects of stability and optimization. This configuration prevents a fuselage landing.

Configuration 3 received the lowest average score of 5.5 (Tab 32), indicating some limitations in terms of static stability and aerodynamic optimization. Although this configuration scored relatively high for moment of stability (Cm), its lower scores in other categories suggest that it may not be the best choice in cases where maximum efficiency is required for all evaluated parameters. This configuration is suitable for fuselage landings.

Conclusions:

The results presented in the table indicate that configuration 2 is optimal choice in the context of multi-criteria analysis, offering the highest level of static stability and aerodynamic performance. Configuration 1 also shows favorable characteristics, but not meeting landing requirements, making it a solid alternative in situations requiring a balanced approach to stability and drag. Configuration 5 may be preferred in cases where minimizing aerodynamic drag is crucial, but at the expense of less stability. Configurations 3 and 4 present moderate results, suggesting that they may be preferred where a compromise approach is required.

6.4. Presentation of the results of the Twin Stratos UAV case study conducted with a pilot

A pilot case study was conducted on the flight of the Stratos UAV with its pilot, which provided key information on the considered configuration. The study looked at the overall layout of the analysed UAV, the position of aerodynamic centers and gravity. The pilot of the Stratos UAV is Dr. Wawrzyniec Panfil, Eng.

The following results were presented on the Polnor Leader project report (Panfil, et al. 2024):

Flights with and without ailerons:

Using the TS110 test platform, maintain the tests to compare the aircraft's behavior in the configuration with and without ailerons. Additionally, the effect of differentiating the left and right engine thrust while making a turn was checked. The tests were performed during repeated flights in a 4-waypoint mission (Fig. 112). Scenarios were as follows:

- With ailerons, no differential thrust;
- With ailerons, differential thrust;
- Without ailerons, differential thrust;
- Without ailerons, no differential thrust.

Fig. 112 Mission for testing the TS110 with and without ailerons (Panfil, et al. 2024)

As it can be observed (Fig. 113), comparing scenarios with and without ailerons, variability of the roll angle (blue line) is smaller when ailerons are used, so the oscillation along the longitudinal axis of the plane are smaller. Furthermore, comparing scenarios with and without thrust differentiation, variability of the roll angle is smaller when thrust is differentiated. The best situation, from the approach of flight stability, is when ailerons are used and thrust is differentiated. Similar conclusions regard yaw angle (orange line in Fig. 113).

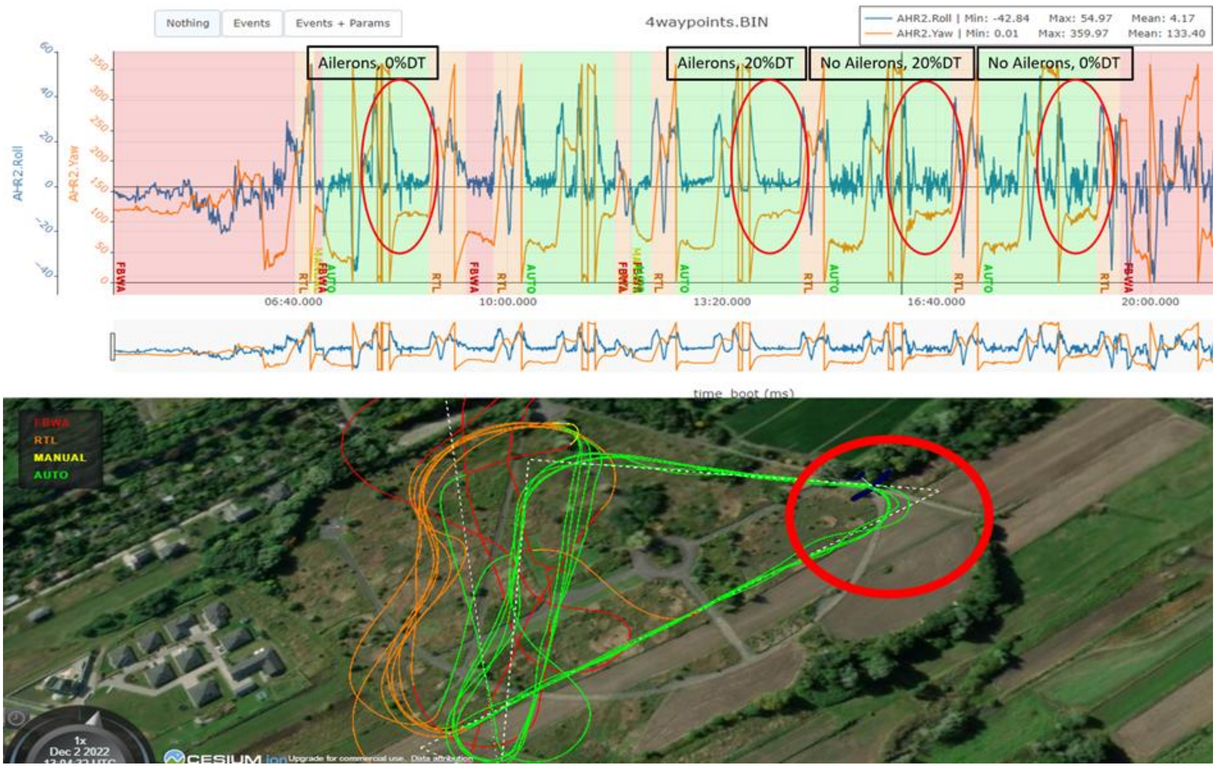

Fig. 113 Roll and yaw angles when testing the TS110 with and without ailerons (Panfil, et al. 2024)

Pilot conclusions:

The drone without ailerons and with the thrust differentiation performs turns in a quite properly coordinated manner. Flying without ailerons is possible, but they improve flight stability reducing oscillations in roll and yaw axes.

In pure horizontal flight, the use of ailerons would be particularly beneficial, as they would effectively counteract the drone's oscillations around its longitudinal axis, which are the result of wind gusts. This phenomenon has been noted in field conditions, where the oscillations were clearly visible. This problem becomes even more significant during landing, especially in situations where the crosswind occures, as was the case at the Gliwice airfield. The lack of effective mechanisms to control oscillations in the longitudinal axis makes it difficult to stabilize the drone, leading to stressful operational situations. When such conditions are encountered, the only solution is to add thrust, which, however, leads to unintended climb, while requiring additional altitude rudder correction by lowering the nose of the drone.

The use of flaps during landing would also be beneficial, as it would reduce speed during the landing approach, which is crucial for precise and controlled maneuvering in difficult weather conditions.

In terms of aerodynamics, the drone's double-hull arrangement introduces significant challenges. Compared to a single-hull design, in which mass is concentrated along the longitudinal axis, the mass in a dual-hull system is distributed beyond that axis. This distribution of mass significantly increases the moment of inertia with respect to the longitudinal axis, requiring more intensive counter-rotation and making it more difficult to stabilize the drone. This problem is particularly acute in the absence of ailerons that can effectively offset these difficulties.

On the positive side, the use of wing tips (vertical stabilization elements) with a certain tilt angle contributes to partial stabilization of the drone. During tilt, the lifting force generated by these elements creates a reaction moment that promotes the drone's return to the horizontal position, which improves its stability in flight.

These observations point to the need for further optimization of control systems and weight distribution in the design of double-hulled drones, especially in the context of their operational applications in harsh weather conditions.

At the end of the case study, the Harper-Cooper study from Chapter 3.4.3, the Harper-Cooper scale is a scale used in aviation to evaluate the performance and stability of aircraft control systems, including drones. A rating of 5 indicates an acceptable, though not ideal, level of control and performance, with noticeable but not critical piloting problems.

A double-body design with an inverted V-shaped tail can affect the distribution of aerodynamic forces, especially in terms of longitudinal and lateral stability. An inverted V- shaped tail provides aerodynamic advantages such as reduced drag, but can also introduce some challenges in control and responsiveness in maneuvering.

This tail arrangement can limit the range of precise control, especially in low-speed maneuvers or in situations requiring high agility. As a result, the drone could be rated lower in terms of control flexibility, which would explain the rating of 5.

The double-hull design can introduce some asymmetry in the distribution of weight and forces, further hampering stability and control accuracy. This can lead to slightly worse results in the Harper-Cooper scale control assessment.

Conclusions:

- **Acceptable level of performance**: A rating of 5 indicates that the system meets basic requirements, but its performance could be improved in terms of control precision, especially under extreme conditions.
- **Steerability optimization**: To increase the rating in the Harper-Cooper test, one could consider modifications to the control system or reducing the impact of aerodynamic asymmetry in a twin-tail inverted V.
- **Balance between drag and control**: The V-tail design may provide aerodynamic advantages, but at the cost of some loss of handling, which may have affected the test result.

6.5. Determination of the optimal tail configuration based on stability criteria

Based on the stability analysis results presented in subsections 6.3. Numerical stability analyses of the considered tail configurations and 6.4, the optimal configuration of the tail unit in terms of flight stability is configuration 1 (configuration A). The configuration is presented in the Fig. 114.

Fig. 114 Optimal tail configuration in cale of stability cryteria

By compiling the data obtained from the numerical analysis of the considered configurations (Tab 31) and the data obtained from the weighted evaluation for steady-state horizontal flight (Tab 32) for all configurations, a table showing the results in points scale form was developed. See Tab 33.

Tab 33 Final determination of the optimal configuration considering the results from Table 30 and Table 31.

The configuration under consideration	I	II	III	IV	V
Evaluation by forces and moments Pitch,Roll Yaw	4	3	3	5	1
Evaluation based on Tab.32	4	5	2	3	1
Landing on the belly	Yes	No	Yes	No	Yes
sum	8	~~8~~	5	~~8~~	2

The final tally shows that configurations 1, 2, and 4 received the same highest number of points, however, configurations 2 and 4 were rejected due to a difficult belly landing.

Thus, taking into account the above results, the thesis presented in Section 1.7 "Thesis" was confirmed.

During the work on the analyzed site, many conclusions were identified, some of which are presented in the next chapter of the above dissertation.

7. Summary

The topic of designing unmanned aerial vehicles with extended flight endurance was discussed in the PhD thesis. This work was carried out as part of the LEADER project, and the main research object was the Twin Stratos aircraft, designed to operate at high altitudes.

The proposed analysis methodology allowed the determination of static stability parameters of horizontal flight and the evaluation of the various considered tail configurations of the adopted test object. And allowed to confirm the thesis that : It is possible to select a configuration for the tail section of a given unmanned aerial vehicle (UAV) that is optimal in terms of meeting stability criteria. This selection considers typical flight profiles and the operational conditions determined by the intended application of the UAV. The optimization process may utilize results derived from both simulation-based and analytical approaches. In the doctoral dissertation, an evaluation of the considered tail configurations was conducted in the section 6.5 , based on evaluation of stability criteria, resulting in the selection of an optimal V-tail configuration for the STRATOS UAV. This evaluation is based on analyses derived from simulations presented in 6.3 as well as the analytical calculation method described in the section 5.3. These analyses took into account various flight profiles (section 2.1) and the potential applications of the STRATOS UAV (section 2.2).

The research carried out within the framework of this dissertation allowed the development of a novel methodology for optimizing UAV HALE, which takes into account the unique requirements and limitations of high-altitude flight. The results obtained and the developed methodology are a valuable contribution to the development of this type of design and can form the basis for future research and applications in the field of UAVs.

In the course of the work, a key problem was identified: the lack of adequate regulations for the flight of unmanned HALE aircraft. Current regulations, both European and Polish, do not take into account the specific requirements and capabilities of such structures, which significantly limits their full operational potential. As a result, designers have to rely on standards for manned aircraft and gliders, which leads to an excessive increase in safety parameters and loads on structures.

The developed methodology and the optimization results obtained can be widely applied in the design of new long endurance unmanned aerial vehicles that can act as an alternative to satellites. The next stages of the research should focus on fully automating the process of optimizing the structure under the atem of stability using ANSYS software and verifying the results in experimental tests.

7.1. Conclusions

The present work includes a detailed comparison of aerodynamic simulation results obtained using two numerical tools: XFLR5 and ANSYS CFX. These results were analyzed in the context of different drone tail configurations to assess their stability. Both tools showed significant convergence of results against the tests of the resulting demonstrator, especially for simpler flight conditions and at moderate angles of attack.

XFLR5, as a tool based on the panel method, has a short calculation time and relatively easy access to the results. However, its flow modeling is based on some simplifications, such as the lack of consideration of fully turbulent flow effects or nonlinear aerodynamic interaction effects, which can lead to some inaccuracies in more complex flow conditions such as near overpressure flight or diving flight.

ANSYS CFX, which uses methods based on Navier-Stokes equations, offers more accurate modeling of the full range of flows, including turbulent and nonlinear phenomena, allowing for more accurate analysis under more complex flight conditions, such as high angles of attack or varying wind speeds.

In the context of the comparison, it was noted that the differences between the results obtained with the two tools are most apparent in cases where the drone is in extreme flight states, such as, high angle of attack. ANSYS CFX shows more stable results and better representation of dynamic effects, such as vibration and nonlinear flows, while XFLR5 can predict results that are less stable or with higher error. These differences may be due to a different approach to computational meshing, where ANSYS CFX allows for more accurate near-surface modeling, as well as differences in the way boundary conditions are modeled, which can affect results in more dynamic scenarios.

Despite these differences, both tools provided valuable information for assessing the stability of the tail configurations under consideration. In terms of overall conclusions, their convergence under typical flight conditions suggests that the two tools can be used complementarily, depending on the specifics of the study, the stage the project is at and the computational resources available.

In-flight stability results derived from analytical calculations are based primarily on the geometric parameters of the object under study. Without knowing the exact position of the aerodynamic middleground of the test object and the position of the center of gravity, it is impossible to perform these calculations.

Due to the labor-intensive nature of the calculations carried out to determine the main points required for the analytical determination of stability, a scheme of proceeding using the initial execution of the object model in the XFLR5 program to obtain the necessary parameters, then carrying out analytical calculations in parallel and in the XFLR5 environment, and finally carrying out tests of the accurate geometric model in the ANSYS environment is adopted as the optimal scheme. The juxtaposition of such analyses allows to obtain the closest to reality results.

Considering the tests performed in flight on the Stratos 1:7 and the results obtained during the numerical representation of flight conditions in both numerical environments, it is correct to state the high accuracy of the results from the adopted and developed computational models.

- **Summary of the results of the stability assessment of the considered configurations:**

V-tail and inverted V-tail (also called A-tail in the dissertation)

The V-tail and inverted V can improve the aircraft's maneuverability and stability at high angles of attack, which is beneficial during takeoff, landing and combat maneuvers. Its design can generate less aerodynamic drag than traditional tail configurations, which benefits energy efficiency. However, this tail can introduce difficulties in maintaining directional stability (yaw) under aerodynamically complex conditions. Compared to conventional configurations, the inverted-V tail may exhibit more drag at low speeds, which affects flight efficiency. Its more complex design requires advanced engineering expertise, which can increase production and maintenance costs.

In summary, the inverted-V tail offers advantages in maneuverability and stability at high angles of attack, but it also comes with design and aerodynamic challenges. The choice of this configuration depends on the specific requirements of the project and the application of the aircraft.

Conventional tail

The conventional tail is characterized by a simple design, which facilitates production, maintenance and repair. It generates low aerodynamic drag, which promotes energy efficiency, and provides good stability during the yaw phase, making it easier to control the aircraft. It is versatile, suitable for a variety of configurations, from small aircraft to large jets. Compared to more advanced configurations, the conventional tail can be less maneuverable and heavier, affecting maneuverability and energy consumption. It can also generate more aerodynamic drag at high angles of attack. In summary, the conventional tail is popular for its simplicity, efficiency and flexibility, although it has some limitations in maneuverability and weight, making it a suitable choice for many applications, especially in civil aviation.

Boom Tail

The boom tail on STRATOS places the vertical stabilizers under the horizontal stabilizer, which can protect them from the effects of air vortices generated by the wings and rotors. This design minimizes interaction between control surfaces, improving control and stability of the aircraft, especially at high angles of attack. However, the "boom tail" can generate additional weight and aerodynamic drag, which affects energy consumption and maneuverability . It can introduce difficulties in the turning phase, especially in complex atmospheric conditions, requiring precise control. In summary, the boom tail offers advantages in terms of stability and control, but comes with some aerodynamic and design limitations.

High Boom Tail

The high boom tail places the horizontal stabilizers at a higher level, which protects them from wing influence and improves control efficiency and stability in severe weather. However, this design can generate additional weight and aerodynamic drag, affecting energy consumption and maneuverability. It also introduces challenges in controlling the UAV during the turning phase, especially in complex atmospheric conditions.

Based on the analysis and simulations, tail configuration 1 emerged as the best in terms of stability for the UAV STRATOS test object. As mentioned in Section 6.3.4. Compared to the other configurations, configuration I is characterized by less fluctuation of moments (especially roll and yaw), which may indicate stability and ease of control in conditions without extreme maneuvers.

7.2. Future work

It is recommended to develop methodologies for automating structural optimization with stability analyses using ANSYS software.

Aerodynamic tests of the tail configuration 1 under critical conditions are planned in accordance with the forces that occur during high-altitude flight. These tests are intended to confirm analytical and numerical results and provide data for further modifications and calibration of numerical models.

It is necessary to develop and refine the existing numerical models to better match the actual operational conditions, and then confront the results obtained in the numerical analyses with the results of experimental tests for the TS17 and Twin Stratos 1:2 UAVs.

It is advisable to conduct more advanced dynamic analyses that cover the full range of flight conditions, including the effects of turbulence, varying wind speeds and different flight profiles. In particular, it is worthwhile to address the modeling of nonlinear behavior and study the response of drones to sudden changes in atmospheric conditions to better understand their behavior in real operational scenarios.

It is recommended that experimental tests be conducted in a wind tunnel to verify and complement simulation results obtained with numerical tools. Such tests will enable a better representation of actual flight conditions and a more accurate understanding of flow phenomena around different tail configurations. These experiments could also provide data for calibrating numerical models and improving their accuracy.

Further research in these areas can contribute to the development of more advanced UAV HALE drone models that can meet the growing demands of high-altitude missions and extreme weather conditions.

Bibliography

Rizzi, Arthur. 2011. "Modeling and simulating aircraft stability and control—The SimSAC project." *Progress in Aerospace Sciences*, 10 26: 573-588.

Abdulwahab, Emad, Qasim Atiyah, Ali Talib, and Ali Abdalzahra. 2013. "Aircraft Lateral-Directional Stability in Critical Cases via Lyapunov Exponent Criterion." *Al-Khwarizmi Engineering Journal. 9.* 29-38.

Adamczuk, Paweł, and Michał Burek. 2019. *Techniki pilotażu w lotach próbnych. Stateczność statyczna i dynamiczna samolotu.* Dęblin: Wydawnictwo Lotniczej Akademii Wojskowej.

Agostino, Shane, Matthew Mammone, Matthieu Nelson, and Tong Zhou. 2006. *CLASSIFICATION OF UNMANNED AERIAL VEHICLES.* The University of Adelaide.

Airbus. 2018. "Airbus.com." Accessed październik 25, 2022. https://www.airbus.com/en/products-services/defence/uas/uas-solutions/zephyr.

Airfoil Tools. 2023. *Airfoil Tools.* AirfoilTools.com. Accessed Feb 2023. http://airfoiltools.com/.

Ananthkrishnan, N. 2004. "Small-Perturbation Analysis of Airplane Flight Dynamics – A Reappraisal. I: Longitudinal Modes." *AIAA Atmospheric Flight Mechanics Conference and Exhibit.* Providence, Rhode Island.

Anderson, John. 2012. *Aircraft Performance & Design.* New Dehli: Tata McGraw-Hill.

—. 2017. *Fundamentals of Aerodynamics.* New York, NY: McGraw-Hill Education.

—. 2000. *Introduction to Flight.* New York: McGraw-Hill.

ANSYS, Inc. 2013. *ANSYS CFX Tutorials.* Canonsburg, P: ANSYS, Inc.

Arjomandi, Maziar. 2007. "Classification of unmanned aerial vehicles." *MECH ENG 3016 - AERONAUTICAL ENGINEERING.*

Babister, A. W. 2013. *Aircraft Dynamic Stability and Response: Pergamon International Library of Science, Technology, Engineering and Social Studies.* Elsevier.

Bertin, John J., and Russel M. Cummings. 2009. *Aerodynamics for engineers.* Upper Saddle River, NJ: Pearson Prentice-Hall.

Boschetti, Pedro J., Elsa M. Cardenas, and Andrea Amerio. 2010. "AIAA Atmospheric Flight Mechanics Conference." *Static-Stability Analysis of a Unmanned Airplane as a Flexible-Body.* Toronto, Ontario Canada.

Carholt, O C, E Fresk, G Andrikopoulos, and G Nikolakopoulos. 2016. "Design, Modelling and Control of a Single Rotor UAV." *24th Mediterranean Conference on Control and Automation (MED).* Athens, Greece.

Caughey, David A. 2011. *Introduction to Aircraft Stability and Control, Course Notes for M&AE 5070.* Ithaca, New York: Sibley School of Mechanical & Aerospace Engineering, Cornell University.

Cesnik, Carlos E, and Weihua Su. 4 - 7 January 2011. "49th AIAA Aerospace Sciences Meeting including the New Horizons Forum and Aerospace Exposition." *Nonlinear Aeroelastic Simulation of X-HALE: a Very Flexible UAV.* Orlando, Florida.

Cesnik, Carlos E. S., Patrick J. Senatore, Weihua Su, and Ella M Atkins. December 2012. "X-HALE: A Very Flexible Unmanned Aerial Vehicle." *AIAA JOURNAL* 50 (12): 2820 - 2833.

Ciliberti, D, F Nicolosi, and P Della Vecchia. 2013. "A NEW APPROACH IN AIRCRAFT VERTICAL TAILPLANE." *Italian Association of Aeronautics and Astronautics, XXII Conference.* Napoli.

Coban, Sezer, and Tugrul Oktay. 2018. "Unmanned Aerial Vehicles (UAVs) According to Engine Type." *Journal of Aviation 2*, 177-184.

Cusati, Vincenzo, Salvatore Corcione, Danilo Ciliberti, and Fabrizio Nicolosi. 2022. "Design Evolution and Wind Tunnel Tests of a Three-Lifting Surface Regional Transport Aircraft." *Aerospace.*

Damiani, Rick, Fabian Wendt, Jason Jonkman, and Jerome Sicard. 2019. *A Vortex Step Method for Nonlinear Airfoil Polar Data as Implemented in KiteAeroDyn.* San Diego, California: National Renewable Energy Laboratory.

Deperrois, Andre. 2019. "Why does a plane fly: the inviscid potential flow." March.

Ding, Lidong. 2023. "Research on Longitudinal Static Stability Compensation of Aircraft." *Journal of Physics Conference Series.*

D'Oliveria, Flavio Araripe, Francisco Cristovão Lourenço de Melo, and Tessaleno C Devezas. 2016. "High-Altitude Platforms — Present Situation and Technology Trends." *São José dos Campos* 8 (3): 249-262.

Donegan, James J. 1954. "Matrix methods for determining the longitudinal-stability derivatives of an airplane from transient flight data." *NATIONAL ADVISORY COMMITTEE FOE AERONAUTICS.*

Dunbar, Brian. 2009. *www.nasa.gov.* NASA. September 28. Accessed 11 14, 2023. https://www.nasa.gov/image-article/helios-prototype-flying-wing-2/.

Edwards Air Force Base. 1974. *U.S. Air Force Test Pilot School, Stability and Control, Volume I, Stability and Control Flight Test Techniques, National Technical Information Service.* California: U.S. Department of Commerce, Air Force Flight Test Center.

Elmeseiry, Nourhan, Nancy Nancy, and Tawfik Ismail. 2021. "A Detailed Survey and Future Directions of Unmanned Aerial." *aerospace*, 11 25.

Embry-Riddle Aeronautical University. 2024. *AIRCRAFT STABILITY & CONTROL.* Accessed 05 11, 2024. https://eaglepubs.erau.edu/introductiontoaerospaceflightvehicles/chapter/aircraft-stability-control/#return-footnote-635-3.

Etkin, Bernard, and Lloyd Duff Reid. 1996. *Dynamics of flight, stability and control.* Canada: John Wiley & Sons, Inc.

European Union Aviation Safety Agency. 2022. *Easy Access Rules for Unmanned Aircraft Systems (Regulations (EU) 2019/947 and 2019/945).* EASA PRO. September 28. Accessed May 8, 2023. https://www.easa.europa.eu/en/document-library/easy-access-rules/easy-access-rules-unmanned-aircraft-systems-regulations-eu.

F. Heintz, P. Rudol i P. Doherty. 2007. "From Images to Traffic Behavior - A UAV Tracking and Monitoring Application." *10th International Conference on Information Fusion.* Quebec, Canada.

Fotouhi, Azade, Haoran Qiang, Ming Ding, Mahbub Hassan, Lorenzo Galati Giordano, Giordano Garcia-Rodriguez, and Jinhong Yuan. 2019. "Survey on UAV Cellular Communications: Practical Aspects, Standardization Advancements, Regulation, and Security Challenges." *IEEE Communications Surveys & Tutorials, vol. 21, no. 4*, 3417-3442.

Frulla, G. 2002. "HELIPLAT: Structural Analysis of High Altitude very-long endurance Solar Powered platform for Telecommunication and earth observation Applications." *Engineering, Environmental Science.*

Gibbs, Yvonne. 2017. *www.nasa.gov.* NASA. August 7. Accessed March 6, 2023. https://www.nasa.gov/centers/armstrong/news/FactSheets/FS-068-DFRC.html.

Glenn Reseaech Center. 2021. *www.grc.nasa.gov.* National Aeronautics and Space Administration. May 13. Accessed August 07, 2024. https://www.grc.nasa.gov/www/k-12/airplane/nseqs.html.

Goetzendorf-Grabowski, Tomasz, and Tomasz Antoniewski. 2016. "Three surface aircraft (TSA) configuration – flying qualities evaluation." *Aircraft Engineering and Aerospace Technology*, 02 13.

Gracia-Hernandez, Luis, Cristina Cuerno-Rejado, and Manuel Perez-Cortes. 2018. "Dynamics and Failure Models for a V-Tail Remotely Piloted Aircraft System." *JOURNAL OF GUIDANCE, CONTROL, AND DYNAMICS*, February 2.

Harper, R. P., and G. E. Cooper. 1966. *Handling Qualities and Pilot Evaluation.* NASA Technical Note.

Heaphy, Marie, Michael S Watt, Jonathan Dash, and Grant D Pearse. 2017. "UAVs for data collection-plugging the ga." *New Zeland Journal of Foresty*, 04: 23-30.

Heintz, Fredrik, Piotr Rudol, and Patrick Doherty. 2007. "From Images to Traffic Behavior - A UAV Tracking and Monitoring Application." *10th International Conference on Information Fusion.* Quebec, QC, Canada, 2007, pp. 1-8, doi: 10.1109/ICIF.2007.4408103.

Hurt, H. H. 1965. *Aerodynamics for Naval Aviators.* California: DIRECTION OF COMMANDER, NAVAL AIR SYSTEMS COMMAND.

Irving, F. G. 2014. *An Introduction to the Longitudinal Static Stability of Low-Speed Aircraft.* London: Whitefriars press LTD.

Joshi, Alaukik, Amritanshu Tripathi, and R N Ponnalgu. 2019. "Modelling and Design of a Hybrid Aerial Vehicle." *2019 6th International Conference on Instrumentation, Control, and Automation (ICA).* Bandung, Indonesia.

Juliawan, Nadhie, Hyoung-Seog Chung, Jae-Woo Lee, and Sangho Kim. 2021. "Estimation and Separation of Longitudinal Dynamic Stability." *Aerospace*, 11 19.

Kamran, Ahmad, and Rahman Hammad. 2013. "Flutter Analysis of X-HALE UAV-A Test Bed for Aeroelastic Results Validation." *Applied Mechanics and Materials Vol. 245*, 303-309.

Kemp. Jr., William B. 2013. "Definition and application of longitudinal stability derivatives for elastic airplanes." *NASA Technical Note*, 9 2.

Kerschen, G, M Peeters, and J C Golinval. 2013. "Nonlinear Modal Analysis of a Full-Scale Aircraft." *JOURNAL OF AIRCRAFT*, 10.

Kubryński, Krzysztof. 1996. *APPLICATION OF THE PANEL METHODTO SUBSONIC AERODYNAMIC DESIGN.* Warsaw: Overseas Publishers Association.

Kurnyta, Artur, Wojciech Zieliński, Piotr Reymer, Michał Dziendzikowski, and Krzysztof Dragan. July 10-13, 2018. "In Flight Load Determination in Critical Structure Elements Based on." *9th European Workshop on Structural Health Monitoring.* Manchester, United Kingdom.

Lee, Cheonghwa, Seolha Kim, and Baeksuk Chu. 2021. "A Survey: Flight Mechanism and Mechanical Structure of the UAV." *International Journal of Precision Engineering and Manufacturing*, 719-743.

Lu, Ke, Chunsheng Liu, Chunhua Li, and Renliang Chen. 2019. "Flight Dynamics Modeling and Dynamic Stability Analysis of Tilt-Rotor Aircraft." *International Journal of Aerospace Engineering - Hindawi*, August 14.

Lungu, Mihai. 2013. "Adaptive backstepping flight control for a mini-UAV." *International Journal of Adaptive Control and Signal Processing*, August.

Mahdi, Mohammed, and Yasser A. Elhassan. 2012. "Stability Analysis of a Light Aircraft Configuration using Computational Fluid Dynamics." *Applied Mechanics and Materials Vol 225*, November: 391-396.

Mańkowski, Jarosław, Jakub Piękoś, Karol Dominiak, Piotr Klukowski, Michał Fotek, Maciej Zawisza, and Piotr Żach. 2021. "A Mandible with the Temporomandibular Joint—A New FEM." *Materials*, 09 2.

Mateja, Krzysztof, Wojciech Skarka, Magdalena Peciak, Roman Niestrój, and Maik Gude. 2023. "Energy Autonomy Simulation Model of Solar Powered UAV." *MDPI Energies*, January 1.

McCormic, Barnes W. 1979. *Aerodynamics, aeronautics and flight mechanics.* Canda: JOHN WILEY & SONS.

Mieloszyk, J, and T Goetzendorf-Grabowski. 2017. "Introduction of full flight dynamic stability constraints in aircraft." *Aerospace Science and Technology*, 05 22: 252-260.

Mohamed Zouhir Dar Ramdane, Miloud Abidat, and Mohamed Hamel. 2015. "Numerical Simulation of Heat Exchanger's Length's Effect in a Thermoacoustic Engine." *Journal of Physical Science and Application.*

Montgomery, Sean A, and Nikos J Mourtos. 2016. "Design of a 5 Kilogram Solar-Powered Unmanned Airplane for Perpetual Solar Endurance Flight." *American Institute of Aeronautics and Astronautics.*

Moore, F.G., and L. Y. Moore. 2008. *2009 Version of the Aeroprediction Code: The AP09.* King George, VA: Aeroprediction, Inc.

Mozaffari, Mohammad, Walid Saad, Mehdi Bennis, Young-Han Nam, and M´erouane Debbah. 2019. "A Tutorial on UAVs for Wireless Networks: Applications, Challenges, and Open Problems." *IEEE Communications Surveys & Tutorials, vol.21*, 334-2360.

Muhammad Ahmad, Zukhruf Liaqat Hussain, Syed Irtiza Ali Shah, and Taimur Ali Shams. 2021. "Estimation of Stability Parameters for Wide Body Aircraft." *Applied Sciences, MDPI*, 11.

Nelson, Robert C. 1998. *Flight Stability and Automatic Control.* Boston, Massachusett: WCB McGraw-Hill.

Nicolosi, Fabrizio, Danilo Ciliberti, Pierluigi Della Vecchia, and Salvatore Corcione. 2020. "Experimental analysis of aircraft directional control effectiveness." *Aerospace Science and Technology*, July 22.

Nicolosi, Fabrizio, Salvatore Corcione, and Pierluigi Della Vecchia. 2016. "Commuter Aircraft Aerodynamic Characteristics Through Wind Tunnel Tests." *Aircraft Engineering and Aerospace Technology.*

Noth, A, R Siegwart, and W Engel. 2006. "Design of Solar Powered Airplanes for Continuous Flight." In *ETHZ - Advances in Unmanned Aerial Vehicles, State of the art and the road to autonomy*. Zurich: Springer.

Noth, Andre, Walter Engel, and Roland Siegwart. 2006. "Design of an Ultra-Lightweight Autonomous Solar Airplane for Continuous Flight." *Field and Service Robotics* 25: 441–452.

Nowakowski, Mirosław. 2019. *Badania w Locie Statków Powietrznych.* Warszawa: WYDAWNICTWO INSTYTUTU TECHNICZNEGO WOJSK LOTNICZYCH.

Panfil, W, W Moczulski, A Pawełczyk, K Targosz, Ł Maliszewski, and D Pająk. 2024. *Report on tests of the integrated system in a laboratory and relevant environment; Project: "Long-endurance UAV for collecting air quality data with high spatial and temporal resolutions".* Gliwice: Program „Badania stosowane" w ramach Norweskiego Mechanizmu Finansowego 2014-2021.

Park, Jangho, Jaw-Young Choi, Yeongmin Jo, and Seongim Choi. 2017. "Stability and Control of Tailless Aircraft Using Variable-Fidelity Aerodynamic Analysis." *American Institute of Aeronautics and Astronautics*, May 19: 2148-2164.

Paskonov, V. M. 2020. *Navier-Stokes equations. Encyclopedia of Mathematics.* 06 06. Accessed 01 21, 2024. http://encyclopediaofmath.org/index.php?title=Navier-Stokes_equations&oldid=47950.

Pietreanu, Casandra Venera, and Valentin Marian Iordache. 2018. "QUALITATIVE AND QUANTITATIVE ASSESSMENT OF RISKS ASSOCIATED TO HELIOS HP 03-2 UNMANNED AERIAL VEHICLE DEVELOPED BY NASA." *U.P.B. Sci. Bull., Series D, Vol. 80*, 39-50.

Polnor Leader. 2019. "Polnor Leader - About Us." Accessed January 21, 2023. https://polnor-leader.eu.

Raymer, Daniel P. 1992. *Aircraft Design: A Conceptual Approach.* Washington, DC: American Institute of Aeronautics and Astronautics.

Rodgers, Edward J. 1965. "The Neutral Point in Stability and Control Analysis." *Journal of Aircraft*, February: 33-38.

Rogalski, Tomasz, Dariusz Nowak, and Łukasz Wałek. 2015. "ALGORYTMY STEROWANIA LOTEM SAMOLOTU BEZZAŁOGOWEGO W NIETYPOWYCH STANY LOTU." *TTS Technika Transportu Szynowego*, 12: 1303-1309.

Rohlf, Detlef, Stefan Schmidt, and Jonathan Irving. 2012. "Stability and Control Analysis for an Unmanned Aircraft Configuration Using System-Identification Techniques." *JOURNAL OF AIRCRAFT*, December: 1597-1609.

Romeo, G, G Frulla, and E Cestino. 2005. "HELIPLAT®: a high altitude very-long endurance solar powered platform for border patrol and forest fire detection." *WIT Transactions on The Built Environment, Vol 82*, 459-469.

Saeed, Adnan S, Ahmad Bani Younes, Shafiqul Islam, Jorge Dias, Lakmal Seneviratne, and Guowei Cai. 2015. "A Review on the Platform Design, Dynamic Modeling and Control of." *2015 International Conference on Unmanned Aircraft Systems (ICUAS).* Denver, Colorado, USA.

Sciences, Aurora Flight. n.d. *High-Altitude Pseudo-Satellite (HAPS).* Aurora Flight Sciences. Accessed 12 03, 2023. https://www.aurora.aero/high-altitude-pseudo-satellite-haps/.

Sieradzki, Adam, Adam Dziubiński, and Cezary Galiński. 2016. "PERFORMANCE COMPARISON OF THE OPTIMIZED INVERTED." *Archive of Mechanical Engineering, VOL.LXIII*, 455-470.

Slingerland, R. 2003. "GROUND EFFECT ON DRAG AND PITCHING MOMENT FOR AIRCRAFT TAIL-OFF CONFIGURATIONS." *AIAA's 3rd Annual Aviation Technology, Integration, and Operations (ATIO) Tech.* Denver, Colorado.

Stafiej, Wiesław. 2000. *Obliczenia stosowane przy projektowaniu szybowców.* Warszawa: Politechnika Warszawska.

Struett, Ryan C. 2012. *Empennage Sizing and Aircraft Stability using Matlab.* San Luis Obispo: California Polytechnic State University, 1 Grand Ave.

Suchocki, Tomasz, Piotr Lampart, and Jan Surwiło. 2015. "Designation of operating characteristics for micro-jet engine and CFD validation." *Mechanik*, 567-820.

Tuzucu, Ilhan. 2008. "On the stability of flexible aircraft." *Aerospace Science and Technology*, January 12: 376-384.

Ucgun, Hakan, Ugur Yuzgec, and Cuneyt Bayilmis. 2021. "A review on applications of rotary-wing unmanned aerial vehicle charging stations." *International Journal of Advanced Robotic SystemsVolume 18, Issue 3*, 05.

Vecchia, Pierluigi Della, Fabrizio Nicolosi, and Danilo Ciliberti. 2015. "Aircraft directional stability prediction method by CFD." *33rd AIAA Applied Aerodynamics Conference.* Dallas, TX.

Wang, Lixin, Kun Yang, Peng Zhao, and Ting Yue. 2021. "Aircraft Configuration Parameter Boundaries Based on Closed-Loop Flying Qualities Requirements." *Aerospace*, 360.

Weiss, Arturo. 2023. *The Pros & Cons Of Twin-Boom Aircraft.* Valnet Publishing Group. 05 26. Accessed 02 11, 2024. https://simpleflying.com/twin-boom-aircraft-pros-cons-guide/.

Whalen, Edward A., Arvin Shmilovich, Marc Spoor, John Tran, Paul Vijgen, John C. Lin, and Marlyn Andino. 2016. "Flight Test of an AFC Enhanced Vertical Tail." *8th AIAA Flow Control Conference.* Washington, D.C.

What, When, How - Tail designs. 2023. *Tail designs.* Accessed 05 02, 2024. https://what-when-how.com/flight/tail-designs/.

Witanowski, Łukasz, Piotr Klonowicz, and Piotr Lampart. 2018. "3D shape optimisation of a low-pressure turbine stage." *International Journal of Energy Production and Management*, January: 10-21.

XFLR5. 2023. *http://www.xflr5.tech.* 05 06. Accessed 04 14, 2024. http://www.xflr5.tech/xflr5.htm.

Zenowicz, Kamil. 2023. *Optimisation of Unmanned Aerial Vehicle of Unlimited Flight Endurance.* Gliwice: Silesian University of Technology. Accessed 10 10, 2023. https://bip.polsl.pl/nadania_dr/kamil-zenowicz/.

Zenowicz, Paulina, and Wojciech Moczulski. 2024. "Comparative study of the UAV configuration during its horizontal flight." *Diagnostyka materiałów inżynierskich. XII Konferencja naukowo-techniczna, 2024.*

Zheng, Juepeng, Haohuan Fu, Weijia Li, Wenzhao Wu, Le Yu, Shuai Yuan, Wai Yuk Tao, Tan Kian Pang, and Kasturi Devi Kanniah. 2021. "Growing status observation for oil palm trees using Unmanned Aerial Vehicle (UAV) images." *ISPRS Journal of Photogrammetry and Remote Sensing, Volume 173*, March: 95-121.

Zhu, Xiongfeng, Zheng Guo, and Zhongxi Hou. 2014. "Solar-powered airplanes: A historical perspective and future challenges." *Progress in Aerospace Sciences 71*, 36-53.

Comparative analysis of the drone configuration in terms of stability criteria

Doctoral Dissertation – Abstract

Author: MSc, Eng. Paulina Zenowicz
Supervisor: Prof. Wojciech Moczulski, PhD, DSc
The Silesian University of Technology, Faculty of Mechanical Engineering

The outcome of the author's work is the determination of the optimal tail configuration for the examined object, tailored to the assumed flight parameters, the defined mission, and the method of takeoff and landing established during the design process. Within the scope of the study, the author also presented alternative tail configurations, specifying their parameters, their impact on flight stability, as well as their advantages and disadvantages. The analysis of the collected research results has confirmed the correctness of the proposed thesis: It is possible to select a configuration for the tail section of a given unmanned aerial vehicle (UAV) that is optimal in terms of meeting stability criteria. This selection considers typical flight profiles and the operational conditions determined by the intended application of the UAV. The optimization process may utilize results derived from both simulation-based and analytical approaches. The analyses presented in the doctoral dissertation confirmed the validity of the test configuration adopted for implementation within the POLNOR LEADER project.

The objective of this doctoral dissertation was to determine, using comparative research methods, the optimal tail configuration of an unmanned aerial vehicle (UAV) in terms of static flight stability. The tail configuration was defined based on the adopted flight parameters. The primary scientific challenge addressed in this work was to demonstrate the feasibility of determining the optimal configuration using numerical computational methods and applying a CFD (Computational Fluid Dynamics) environment.

Based on a review of existing solutions, tail configurations applicable to the research object—the 1:7 scale BSP Twin Stratos (TS17)—were identified. Due to the unconventional design, which employs two fuselages symmetrically positioned at a precisely defined distance from the drone's axis of symmetry, an additional challenge was identified. This involves the need to connect both fuselages using the considered tail configurations to ensure structural rigidity and maintain the flight parameters of the research object.

To validate the formulated thesis, a methodology for conducting analyses was proposed, adaptable to the computational environments under consideration. The analyses were performed using two computational environments: ANSYS CFX and XFLR5. The results obtained in both environments were determined for fixed and predefined flight parameters and subsequently compared. To verify the accuracy of the results and assess the degree of deviation from the actual system, both environments simulated the conditions observed during test flights of the TS17 demonstrator equipped with an inverted "V" tail configuration. Based on these tests, a computational environment was selected as the foundation for conducting analyses to determine the optimal tail configuration for the intended mission and flight parameters.

Keywords: Unmanned Aerial Vehicle, stability, aerodynamics, numerical analyses, CFD, tail configuration.

Porównawcza analiza konfiguracji drona w odniesieniu do kryteriów stateczności

Praca doktorska – Streszczenie

Autor: mgr inż. Paulina Zenowicz
Promotor: prof. dr hab. Wojciech Moczulski
Politechnika Śląska w Gliwicach, Wydział Mechaniczny Technologiczny

Wynikiem pracy autorki jest określenie optymalnej konfiguracji ogonowej badanego obiektu dla zakładanych parametrów lotu, przyjętej misji oraz ustalonej podczas prac nad projektem metody startu oraz lądowania. W ramach pracy, autorka przedstawiła także pozostałe możliwe do zastosowania konfiguracje ogonowe określając ich parametry, wpływ na stateczność w locie, wady oraz zalety. Analiza zebranych wyników badań potwierdziła słuszność postawionej tezy: Możliwe jest dokonanie wyboru konfiguracji części ogonowej danego bezzałogowego statku powietrznego (BSP), optymalnej pod względem spełnienia kryterium stateczności. Wybór ten uwzględnia typowe profile lotu oraz warunki ich wykonywania wynikające z przeznaczenia rozpatrywanego BSP. Proces optymalizacji może opierać się na wynikach uzyskanych zarówno metodami symulacyjnymi, jak i analitycznymi. Analizy przedstawione w rozprawie doktorskiej potwierdziły słuszność przyjętej do wykonania w ramach projektu POLNOR LEADER konfiguracji testowej.

Celem niniejszej rozprawy doktorskiej było określenie metodami badań porównawczych optymalnej pod względem stateczności statycznej lotu konfiguracji ogonowej bezzałogowego statku powietrznego. Konfiguracja ogonowa została określona dla przyjętych parametrów lotu. Podstawowym problemem naukowym podjętym w pracy było udowodnienie możliwości określenia optymalnej konfiguracji za pomocą numerycznych metod obliczeniowych oraz zastosowaniu środowiska CFD.

Na podstawie przeglądu istniejących rozwiązań określone zostały możliwe do zastosowania w obiekcie badań, którym został BSP Twin Stratos w skali 1:7 (TS17), konfiguracje ogonowe. Ze względu na nietypowy układ wykorzystujący dwa kadłuby umiejscowione symetrycznie, w ściśle określonej odległości od osi symetrii drona, zidentyfikowany został kolejny problem, którym jest konieczność połączenia obu kadłubów rozpatrywanymi konfiguracjami ogonowymi w celu zachowania sztywności i parametrów lotu obiektu badań.

W celu wykazania słuszności sformułowanej tezy zaproponowano metodykę prowadzenia analiz możliwą do zaadaptowania dla rozpatrywanych środowisk obliczeniowych. Analizy zostały wykonane z zastosowaniem dwóch środowisk obliczeniowych, jakimi są ANSYS CFX oraz XFLR5. Wyniki analiz uzyskiwane w obu środowiskach obliczeniowych określane były dla stałych i przyjętych odgórnie parametrów lotu a następnie porównywane. Dla określenia poprawności wyników oraz określenia stopnia rozbieżności względem układu rzeczywistego, w obu środowiskach odwzorowano warunki panujące podczas lotów testowych demonstratora TS17 wyposażonego w konfigurację ogonową tylu odwrócone „V". Na podstawie przeprowadzonych testów wytypowane zostało środowisko na bazie którego przeprowadzono analizy umożliwiające określenie optymalnej konfiguracji ogonowej dla zakładanej misji oraz parametrów lotu.

Słowa kluczowe: Bezzałogowy Statek Powietrzny, stateczność, aerodynamika, analizy numeryczne, CFD, konfiguracja ogonowa.